Democratic and Popular Republic of Algeria

Ministry of Higher Education and Scientific Research

University Mohamed Khider of Biskra

Faculty of Exact Sciences and Science of Nature and Life

Department of Material Sciences

Thesis

Presented to obtain the degree of

Doctorate

Option: Physics of Materials.

Entitled:

Study of the effect of dopant on oxide thin films for optoelectronic applications.

Presented by:

M^me^. BENCHAREF Zahia

Publicly defended on: 19 / 12 / 2022

In front of the Jury committee composed of:

M^r^. A. ATTAF	Professor	University of Biskra	President
M^r^. A. CHALA	Professor	University of Khenchela	Supervisor
M^r^. S. RAHMANE	Professor	University of Biskra	Examiner
M^r^. A. DJELLOUL	Professor	University of Khenchela	Examiner

Acadymic year 2022-2023

Dedication

I would like to dedicate this work

To my dear Parents;

To my dear husband and dear children;

To my dear sisters and dear brothers;

To all my relatives and neighbors;

To all my friends and colleagues.

Zahia BENCHAREF

Acknowledgements

First and for most, I would like to thank **ALLAH** for his helping me in making this quest of knowledge possible.

Apart from the efforts of me, the success of this work depends on the encouragement and support of many others. I take this opportunity to express my gratitude to people who help to complete this project successfully.

Initially, I would like to acknowledge my heartfelt gratitude to my supervising guide, Mr. **Abdelouahad CHALA** his willingness to motivate me contributed tremendously to my research work. Without his insightful guidance and persistent help, this thesis would never have been accomplished. I am thankful for his guidance, enthusiastic encouragement, valuable suggestions and useful critiques he gave me during the course of this research work.

I express my sincere gratitude and appreciation to my reading committee members, Professor **Abdallah. ATTAF** of Biskra University, Professor **Saäd RAHMAN** of Biskra University, and Professor **Abdelkader DJELLOUL** of **Khenchela** University for their precious time to read my thesis and for ac-accepting to judge it.

I would like to extend my special thanks to Professor **Saäd RAHMANE**, Professor **Said BENRAMACHE,** Doctor **R. Messemeche** and Doctor **Y. Benkhetta** for helping me especially at this research. I would also like to thank everyone who works in laboratory of the thin films of our university.

Finally, I express my sincere thanks to all my, family, friends, colleagues, and to everyone who helped me to accomplish this research work.

Table of contents

CHAPTER THREE : Structural, compositional and morphological study of Co_3O_4:N (N= Mn, La, Sn and Zn) Thin Films.

CHAPTER FOUR : Optical and electrical study of Co_3O_4:N (N= Mn, La, Sn and Zn) Thin Films

General introduction

General introduction

Absorbent conducting oxide (ACO) materials such as Fe_2O_3, Cu_2O, NiO and Co_3O_4 have attracted a lot of researchers. The development of ACO are important to their interest of optoelectronic, chemical optical and physical properties [1]. Among them ACO cobalt oxide, which is one of the most remarkable material in experimental examination of scientific and technological importance [1]. Cobalt oxide has three phases different crystalline are: Co_2O_3 (cubic structure), CoO (cubic structure) and Co_3O_4 (cubic spinel structure of the type AB_2O_4; where Co^{3+} ions occupy the octahedral sites and Co^{2+} occupy the tetrahedral sites) is high stability in comparison to other phases [2]. It has a high optical absorbance in the spectral range of UV-Vis and electrical conduction.

Until now, Co_3O_4 thin films is prepared by a variety of thin film deposition techniques such as magnetron sputtering (MST), pulsed laser deposition (PLD), 400 °C molecular beam epitaxy (MBE), sol-gel process (SGP), reactive evaporation (RE), electrochemical deposition (ECD), chemical vapor deposition (CVD) and pneumatic spray method (PSM)...etc. Among these techniques, Co_3O_4 thin films are deposited using a homemade pneumatic spray method (PSM). It can produce homogeneous thin films with a very regular crystallites sizes [3-4]. The PSM has many advantages, such as: control of solution concentration, temperature stabilization, control for glass substrates, time control for spraying, large-area spraying, and control of composition so that the morphology of films can be controlled (dense or thickness of films). Therefore, it is one of the most important methods for the preparation of functional Co_3O_4 films.

In the last decades, several published researches studied cobalt oxide thin films properties which was prepared by SPM by varying multiple deposition parameters such as: doping of the transition metal elements (Fe, Mn, Cu, Cr, Ni) in Co_3O_4 can enhance electrocatalytic activity [5-9], Mn doping [10], Cu doping [11] .... etc.

In this work, an attempt is made to optimize optical and electrical properties of cobalt oxide thin films using PSM, by changing the following parameters: Mn, La, Sn and Zn doping. The prepared Co_3O_4:N (N= Mn, La, Sn and Zn) thin films are characterized by X-ray diffraction, UV-Vis spectroscopy, atomic force microscopy (AFM) the three-dimensional (3D),scanning electron microscopy, energy dispersive spectroscopy (EDS), and four points probe measurements.

This thesis is divided into four chapters:

Chapter one deals with a bibliographic study of cobalt oxides.

The second one focuses on a description of the elaboration pneumatic spray method (PSM) used to prepared Co_3O_4:N (N= Mn, La, Sn and Zn) thin films. The second one focuses on the description of the elaboration pneumatic spray method (PSM) used to prepare Co_3O_4:N (N= Mn, La, Sn and Zn) thin films as well as the deposition process of the films and the various characterization techniques that are used to analyze the prepared thin films.

Chapter three presented structural and morphological properties of doped Co_3O_4:N (N= Mn, La, Sn and Zn) thin films that are prepared by pneumatic spray method (PSM) on glass substrate at 400°C.

In chapter four Optical and electrical properties of doped Co_3O_4:N (N= Mn, La, Sn and Zn) Thin Films are investigated.

Finally, a concluding section closes the dissertation where the important results as well as the future work scope are highlighted.

References

[1] A. Louardi, A. El Bachiri, L. Soussi, H. Erguig, B. Elidrissi, M. Khaidar, M. Monkade, Optical Properties of Mg Cobalt Oxide ($Mg_x Co_{3-x} O_4$) Thin Films, Materials Focus 7 (2018) 459-463.

[2] Fikadu Alema, Andrei Osinsky, Partha Mukhopadhyay, Winston V.Schoenfeld, Epitaxial growth of Co_3O_4 thin films using $Co(dpm)_3$ by MOCVD, Journal of Crystal Growth525(2019)125207.

[3] Warda Daranfed1, Noubeil Guermat, Kamel Mirouh, Experimental Study of Precursor Concentration the Co_3O_4 Thin Films Used as Solar Absorbers, Annales de Chimie - Science des Matériaux, 44 (2020). 121-126

[4] Sami Salman Chiad, Hussein Ali Noor, Oday Mazin Abdulmunem and Nadir Fadhil Habubi, Optical and Structural properties of Ni-doped Co_3O_4Nanostructure Thin films Via CSPM, Journal of Physics: Conference Series, 1362 (2019) 012115.

[5] A.I. Nguyen, D.L. Suess, L.E. Darago, P.H. Oyala, D.S. Levine, M.S. Ziegler, R.D. Britt, T.D. Tilley. Manganese-Cobalt Oxido Cubanes Relevant to Manganese-Doped Water Oxidation Catalysts, Journal of the American Chemical Society. 139 (2017) 5579–5587.

[6] S. Liu, K. Hui, K. Hui, ACS Appl. Vertically stacked bilayer CuCo 2 O 4/MnCo 2 O 4 heterostructures on functionalized graphite paper for high-performance electrochemical capacitors. Journal of Materials. Interfaces 8 (2016) 3258–3267.

[7] X. Zou, J. Su, R. Silva, A. Goswami, B.R. Sathe, T. Asefa, Efficient oxygen evolution reaction catalyzed by low-density Ni-doped Co3O4 nanomaterials derived from metal-embedded graphitic C3N4, Chem. Commun. 49 (2013) 7522–7524.

[8] T. Baidya, T. Murayama, P. Bera, O.V. Safonova, P. Steiger, N.K. Katiyar, K. Biswas, M. Haruta,Low-Temperature CO Oxidation over Combustion Made Fe- and Cr-Doped Co_3O_4 Catalysts: Role of Dopant's Nature toward Achieving Superior Catalytic Activity and Stability,Journal of Physical Chemistry. 121 (2017) 15256–15265.

[9] T. Grewe, X. Deng, H. Tüysüz, Influence of Fe Doping on Structure and Water Oxidation Activity of Nanocast Co3O4, Chemistry of Materials. 26 (2014) 3162–3168.

[10] Abdelhak Lakehal, Bedhiaf Benrabah, Amar Bouaza, Cherifa Dalache, Benhebal Hadj. Tuning of the physical properties by various transition metal doping in Co_3O_4: TM

(TM = Ni, Mn, Cu) thin films: A comparative study. Chinese Journal of Physics. 56 (2018) 1845-1852.

[11] R. Venkatesha, C. Ravi Dhasa, R. Sivakumarb, T. Dhandayuthapanib , B. Subramanianc, C. Sanjeevirajad , A. Moses EzhilRaje, Tailoring the physical properties and electrochromic performance of nebulizer spray coated Co3O4 films through copper doping ,Solid State Ionics. 334 (2019) 5-13.

CHAPTER ONE

Bibliographic Study of Cobalt Oxides Thin Films.

This chapter deals with a bibliographic study of the physical properties of cobalt oxide thin films. A brief review on the structural, compositional, optical, electrical and magnetic properties of Co3O4 and Co3O4 doped thin films is presented.

I.1. Introduction

Cobalt oxide is a semiconductor material p-type that is a part of family of ACO, it occurs in three different phases with stoichiometry such as cobalt oxide (Co_3O_4: cubic spinel structure of the type AB_2O_4; where Co^{+3} ions occupy the octahedral sites and Co^{+2} occupy the tetrahedral sites), cobaltous oxide (CoO: cubic structure) and cobaltic oxide (Co_2O_3: cubic structure)[1].Among the cobalt oxides, Co_3O_4 which is the most stable and our focus is on this oxide of cobalt [2].Co_3O_4 thin films .It is suitable for many applications such as catalyst for gas sensors [3] and catalysers [4-5], super-capacitors [6],solar selective absorber due to the p-type semiconducting [7], energy storage [8],photocatalytic [9] due to having a good structure crystallinity, good electrical conductivity and high absorbency in the visible region.

Table.1 shows the physical and chemical properties of Co_3O_4 thin films, it is found that the Co_3O_4 has a low band gap energy (Eg) with a refractive index of 2,4. The Co_3O_4 as a thin film is studied on verities of substrates with chemical and physical methods; it was used to improve the structural optical and electrical properties. The magnetron sputtering (MST), pulsed laser deposition (PLD), chemical vapor deposition (CVD), sol-gel process (SGP), reactive evaporation (RE), electrochemical deposition (ECD) and spray pyrolysis techniques (SPT), are used to prepare the Co_3O_4 thin films, the spray techniques also are favorites in comparison to other methods due to control of solution concentration, temperature stabilization control for glass substrates, time control for spraying, large-area spraying, and control of composition.

Table. 1: *Summary of the basic physical and chemical properties of Co_3O_4 thin films*

Property	**Value**
Appearance	Fine dark gray to black
Molecular mass	74,9326 g/mol
Stable phase Energy at 298,15 K	9,23 eV
Conductivity σ $(\Omega cm)^{-1}$	10^{-4} -10^{-2}
Melting Point	895 °C (1643 °F)
Refractive index	2,4
Density (Volumic mass)	6,11 g/ mol

Direct band gap energy (Eg)	2,0-2,7 eV
Crystal structure	cubic spinel
Lattice parameter (a_0)	8, 080 Å
Space group	Fd-3m
Electrical properties at room temperature	p-type

The main objective of this research is to study the physical and chemical properties of Co_3O_4 thin films based on past research. In this work; we have proposed a review of original research to nanostructured Co_3O_4 prepared by spray techniques.

I.2. Structural and microstructural properties

I.2.1 Co_3O_4 thin films

In order to elaborate Co_3O_4 thin films, various growth techniques have been used such as magnetron sputtering (MST), pulsed laser deposition (PLD), chemical vapor deposition (CVD), sol-gel process (SGP), reactive evaporation (RE), electrochemical deposition (ECD), spray pyrolysis technique (SPT) and pneumatic spray method (PSM).

According to the growth conditions, more crystallized Co_3O_4 thin films can be obtained. Kouidri Nabila et al. [10] prepared cobalt oxide thin films at different temperature by CVD on a glass. Their X-ray diffraction (XRD) patterns are collected in figure 1. Found that the Co_3O_4 thin film has a polycrystalline nature with preferentially (111) at temperature 400°C. It is high than other diffractions which indicating that the preferred orientation with (111) plan. The Co_3O_4 films are polycrystalline in nature crystallized in the cubic spinel structure as shown in the figure 2 [11].

C. Ravi Dhas et al. [12] investigated the effect of precursor molarity on the structural property. They discussed that the high crystalline structure of Co_3O_4 thin films was obtained in the film prepared with 0.1 M (see figure 3). They found that the Co_3O_4 thin films have preferential orientation along (311) direction peak, so that the deposition under different molar concentration was affected on the structural property.

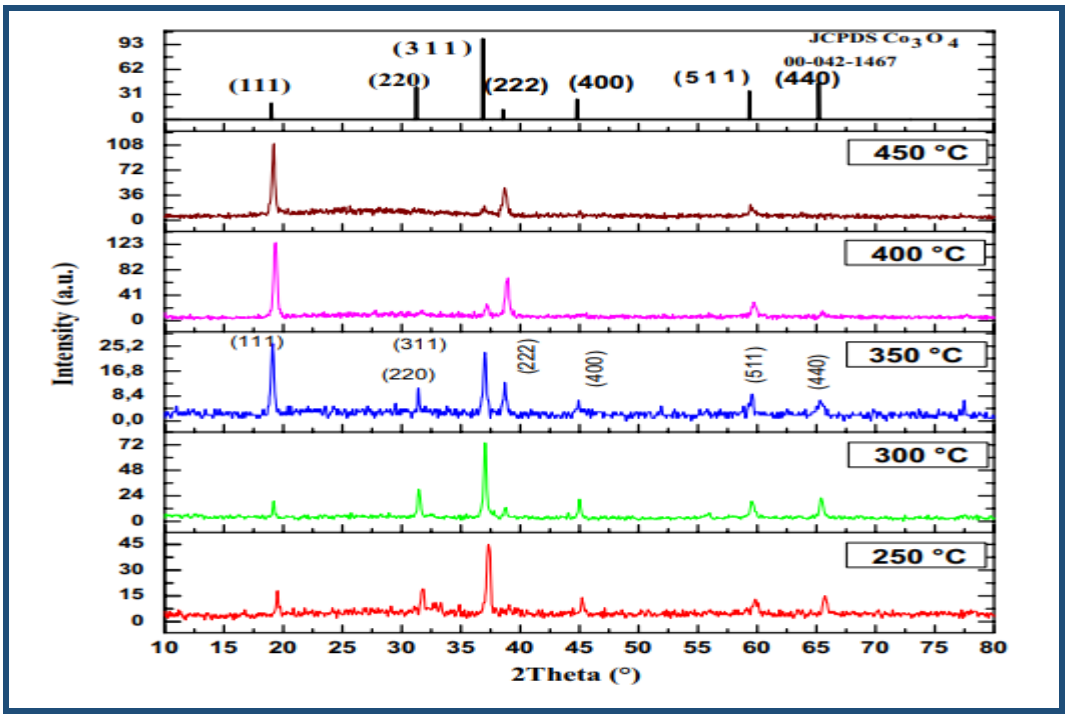

Figure 1:XRD patterns of Co_3O_4 thin films as function of substrate temperatures [10].

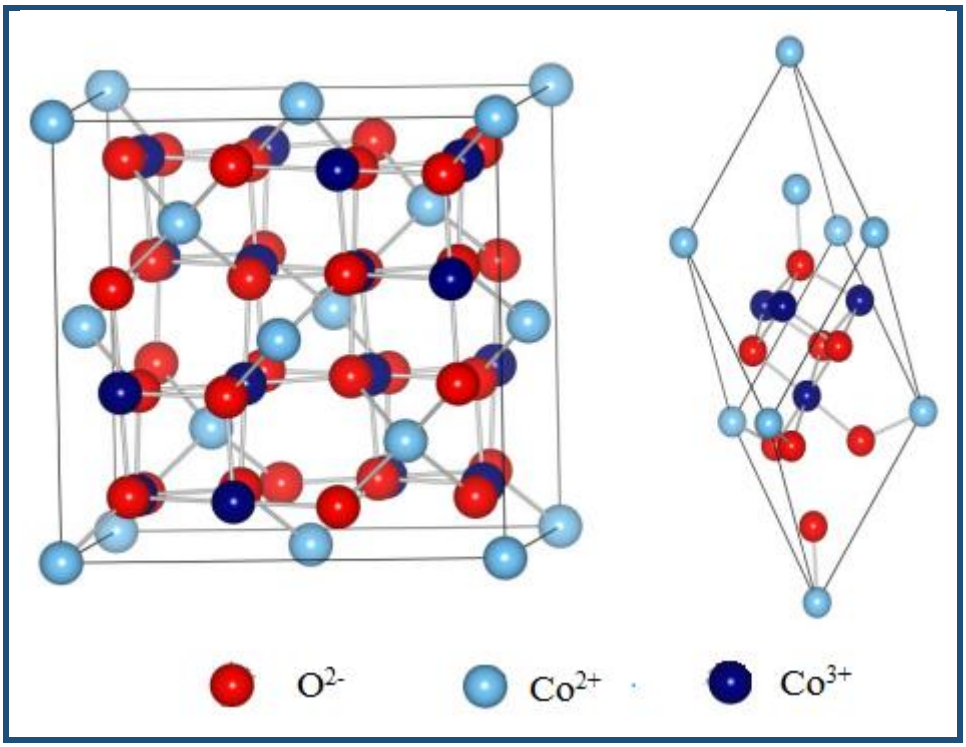

Figure 2: Unit cell (on the left) and primitive cell (on the right) of Co_3O_4[11].

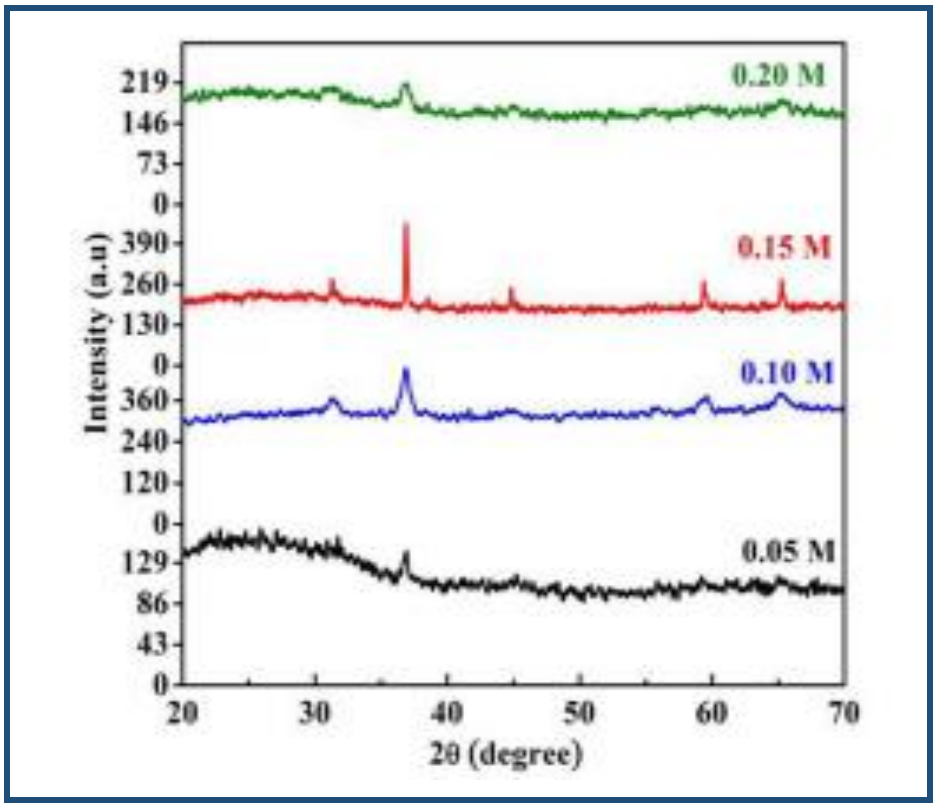

Figure 3:X-ray diffraction patterns of Co_3O_4 thin films deposited under different molar concentration[12].

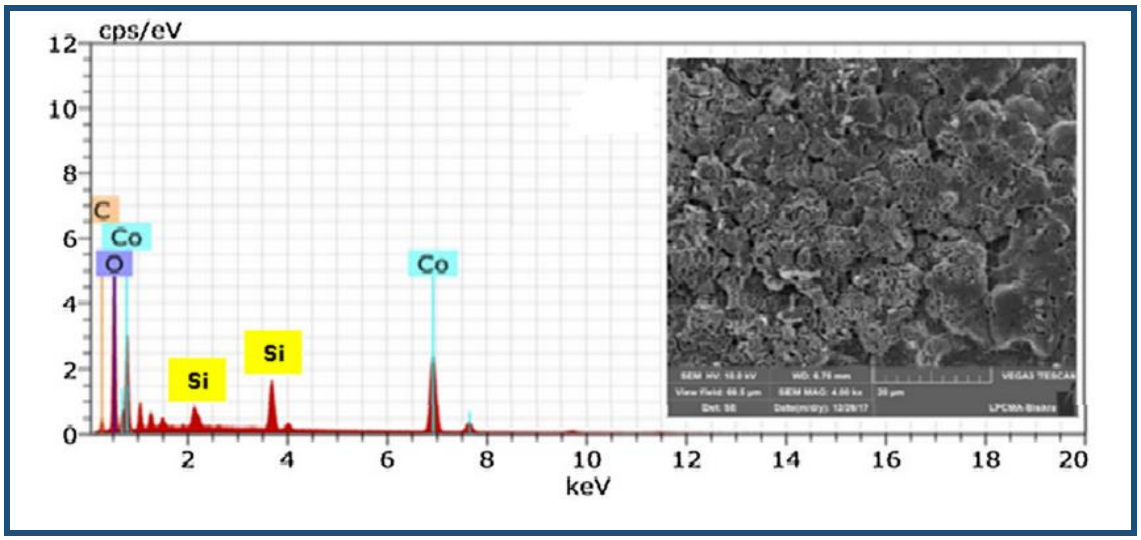

Figure 4: EDS spectrum with SEM image (inset) of Co3O4 thin films deposited at 400 °C[10].

The growing conditions affect also the morphology of the produced films. Kouidri Nabila et al. [10] reported theEDS spectrum with scanning electron microscopy (SEM) images of CVD made Co_3O_4 thin film (Figure 4). They revealed overgrowth of clusters, which is clearly seen and pointed outnanograins have increased their size by further deposition and come closer to each other.Thus, the films follow the cluster by cluster growth process compactness of the formed dispersed structures.

I.2.2 Doped Co_3O_4 thin films

Several doping are performed on Co_3O_4 thin films to tentatively improve their opto-electronic and catalytic properties. The same thin film growth techniques are used to produce such thin films than those practiced for pure Co_3O_4thin films. In most the cases, the stabilization of the blende spinel structure in these films is much more attributed to the deposition conditions than to the doping nature.

I.2.2.A. Mn doping

A group of researchers studied manganese doped Co_3O_4 thin films by CVD. The obtained patterns are depicted in figure 5. As it can be seen from the figure below ,the diffraction peaks corresponding to (111), (220), (400), (511) and (440) planeswhich are good in agreement with Co_3O_4 cubic spinel structure. Their slight2θposition shift reveals the incorporation of manganese cations and finally the relatively high intensity of the (311) peak suggests a preferred growth along the [311] direction.The peak shifts towards higher diffraction angles due to the difference in ionic radii of Mn^{2+} (0.67 Å) and Mn^{3+} (0.58 Å) compared to Co^{2+} (0.65 Å) and Co^{3+} (0.61 Å).The replacement of Mn^{3+} ions at the Co sites causes the unit cell to contraction and thereby increases the strain of the deposited films.

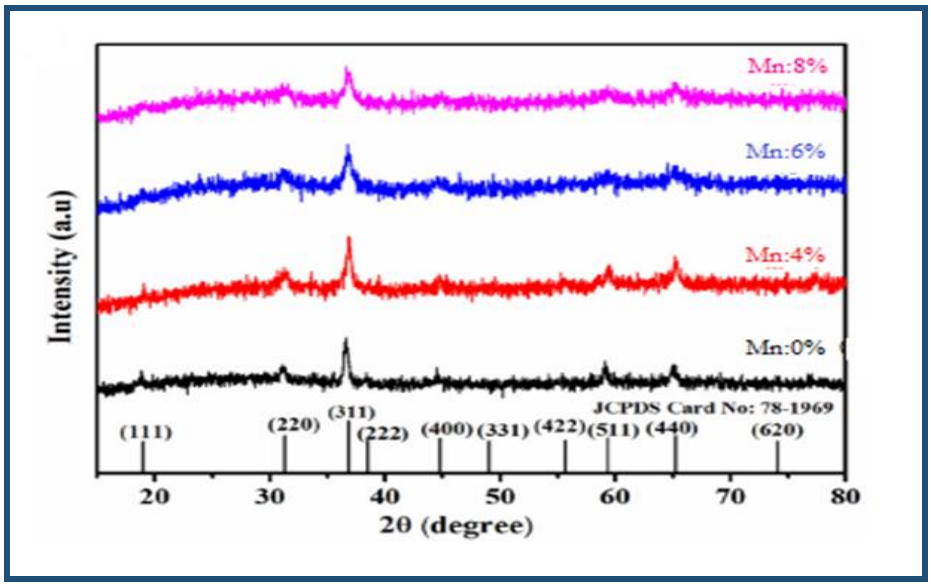

Figure 5: XRD patterns of *Co_3O_4:Mn* thin films is prepared by CVD with different Mn concentration [13].

R. Venkatesha et al. [13] showed that Mn doping affect significantly the surface topography of Co_3O_4 thin films. Indeed, figure 6depicts the SEM top views of Co_3O_4 thin films are deposited at various Mn doping level where pristine Co_3O_4 (Mn 0%) exhibited an agglomerated grain, whereas thin films of Mn-doped Co_3O_4 (MC4% and MC6%) are displayed dendrite shaped structures.

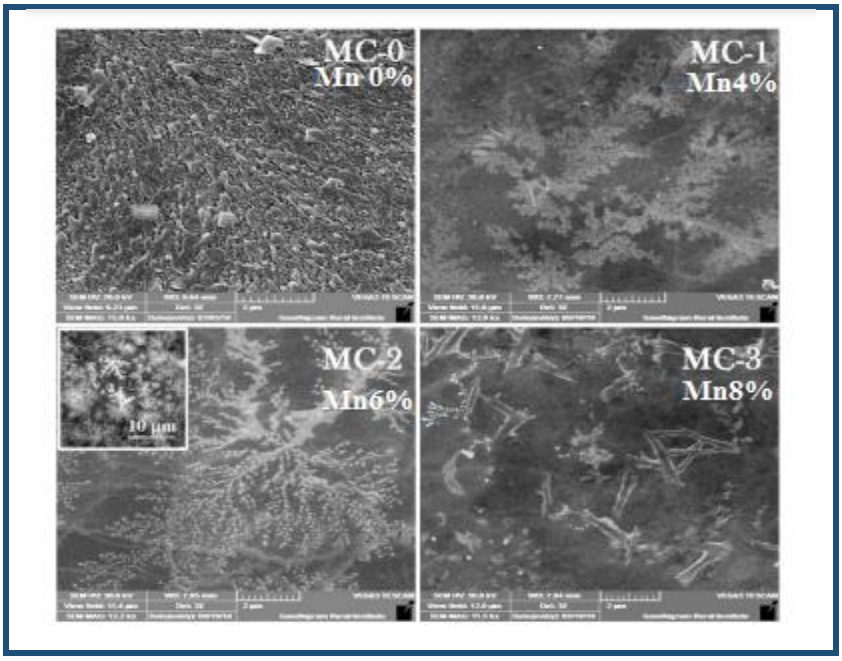

Figure 6: SEM micrographs of pristine and Mn-doped Co_3O_4 thin films[13].

I.2.2.B. Cr doping

Several groups studied the effect of Cr doping on the structural properties of Co_3O_4 thin films. Among them, C. Ravi Dhaset al. [14] prepared Co_3O_4:Cr thin films using by spray technique. figure 7 displays the XRD patterns of Co_3O_4:Cr thin films for different doping percent atomic.

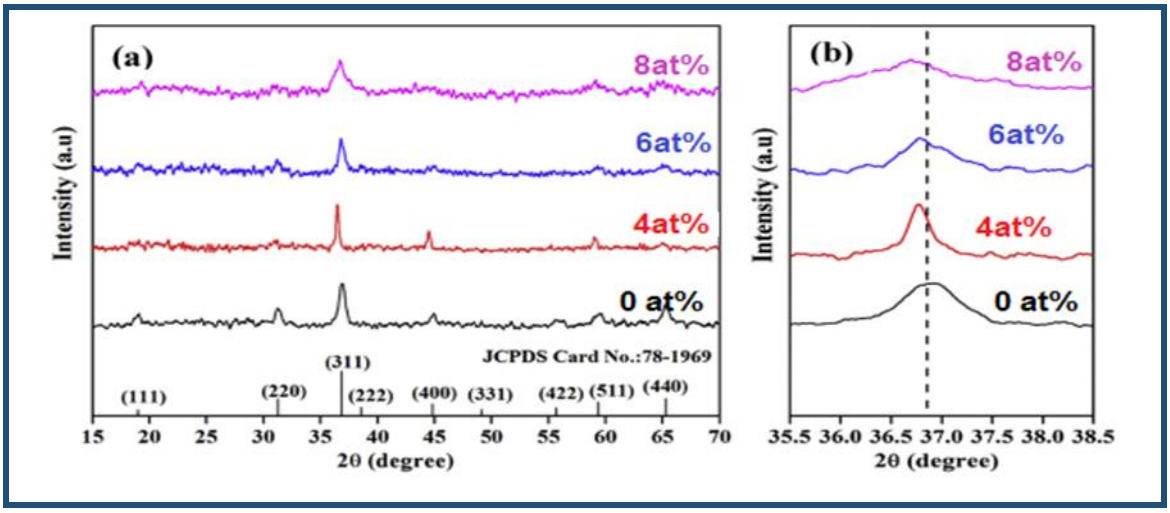

Figure 7:(a) XRD patterns of *Co_3O_4:Cr* thin films are prepared by Spray with different Cr percent atomic and (b) magnified version of (311) plane [14].

The characteristic (111), (220), (311), (400) and (511) diffraction lines of the cubic spinel Co_3O_4 structure are observed. The relatively high intensity of [311] line suggests a preferred orientation growth for the produced thin films along the corresponding crystallographic direction. The formation of nanocrystallites are revealed by the broadening of diffraction peaks. This difference in ionic radius of Cr and Co causes a lattice disorder leads to the increase in expansion of unit cell volume for Cr doped Co_3O_4 films.The same observation is made by Larbi et al. [15]for spray deposited Cs doped Cr_2O_3 thin films.

C. Ravi Dhaset al.[14] show that Cr doping affect significantly the surface topography of Co_3O_4 films. The morphological arrangement is converted from petal-shaped granules homogeneously distributed on the film surface to needle-shaped grains irregularly distributed on the surface of the film. Appearance of clusters consisting of spherical flower-like granules arranged uniformly and as observed a rough pattern, heterogeneous, lumpy film pattern(see figure8).The spherical

flower morphology with small pores deliver larger surface area and might create a good contact between film surface and electrolyte for efficient charge insertion and extraction in electrochromic devices. A similar type of morphological anisotropy is observed for the spray-deposited MoO_3 films with incorporation Ti as dopant to S. Mahajan et al [16].

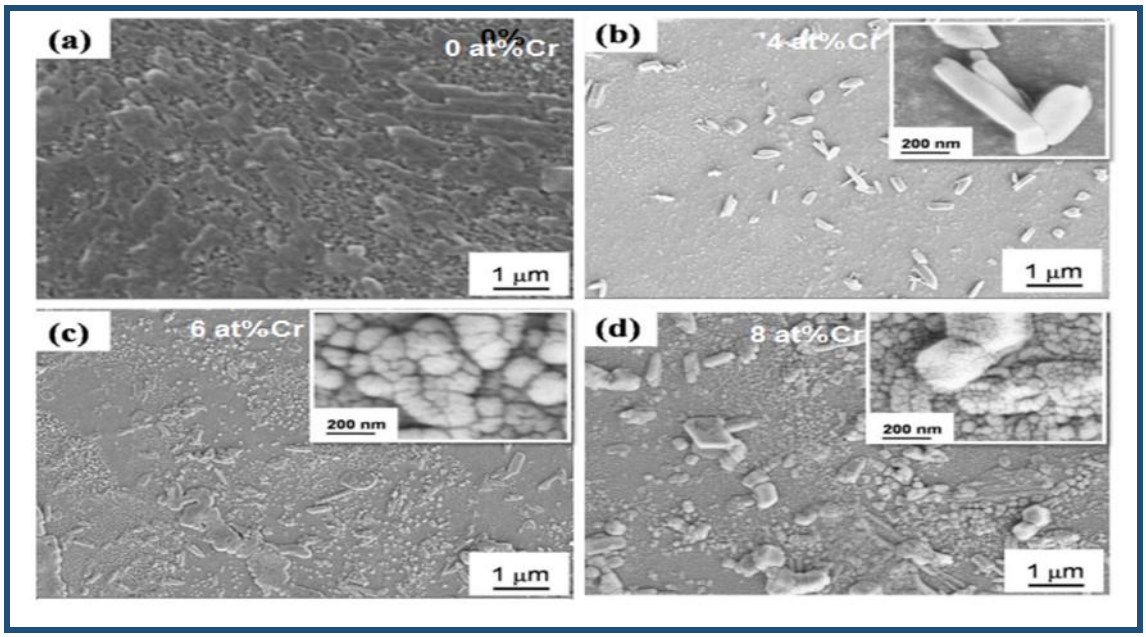

Figure 8.SEM images for pristine and Cr-doped Co_3O_4 thin films [14].

I.2.2.C. Gd doping

Mohd Shkir et al [17] studied a comprehensive on structure, opto-nonlinear and photoluminescence properties of doping Co_3O_4:Gd thin films. The XRD patterns, shown in figure 9, presents of Co_3O_4 films on glass substrates with 0.0, 1.0, 3.0 and 5.0 wt% Gd doping concentrations. XRD results suggest the growth of films with Co_3O_4 pure phase with clear peaks at 2θ angle~19.00◦, 31.36◦, 36.99◦, 59.38◦, 65.12◦ along (111), (220), (311), (511) and (440) diffraction plane, respectively. Gd doping in Co_3O_4 were shows noticeable effect on the structural properties of the prepared thin films. The incorporation of the Gd^{3+} doping element into the Co_3O_4 matrix deteriorated the crystalline quality of the thin films as can be seen from the XRD patterns. The presence of dislocations such as vacancies, interstitials, and substitutional in samples are responsible to occur in the lattice of the crystal structure.

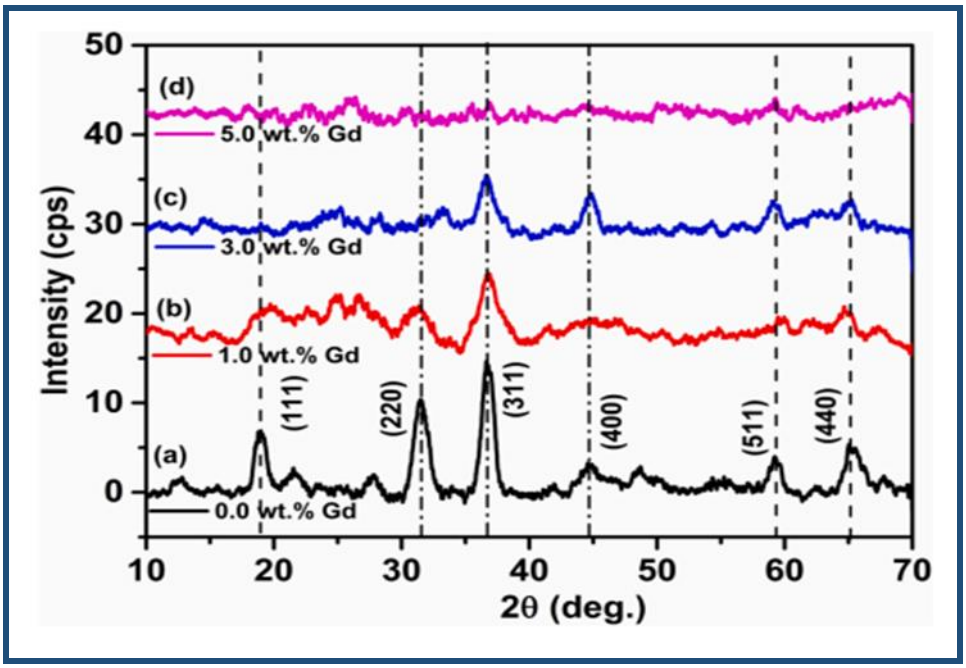

Figure 9:XRD patterns of *Co_3O_4:Gd*thin films are prepared by spray [17].

Raman spectroscopy is undertaken to explore spectroscopic properties of Gd:Co3O4 films. The recorded profiles on all the produced thin films are given hereafter. Figure 10 shows the peaks that are located at 190,262,477,518,682.18 and 1247.70 cm− 1, respectively [18,19]. These results are determined to the Co3O4 tetrahedral sites and to Co–O bond in octahedral sites in agreements with the previous results [20,21]. The change in the intensity of the Raman spectra of the prepared thin firms is due to the existence of lattice strain in the crystal structure. It is due to the existence of more values of dislocation density, thereby the crystal quality of the films decreases with increasing Gd contests.

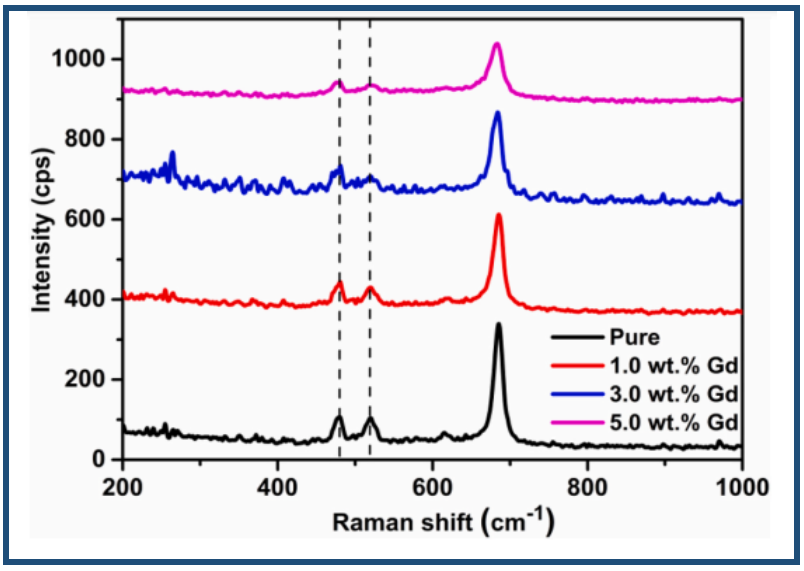

Figure 10: FT-Raman profiles for*Co_3O_4:Gd* thin films are prepared by spray [17].

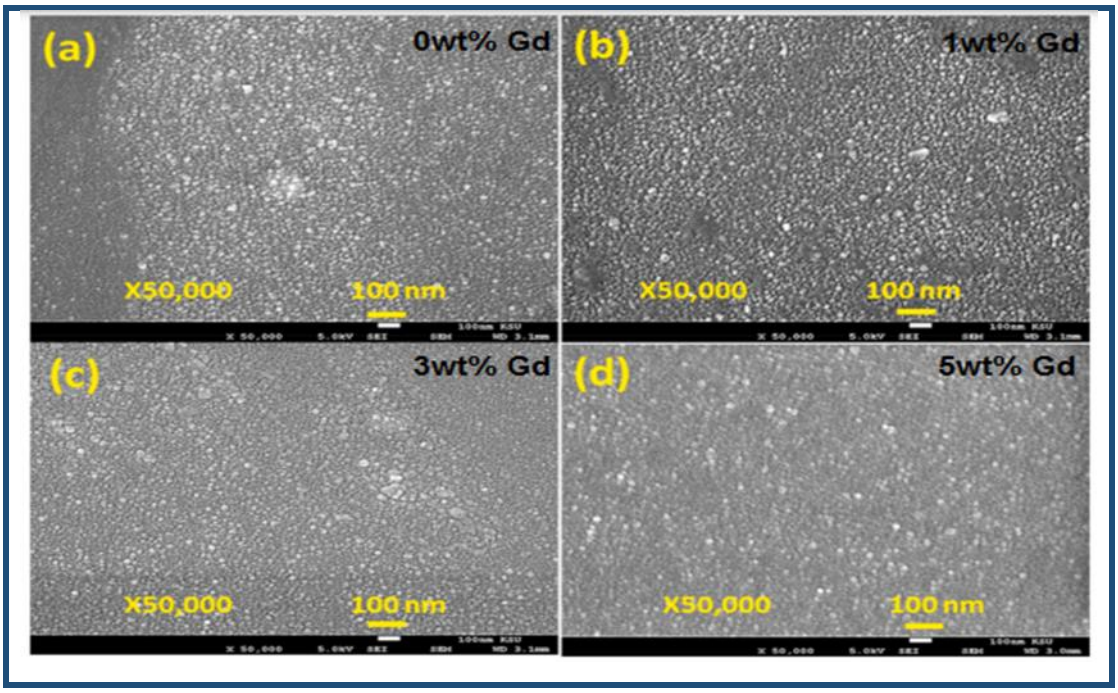

Figure 11. FESEM images for pristine and Gd-doped Co_3O_4 thin films [17].

Mohd Shkir et al [17] showed that Gd doping does not affect significantly the surface topography of Co_3O_4 thin films. Indeed, figure 11 depicts the FESEM top views of Co_3O_4 thin films deposited at various Gd doping level. FESEM micrographs show the compact morphology

of round shapes with nanometer size. It is also observed that all nanoparticles were uniformly distributed throughout the substrates.

I.2.2.D. Nd doping

The study of influence of Neodymium doping is also investigated. In this context, Mohd Shkir et al. [22] elaborated cobalt oxide (Co_3O_4) thin films at 400 ◦C substrate temperature by CVD method. The XRD patterns of the deposited films are displayed in figure12.

The collected XRD patterns match very well with the cubic Co_3O_4 structure with the patterns of pure and Nd doped Co_3O_4 films. The presence of Nd doping in Co_3O_4 show noticeable effect on the structural properties of the prepared thin films. For this the increase of the lattice constants (a) values are increasing with rising of the Nd content. These results are also observed by Ravi Dhas et al. in Cr doped Co3O4 [14] and Mohd Shkir et al. in Gd doped Co3O4 [17].

Shkir et al. [22] collected the FT-Raman profiles for Co_3O_4:Nd thin films prepared by spray, for different Nd concentration. The obtained spectra are given in figure 13. From this figure, it is clearly visible from vibrational profile that the intensity of Raman peaks and FWHM of Co3O4 is increasing with Nd doping content which indicates the reduction in grain size. It was in accordance with XRD outcomes. There are four positions major Raman modes situated at 479, 518, 615 and 686 cm^{-1} which are assigned to E_g, F_{2g} (2) and F_{2g} (1) and A_{1g}, correspondingly. They indicate, the doping of Nd in Co_3O_4 consequences to generate tensile stress that not only producing the shift of Raman peaks towards lower wavenumber but also waned the crystallinity of the grown films.

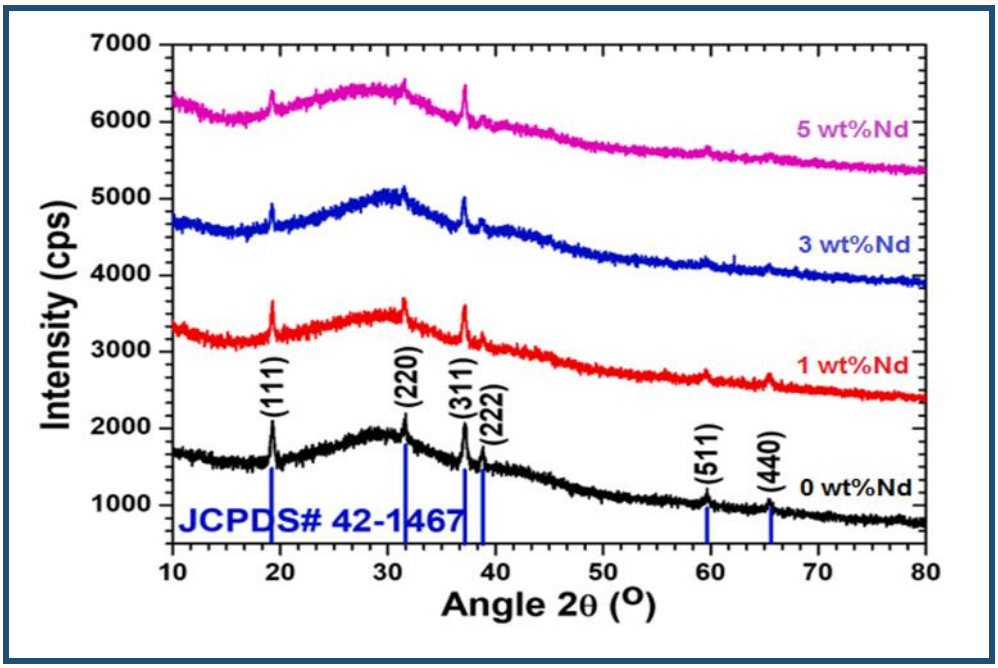

Figure 12:XRD patterns of *Co_3O_4:Nd* thin films are prepared by spray [22].

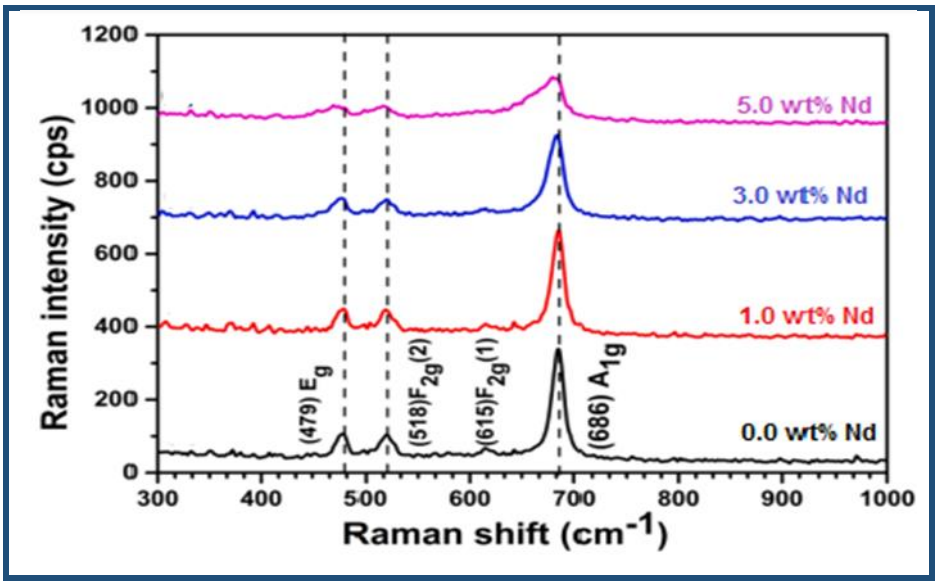

Figure 13:FT-Raman profiles for *Co_3O_4:Nd* thin films are prepared by spray [22].

The authors studied also the surface morphology and grain size of the prepared Co_3O_4 thin films. They reported for the thin films a closely packed with spherical shape and no void/pinhole/crack

is observed and no morphological change has observed with Nd doping, as displayed in figure 14. By introducing increasing amounts of Neodymium, the grains size is reducing in Co_3O_4films, in agreements with of results Fareed et al in Gd doped Co_3O_4 [23]. Also Švegl et al. reported the spherical shape grains formation in Li:Co_3O_4 films are deposited via dip-coating process [24].

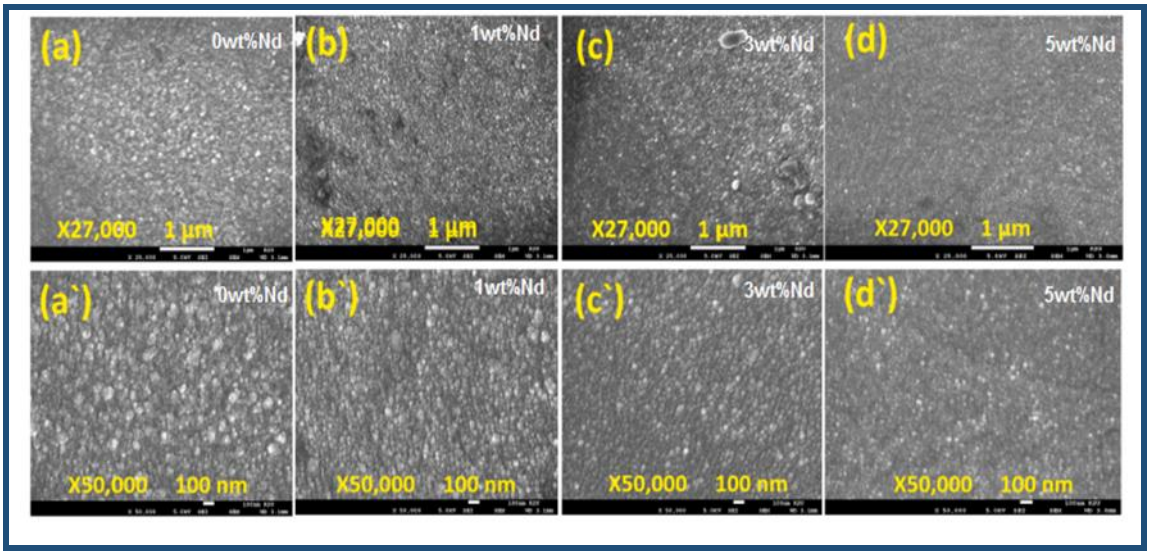

Figure 14. FESEM images for pristine and Nd-doped Co_3O_4nanostructured thin films [22].

The authors also performed Scanning Probe Microscope (SPM) analysis on all developed films as displayed in figure 15. From these SPM images they discovered that the grain size in the developed films is very low, which this is in agreement with the XRD and FESEM analysis. They have estimated the root mean square (RMS) roughness (Rq) as ~ 10.45, 13.41, 48.48, and 44.47 nm with means/average roughness (Ra) values of 6.71, 15.79, 29.86, and 33.70 nm for Co3O4 films doped with 0, 1, 3 and 5 wt% of Nd, respectively. From the obtained values of roughness that the films possess low roughness, which means more compact films, they reveal say that the films were achieved with better quality. And to know the statistical properties/info related to surface profile of films, they have studied the skewness (R_{sk}) and kurtosis (R_{ku}) both and these estimated values are provided in table **2**. The R_{sk} and R_{ku} are defining the films surface, if R_{sk} = 0 indicates symmetric hight distribution and if R_{sk} = 3 shows moderately sharp films.The + ve and -ve values of R_{sk} signify high peaks and occupy valley and deep scratches and lack of peaks, respectively. So, when R_{ku} > 3, it is related to high peaks/low valleys and when it is < 3 indicates low peaks/valleys. From this table that the values of Skewness of both films are in

range of 0.96–3.32. This means that the lowest skewness value (0.68) is for the film grown with 0.0 wt% of Nd doping, which proposes higher symmetry compare to other films. These constraints define the symmetrical grains spreading all over the films. Correspondingly, the pure thin film possesses lower kurtosis value compare to other films which signify that the film developed without Nd doping shows high peaks and low valleys compare to other films.

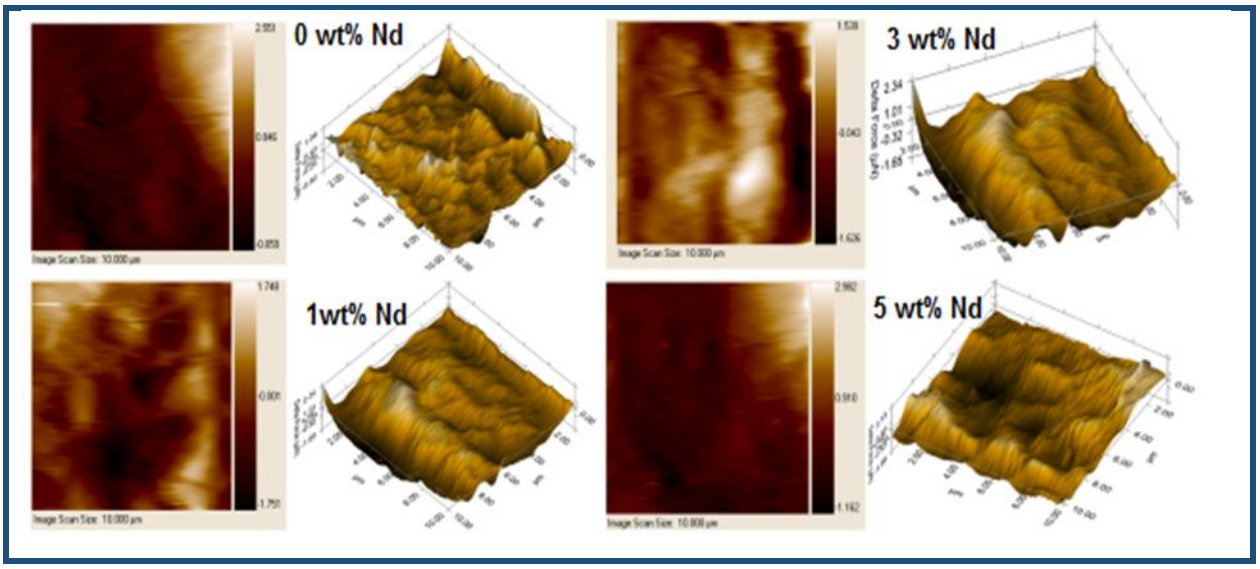

Figure 15. Scanning Probe Microscope (SPM) images for pristine and Nd-doped Co_3O_4 nanostructured thin films [22].

Table. 2: *Scanning Probe Microscope (SPM) results for all developed films*.

Films (Nd: Co3O4)	Grain size and roughness parameters		Shape parameters	
	RMS roughness R_q (nm)	Average roughness R_a (nm)	R_{ku} (Kurtosis)	R_{sk} (Skewness)
0.0 wt% Nd	10.55	6.71	2.61	0.96
1.0 wt% Nd	13.41	15.79	25.07	3.32
3.0 wt% Nd	48.48	29.86	8.94	2.69
5.0 wt% Nd	44.47	33.70	4.02	0.95

I.2.2.E. Sn doping

The study of influence of Tin doping are also investigated. In this context, Hasan Albargiaet al. [25] elaborated cobalt oxide (Co_3O_4) thin films for different doping level including 0, 2, 4, and 6 wt% at 450 ◦C substrate temperature by nebulizer spray pyrolysis (CVD) method. The XRD patterns of the deposited films are displayed in figure16.

The collected XRD patterns match very well with the face-centered cubic Co_3O_4 structure with thepatternsof pure and Sn doped Co_3O_4 films. The presence of Sn doping in Co_3O_4 shows noticeable effect on the structural properties of the prepared thin films.The suppressed intensity affirmed the decreased crystallinity upon the addition of Sn ions. Moreover, the average crystallite size are found to be decreased while increasing Sn doping level. This result suppresses the grain growth of the Sn-doped Co_3O_4 films. In general, the doping oppened up defects [26], and thus, incorporation of Sn into the Co_3O_4 structure confirmed.

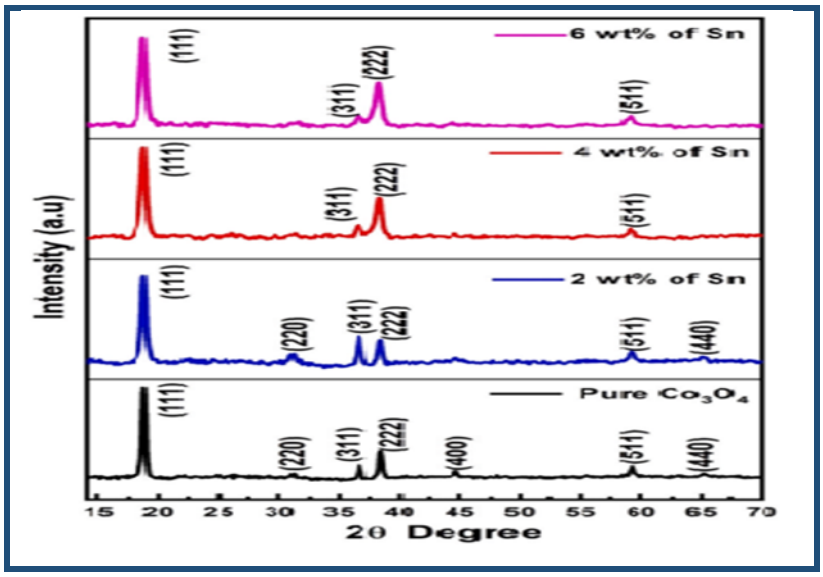

Figure 16:XRD patterns of *Co_3O_4:Sn*thin films are prepared by spray [25].

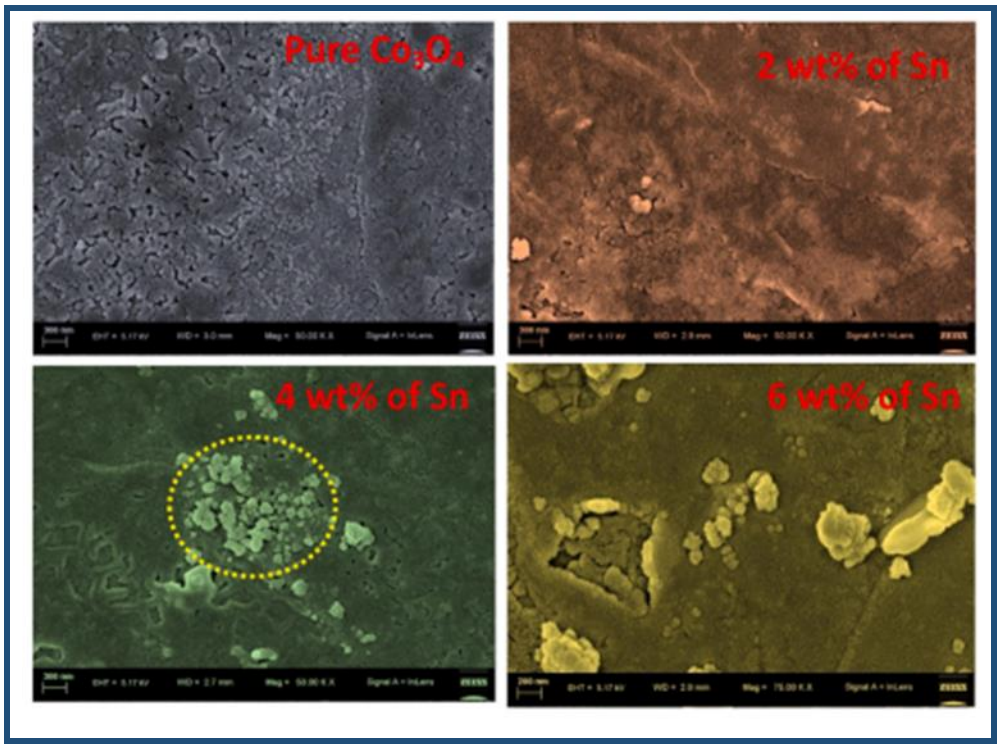

Figure 17. FESEM images for pristine and Sn-doped Co_3O_4 thin films [23].

The authors studied also the surface morphology and grain size of the prepared Co_3O_4 thin films. They reported for the thin films a closely packed with spherical-shaped grains and randomly arranged for all the coated films. They also found that the size of each grain size varies with the Sn doping level(see figure 17). As increase of Sn doping, the size of each grain seems to be suppressed without changing its shapes. Due to doping, some of the bigger grains are developed on the surface of the Co_3O_4 thin films.

Most of the films showed closely packed nanosized crystal grains with lesser grain boundary, which will definitely improve the carrier transport properties of the diode. This is the one of the advantages of Co_3O_4 thin films.

I.3. Optoelectronic properties

I.3.1 Co_3O_4 thin films

Nabila Kouidri et al. [10] studied the effect of temperatures of the substrate on the optical properties of Co_3O_4 thin films were prepared by CVD. They recorded the optical transmittance

spectra of Co3O4 thin films deposited at different temperatures of the substrate as a function of wavelength in the visible and NIR regions they shown in figure 18.

The transmittance values increase with increase as the substrate temperatures increases. This could be explained by a decrease in the mass transported to the heated substrate at elevated temperatures with the increase of the ascending convective flow of the hot air.

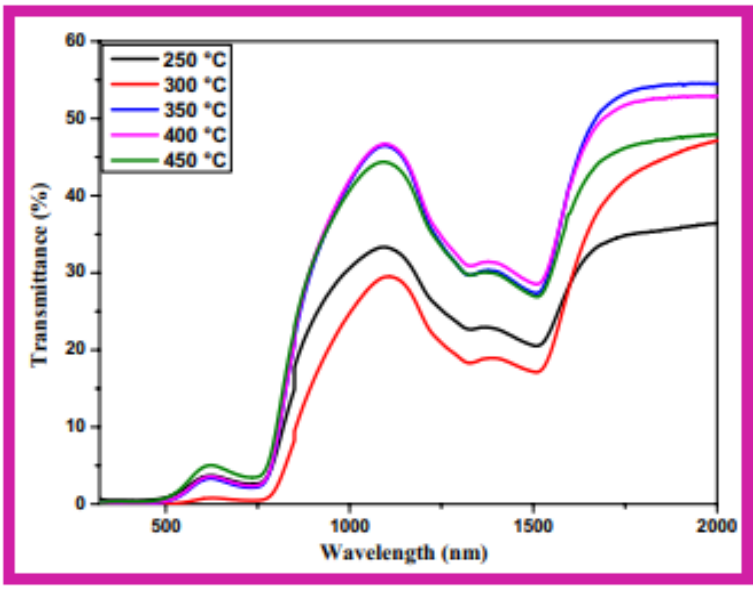

Figure 18: Optical transmittance of Co_3O_4 thin films as a function of substrate temperatures [10].

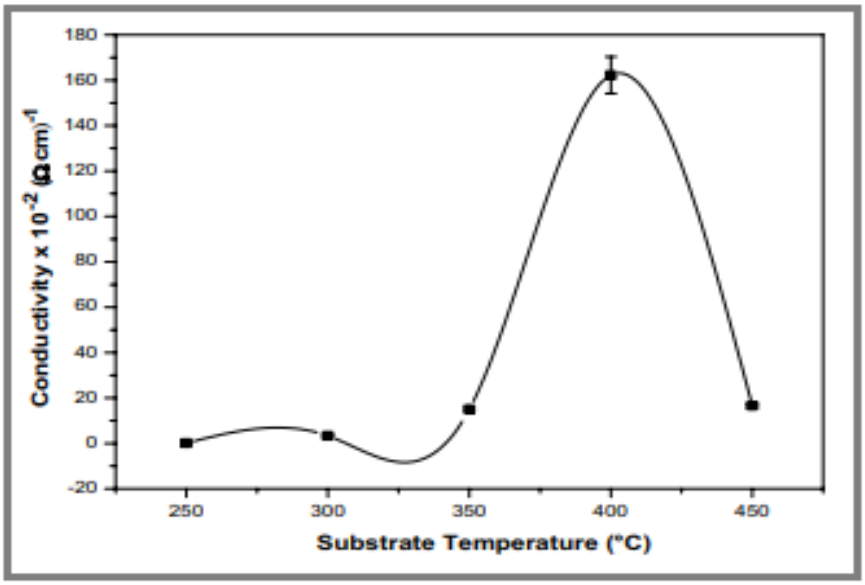

Figure 19: Dependence of electrical conductivity in Co_3O_4 films on substrate temperature[10].

They presented in figure 19 the variation of electrical conductivity as a function of the substrate temperature. They noted that σ increases with increasing substrate temperature up to 400 °C where it decreases.

They traced it back to the fact that stoichiometric Co_3O_4 and its electrical properties depend on the amount for adsorbed oxygen at the surface; Co_3O_4 films adsorb oxygen from air and create surface states, these surface states allow the electron to be excited from the valence band. And as a result, more holes are induced in p-type Co_3O_4 grains.

I.3.2 Doped Co_3O_4 thin films

I.3.2.A. Mn doping

R. Venkatesha et al. [13] studied the effect of Mn doping concentration on the optical properties of Co_3O_4 thin films prepared by CVD. They recorded the optical transmittance of pristine and Mn-doped Co_3O_4 films. The average transmittance values decrease with increase in Mn dopant concentration (see figure 20 (a)). This could be attributed to increasing the scattering centers or defects created upon manganese addition.

Figure 20 (b): The probable reason for this kind of observed variation in band gap energy Eg could be related to the synergistic effect of quantum confinement due to the reduction in the crystallite size, and also the incorporation of Mn atoms alters the bond length between metallic cations (Mn, Co) and O. Both of the above-mentioned phenomena result in poor interaction between the localized orbitals and less overlapping of energy levels.

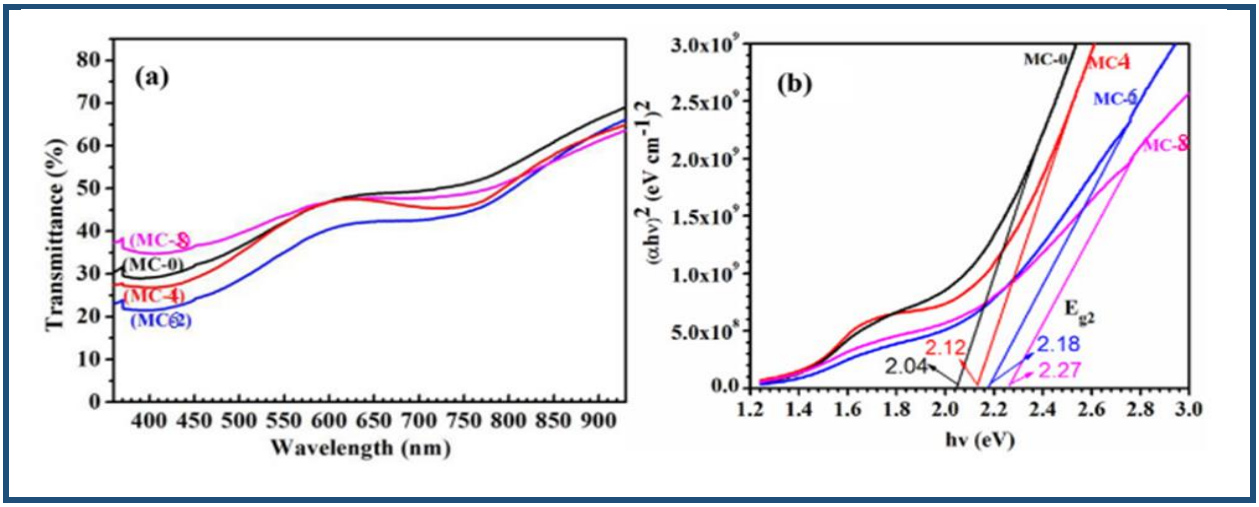

Figure 20: (a) Transmittance spectra and (b) Tauc plot of pristine and Mn-doped Co_3O_4 thin films [13].

From table 2 it can be observed that resistivity of Mn doped Co_3O_4 films decreases with increase in Mn dopant concentration upto 6 at.%. Co_3O_4 compared to pristine Co3O4 film. The partial occupation of mixed valance states Mn^{+2} (3d4) and Mn^{+3}(3d3) at the lattice sites of Co^{+2}(3d7) and Co^{+3}(3d6) in the complex spinel structured cubic Co_3O_4 eventually boosts the hole concentration and thereby enhances the electrical conductivity. The decrement in the sheet resistance is presumably due to the reduction in the number of grain boundaries as the other peaks than the predominant plane (311) which suppresses to a greater extent upon Mn doping. Further increase in Mn concentration to 8 at% leads to a decline of electrical conductivity as the excess Mn content segregates at grain boundaries which in turn contributes to trapping of charge carriers.

Table2 : *Electrical parameters of Co_3O_4 and Mn doping Co_3O_4 thin films [13].*

Sapmle	Sheet resistance R_{sh}(Ω/Sq)	Resistivity $\boldsymbol{\rho}$(Ω/cm)	Activation energy E_a (eV)
Mn 0%	9.1×10^3	2.59	0.52
Mn 4%	3.7×10^3	1.08	0.40
Mn 6%	1.2×10^3	0.34	0.38
Mn 8%	6.2×10^3	1.80	0.43

I.2.2.B. Cr doping

The optical transmission spectra of Cr-doped Co_3O_4 are shown in figure21 (a)[14]. The variation in the transmittance spectra for Cr-doped Co_3O_4 films could be attributed to crystalline quality, morphology and free carrier density in deposited films upon Cr doping. The band gap values are estimated by drawing tangent lines and extrapolating them to the energy axis($\alpha = 0$) (see figure21 (b)). The obtained Eg values of the deposited thin films are found to be 2.1, 2.04, 1.95 and 2.08 eV for 0 at% Cr, 4at% Cr, 6at% Cr and 8 at% Cr thin films respectively. The marginal variation inEg values might be due to formation of impurity energy levels or localized energy states that are created between conduction band and valance band upon Cr doping and also the oxygen vacancies reduces the width of the band results in band shrinkage effect.

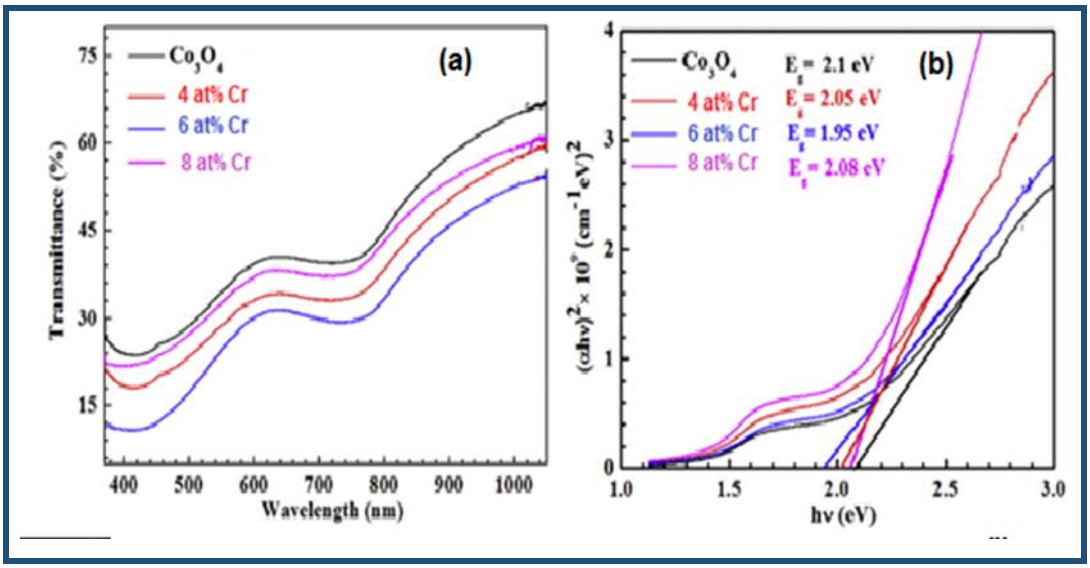

Figure 21: (a) Transmittance spectra and (b) Tauc plot of pristine and Cr-doped Co_3O_4 thin films [14].

Figure 22shows the Arrhenius behavior of the deposited Cr-doped Co3O4 thin films. From the plots, it is observed that all the thin films exhibit semiconducting nature as the resistivity decreased with increase in temperature. The slope which is estimated from the linear fit of the plots is used to determine the activation energy of the thin films using the well-known Arrhenius relation. The obtained activation energy values are given. The variation in activation energy values for Cr-doped Co3O4 thin films could be due to the formation of impurity energy levels between conduction and valence band upon Cr incorporation.

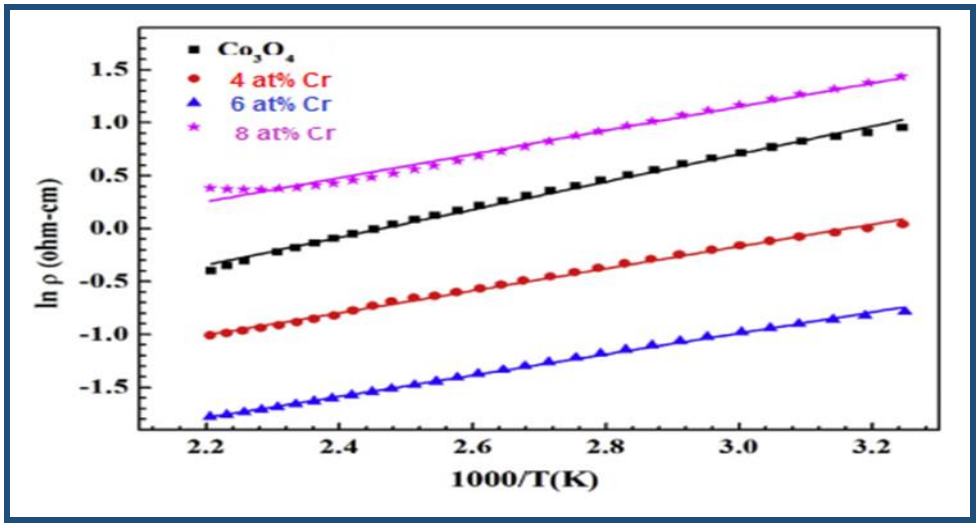

Figure 22: Arrhenius plot (ln r vs. 1000/T(K)) of Co_3O_4 and Cr-doped Co_3O_4 films [14].

The observed values are abridged in table 3. The sheet resistance and resistivity values decidedly are decreased with an increase in Cr dopant concentration, except for the film which contains 8 at% of Cr. This could be explained by the fact that preferential orientation of (311) plane and suppression of other planes due to Cr addition as witnessed from XRD results minimizes the carrier scattering mechanism at grain boundaries. Additionally, the formation of oxygen defects and reduction of chemisorbed oxygen species for 6 at% Cr thin film at the surface sites upon Cr promoted the electrical conductivity. T.P. Rao et al. [27] they confirmed that chemically absorbed oxygen is responsible for the formation of trapping states capable of immobilizing charge carriers. The large electrical resistivity is observed for 8at% Cr thin film may be attributed to the formation of Cr interstitials and poor crystalline nature observed from XRD leads to scattering of charge carriers.

Table3: *Electrical parameters of Co_3O_4 and Cr doping Co_3O_4 thin films [14].*

Sapmles	**Sheet resistance R_{sh}(kΩ/Sq)**	**Resistivity ρ(Ω/cm)**	**Activation energy E_a (eV)**
Crat 0%	9.1	2.59	0.52
Cr at 4%	5.2	1.10	0.42
Crat 6%	2.2	0.47	0.38
Crat 8%	21.2	4.51	0.44

I.2.2.C. Gd doping

Mohd Shkir et al [17] plotted the wavelength,λ, dependences of the absorbance, transmittance and reflectance (figure 23 (a), (b)and (c)) for pure and Gd doped Co_3O_4 thin films show, exclusively are prepared by spray method. They reveal that a noticeable impact of Gd doping on the absorption behavior of films and that most of the transmittance the films increase with Gd content and is found 25% in the visible region. The deposited thin films have low reflectance about 13–20% in visible region compared to the NIR region.

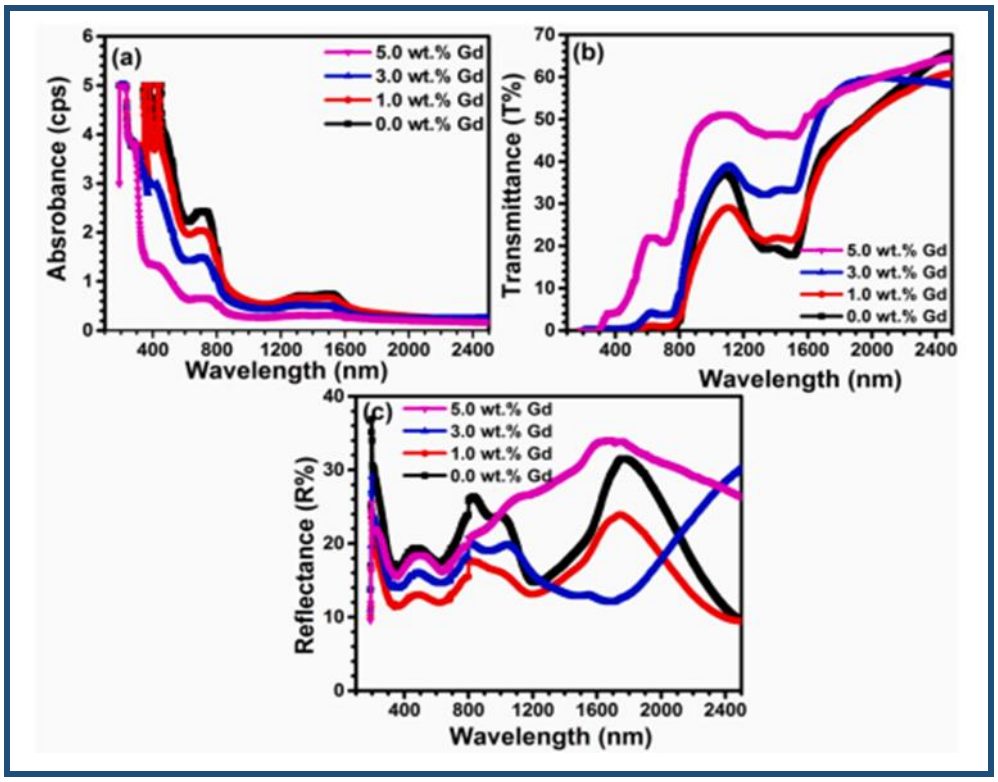

Figure23: (a) Absorbance (b) Transmittance (T%) (c) Reflectance (R%) spectra of pure and Gd doped Co_3O_4 thin films [17].

Mohd Shkir et al [17] studied the effect of gadolinium doping concentration on the band gap energy of Co_3O_4 thin films are elaborated by spray method. Tauc's graphs of films with different Gd concentrations are presented in figure 24. Obviously, two direct Eg can be seen from the previous figure, which are presented in Table 4.A remarkable effect of Gd doping on the band gap of Co_3O_4 films is observed, first band gap reduces slightly, and second band gap enlarged with the rise in Gd contents, in agreements with previous results[28-29].

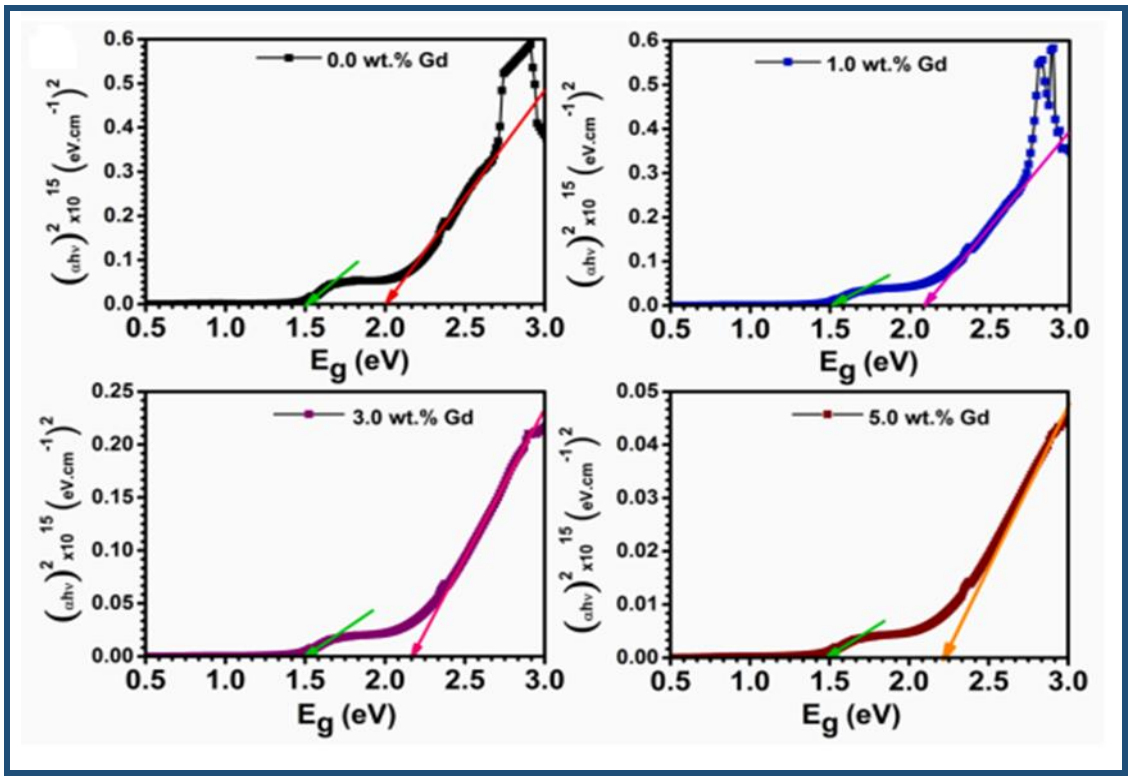

Figure 24: Tauc's plots $(\alpha h\nu)^2$ vs Eg of pristine and Gd-doped Co_3O_4 thin films prepared by spray method [17].

Table4: *Optical band gap of films with different Gd doping concentrations in the Co3O4 thin films.*

Sapmles	Eg1 (eV)	Eg2 (eV)
0.0 wt% Gd@Co3O4	1.52	2.01
1.0 wt% Gd@Co3O4	1.53	2.10
3.0 wt% Gd@Co3O4	1.49	2.09
5.0 wt% Gd@Co3O4	1.49	2.58

Mohd Shkir et al [17] plotted the wavelength (λ) dependences of the extinction coefficient (k) as well as the refractive index (n) (Figure 25 (a) and (b)) of Gd:Co3O4 thin films show, exclusively prepared by spray method. The values of absorption index were found [0.063–0.23] in range of electromagnetic spectrum [190–2500] nm.Refractive indices of thin films are obtained in range [1.87–3.81] for all compositions. They observed that the effect of Gd doping on refractive index of thin films can be seen clearly from Figure (b). They also noticed that the refractive index of

films reducing with easing the Gd concentrations in visible region whereas 5.0 wt% doped films shows significant enhancement in 1200–2400 nm.

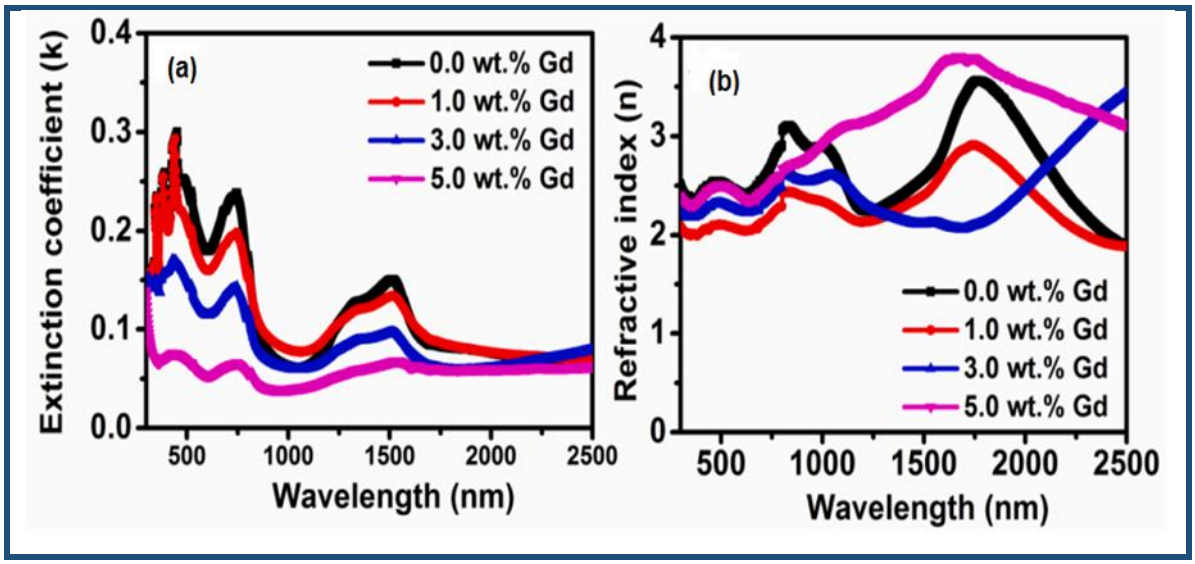

Figure 25: Tauc'splots (a) extinction coefficient (k) and (b) refractive index (n)of pristine and Gd -doped Co_3O_4 thin films prepared by spray method [17].

The authors reported also the variation of the real (ε_1) and the imaginary part (ε_2) of the complex dielectric constant of all Gd: Co_3O_4 thin films respectively (Figure 26). They observed that the values of ε_1 are found to be 4.24–14.4 eV in visible region. The spectra of ε_1 is reflects the absorption edge characteristics of films, from spectra of ε_1, two clear band edge can be seen. From their tip are obtained the values of imaginary part of dielectric constant ε_2 were obtained in range of 0.33–1.21.

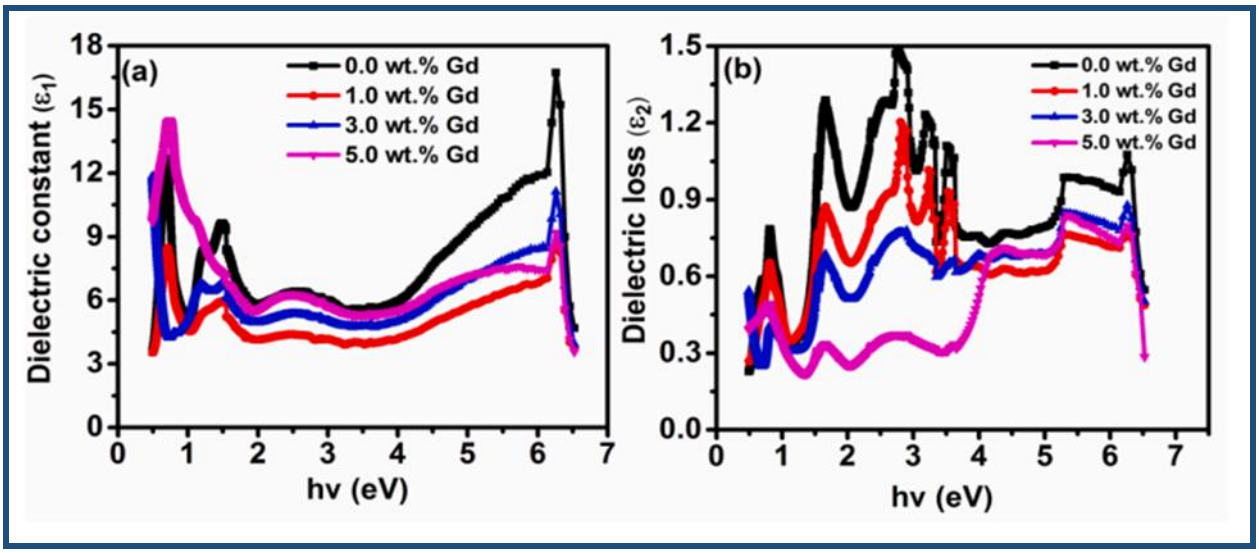

Figure 26: Dielectric constant (a), and dielectric loss (b) of pure and Gd doped Co3O4 thin films.

I.2.2.D. Nd doping

Mohd. Shkir et al [22] studied the effect of Neodymium doping concentration on the optical properties of Co_3O_4 thin films are elaborated by spray method. They recorded that the optical absorbance spectra of all the produced thin films and noticed that the high absorption peak was shown in case of 5% Nd doped in Co_3O_4 film which is due to the high thickness or roughness of the film (see figure 27(a)). They also reported the transmittance spectra (Figure 27 (b)) of Nd doped Co3O4 thin films are depicted increased transmittance in the visible region while as reflectance spectra (Figure 27(c)) shows a decreasing trend upon Nd doping which they attribute for the sensitivity of the films towards roughness or thickness of the film, and the occurrence of coloring as a result of the decrease in the intensity of reflection when the concentration of the dopant increases.

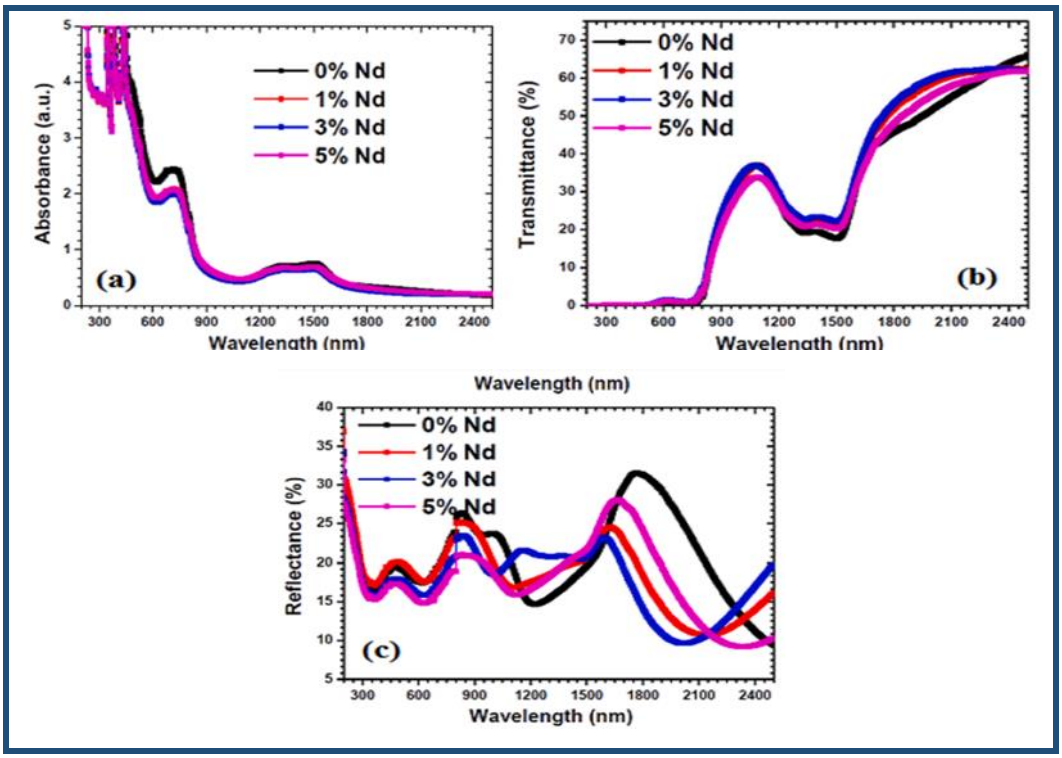

Figure 27:(a) Absorbance (b) Transmittance (T%) (c) Reflectance (R%) spectra for pure and Nd doped Co3O4 thin films[22].

Mohd. Shkir et al [22] extrapolated of the photon energy (h v) on the x-axis versus linear region of a plot of the graph of (αh v) 2 on the y-axis for Nd:Co_3O_4 films as it is illustrated in figure 28. They observed that the range of optical bans gaps 2.03–2.15 eV and 1.49–1.55 eV respectively and noticed an increase of the optical bans gap when the Nd concentration in increases. The authors explained the enhancement trend in the optical band gap by the effect of introduction of Nd doping which cause a distortion of network within Co_3O_4 matrix and forming an impurity energy levels (acceptor level) within the band gap [30] or due to degeneracy of the valence band (VB) [31].

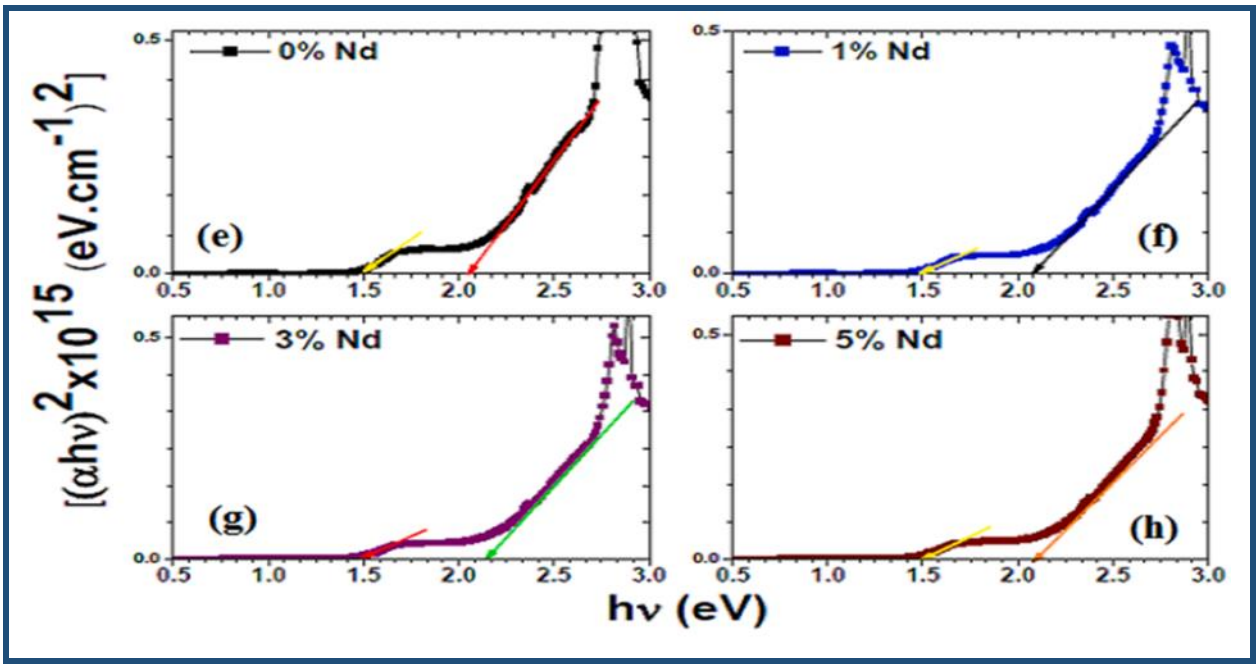

Figure 28: (e, f, g, h) Individual Tauc's plots for direct band gap of pure and Nd doped Co3O4 thin films [22].

I.4. Conclusion

To conclude, cobalt oxide thin films and their Mn, Cr, Gd, Nd and Sn doped counterparts attract a great interest in material science owing to its wide range of technological applications as well as its interesting physical properties. They can be easily produced by different techniques, the CVD route appearing as an easy - to achieve one and as an efficient one to produce pure and crystallized phases. Focusing on this growing thin film method, the obtained films are crystallized in the spinel cubic structure. In all the cases, they evidenced a uniform surface with a granular morphology. Doping did not seem to affect significantly their structure neither their microstructure.

So, we specifically use this technique to produce several Co3O4 and Co3O4:N (N = Mn, Cr, Gd, Nd and Sn) thin films , fixing the deposition conditions . The next chapter will be on the description of these elaboration conditions and summarizes the different characterization techniques used to analyze the prepared films along this work.

References

[1] Raphael M. Obodo, Ugochi Chime, Agnes C. Nkele, Assumpta .Nwanya, A.K.H Bashir, I.G. Madiba, M. Asjad , I. Ahmad, T. Zhao, N. Thovhogi, Fabian I. Ezema, Effect of annealing on hydrothermally deposited Co3O4-ZnO thin films for supercapacitor applications, Materials Today: Proceedings.36 (2021) 374-378.

[2] Assumpta C Nwanya, Daniel Obi, Rose U. Osuji, R. Bucher, Malik Maaza, Fabian I. Ezema, Simple chemical route for nanorod-like cobalt oxide films for electrochemical energy storage applications, J Solid State Electrochem (2017) 21:2567–2576.

[3] R.Perekrestov, A.Spesyvyi, J.Maixner, K.Mašek, O.Leiko, I.Khalakhan, J.Maňák, P.Kšírová, Z.Hubička, M.Čada, The comparative study of electrical, optical and catalytic properties of Co_3O_4 thin nanocrystalline films prepared by reactive high-power impulse and radio frequency magnetron sputtering, Thin Solid Films, 686 (2019) 137427.

[4] O.Kilo, J.Jabbour, R.Habchi, N.Abboud, M.Brouche, A.Khoury, D.Zaouk, Electrospray deposition and characterization of cobalt oxide thin films, Materials Science in Semiconductor Processing, 24(2014)57-61.

[5] P. Shia, R. Sua, S. Zhua, M. Zhua, D. Li, S. Xu.Supported cobalt oxide on graphene oxide: Highly efficient catalysts for the removal of Orange II from water.Journal of Hazardous Materials.229–230 (2012) 331-339.

[6] S.G. Kandalkar, J.L. Gunjakar, C.D. Lokhande, Preparation of cobalt oxide thin films and its use in supercapacitor application. Applied Surface Science. 254 (2008) 5540–5544.

[7] AbdelhakLakehal, BedhiafBenrabah, AmarBouaza, CherifaDalache, BenhebalHadj. Tuning of the physical properties by various transition metal doping in Co_3O_4: TM (TM = Ni, Mn, Cu) thin films: A comparative study. Chinese Journal of Physics. 56 (2018) 1845-1852.

[8] L. Yao, Y. Xi, G. Xi, Y. Recycling and synthesis of LiNi 1/3 Co 1/3 Mn 1/3 O 2 from waste lithium-ion batteries using d, l-malic acid. Feng, J. Alloys.Compd. 680 (2016) 73-79.

[9] A.B. Vennela, D. Mangalaraj, N. Muthukumarasamy, S. Agilan, K.V. Hemalatha. Structural and Optical Properties of Co3O4 Nanoparticles Prepared by Sol-gel Technique for Photocatalytic Application. International Journal of Electrochemical science. 14 (2019) 3535 – 3552.

[10] Nabila Kouidri ·Saâd Rahmane · Abdelkrim Allag, Substrate temperature-dependent properties of sprayed cobalt oxide thin films, Journal of Materials Science: Materials in Electronics 30, (2019) 1153–1160.

[11] Jia Chen, Xifan Wu, AnnabellaSelloni. Electronic structure and bonding properties of cobalt oxide in the spinel structure. PHYSICAL REVIEW B 83, 245204 (2011) 1-7.

[12] C. Ravi Dhas, R. Venkatesh, R. Sivakumar, A. Moses Ezhil Raj, C. Sanjeeviraja. Effect of solution molarity on optical dispersion energy parameters and electrochromic performance of Co3O4 films. Journal of Optical Materials 72 (2017) 717-729.

[13] R. Venkatesha, C. Ravi Dhasa, R. Sivakumarb, T. Dhandayuthapanib, P. Sudhagarc , C. Sanjeevirajad , A. Moses EzhilRaje. Analysis of optical dispersion parameters and electrochromic properties of manganese-doped Co3O4 dendrite structured thin films. Journal of Physics and Chemistry of Solids 122 (2018) 118–129.

[14] C. Ravi Dhas, R. Venkatesh, R. Sivakumar, T. Dhandayuthapani, B. Subramanian, C. Sanjeeviraja, A. Moses Ezhil Raj. Electrochromic performance of chromium-doped Co3O4 nanocrystalline thin films prepared by nebulizer spray technique. Journal of Alloys and Compounds 784 (2019) 49-59.

[15] T. Larbi, M. Amara, B. Ouni, M. Amlouk.Enhanced photocatalytic degradation of methylene blue dye under UV-sunlight irradiation by cesium doped chromium oxide thin films.Materials Research Bulletin. 95 (2017) 152-162.

[16] S. Mahajan, S. Mujawar, P. Shinde, A. Inamdar, P. Patil. Structural, morphological, optical and electrochromic properties of Ti-doped MoO_3 thin films. Solar Energy Materials and Solar Cells
93 (2009) 183-187.

[17] MohdShkir, Z.R. Khan, Aslam Khan, Kamlesh V. Chandekar, M.A. Sayed, S. AlFaify. A comprehensive study on structure, opto-nonlinear and photoluminescence properties of Co3O4 nanostructured thin films: An effect of Gd doping concentrations. Journal of Ceramics International (2022).

[18] A.R. Ansari, S. Hussain, M. Imran, M. Sh Abdel-wahab, A. Alshahrie. Synthesis, characterization and oxidation of metallic cobalt (Co) thin film into semiconducting cobalt oxide (Co_3O_4) thin film using microwave plasma CVD. Materials Research Express 5 (2018) 065003.

[19] V.G. Hadjiev, M.N. Iliev, I.V. Vergilov, The Raman spectra of Co3O4.Journal of Physics C: Solid State Physics. 21 (1988) L199.

[20] J. Jiang, L. Li. Synthesis of sphere-like Co3O4 nanocrystals via a simple polyol route.Materials Letters 61 (2007) 4894–4896.

[21] T. Yu, Y. Zhu, X. Xu, Z. Shen, P. Chen, C.-T. Lim, J.T.-L. Thong, C.-H. Sow, Controlled growth and field-emission properties of cobalt oxide nanowalls. Advanced Materials 17 (2005) 1595.

[22] Mohd. Shkir, Aslam Khan, Mohd Imran, M. Ajmal Khan, Rayees Ahmad Zargarf, ThamraaAlshahrani g, K. Deva Arun Kumar, P. Mohanraji, Kamlesh V. Chandekarj , S. AlFaify. Spray pyrolysis developed Nd doped Co3O4 nanostructured thin films and their structural, and opto-nonlinear properties for optoelectronics applications. Optics and Laser Technology 150 (2022) 107959.

[23] S. Fareed, R. Medwal, J.V. Vas, I.A. Khan, R.S. Rawat, M.A. Rafiq, Tailoring oxygen sensing characteristics of Co3O4 nanostructures through Gd doping, Ceramics International. 46 (7) (2020) 9498–9506.
[24] F. Švegl, B. Orel, I. Grabec-Švegl, V. Kaučič, Characterization of spinel Co3O4 and Li-doped Co3O4 thin film electrocatalysts prepared by the sol–gel route, Electrochim. Acta 45 (2000) 4359–4371.
[25] Hasan Albargia, R. Marnaduc, G. Sujithkumard , Ali S. Alkorbie , Hassan Algadib,f , Mohd. Shkirg , Ahmad Umarb,h , GediSreedevii, Deposition of nanostructured Sn doped Co3O4 films by a facile nebulizer spray pyrolysis method and fabrication of p-Sn doped Co3O4/n-Si junction diodes for opto-nanoelectronics. Sensors and Actuators: A. Physical 332 (2021) 113067.
[26] Mahabubur Chowdhury, Carelle Ossinga, Franscious Cummings, Jessica Chamier, and Mesfin Kebede, Novel Sn Doped Co3O4 Thin Film for Nonenzymatic Glucose Bio-Sensor and Fuel Cell, Electroanalysis vol. 29, (2017) 1–12.
[27] T.P. Rao, M.S. Kumar, N.S. Hussain. Effects of thickness and atmospheric annealing on structural, electrical and optical properties of GZO thin films by spray pyrolysis.Journal of Alloys and Compounds. 541 (2012) 495-504.
[28] T.A. Hameed Abbas, L.H. Slewa, H.A. Khizir, S.A. Kakil. Synthesis of cobalt oxide (Co3O4) thin films by electrostatic spray pyrolysis technique (ESP), J. Mater. Sci. Mater. Electron. 28 (2017) 1951–1957.
[29] D. Barreca, C. Massignan, S. Daolio, M. Fabrizio, C. Piccirillo, L. Armelao, E. Tondello, Composition and microstructure of cobalt oxide thin films obtained from a novel cobalt (II) precursor by chemical vapor deposition, Chem. Mater. 13 (2) (2001) 588–593.
[30] A. Lakehal, B. Bedhiaf, A. Bouaza, B. Hadj, A. Ammari, C. Dalache, Structural, optical and electrical properties of Ni-doped Co3O4 prepared via Sol-Gel technique, Mater. Res. 21 (3) (2018).
[31] R. Vijaya Kumar, Y. Diamant, A. Gedanken, Sonochemical synthesis of amorphous Cu and nanocrystalline Cu2O embedded in a polyaniline matrix, Chem. Mater. 12 (2000) 2301

CHAPTER TWO

Elaboration and Characterizations Techniques

In this chapter particular attention is paid to describe the Co3O4:N (N= Mn, La, Sn and Zn) thin films elaboration technique "spray pneumatic deposition" as well as the deposition process. The different characterization technique used such as X-ray diffraction, UV-Vis spectroscopy, atomic force microscopy (AFM) the three-dimensional (3D), energy dispersive spectroscopy (EDS), and four points probe measurements are briefly described.

I. Description of the elaboration techniques and the deposition process

Generally, any thin film deposition follows the sequential steps: a source material is converted into the vapor form (atomic/molecular/ionic species) from the condensed phase (solid or liquid), which is transported to the substrate and then it is allowed to condense on the substrate surface to form the solid film [1]. Depending on how the atoms/molecules/ions/clusters of species are created for the condensation process, the deposition techniques are broadly classified into two categories: physical methods and chemical methods [2].

The properties of thin films are extremely sensitive to the method of preparation, several techniques have been developed (Depending on the desired film properties) for the deposition of the thin films of the metals,alloys,ceramic,polymer and superconductors on a variety of the substrate materials.Each methods has it's own merits & demerits and of course no one technique can deposit the thin films covering all the desired aspects such as cost ofequipments, deposition conditions and nature of the substrate material etc.

I.1. Glass slides activation

For the deposition of the Co_3O_4 thin films, we use ordinary glass slides. Thus, to activate the glass surface we make the following steps: firstly using a pen with diamond to cut the substrates, rinsing with the water distilled and then with acetone during 5 min, rinsing with distilled water, washing in methanol at ambient temperature in a bath to eliminate the traces from greases and impurities stuck to surface of substrate then they are cleaned in a water bath distilled and drying using a drier in the same condition as previously reported [3-4].

I.2. Co_3O_4 thin films preparation

Co_3O_4 thin films are prepared using a simple homemade PSM on highly cleaning glass substrates. Cobalt chloride dehydrate (CoCl2.6H2O) with 0,1 M (mol/l), manganese (II) chloride tetrahydrate ($MnCl_2.4H_2O$), Lanthanum(III) chloride heptahydrate ($LaCl_3.7H_2O$),tin

tetrachloride or stannic chloride ($SnCl_4.2H_2O$)and zinc chloride($ZnCl_2$)are used as chemicals sources in the solvent which contained equal volumes of distilled water (H_2O) with a volume of 50 ml too and two drops of chloride acid (HCl) also used as a stabilizer for the all samples in this work. Then, the doping concentration is adjusted by adding different amount of doping agent to the solution to give 2, 4,6, 8 and 10 wt % doping levels (N= Mn, La, Sn and Zn) PWN (N/Co = 0; 2; 4; 6; 8 and 10 weight %) (N= Mn, La, Sn and Zn). The produced mixture was stirred for 1 hour at temperature between 50°C –60°C to yield a transparency and homogenous solutions. The normalized distance of 20 cm between the spray nozzle (0,5 mm) and the substrates was maintained. The solution quantity of 50 ml is fixed during the preparation of thin films. The spray rate of 3 (ml/min) was maintained by using filtered compressed air (1bar) as a gas carrier. The deposition time is fixed to 4 min at 400 ◦C as substrate temperature for each film. After deposition, the substrate is cleaned with distilled water in order to remove loosely adherent Co_3O_4 particles from the surfaces. Finally, a very thin and uniform layer is obtained having good adherent property.

I.3. Description of the spray pneumatic deposition method

Several techniques are used to elaborate cobalt oxide thin films. Among them, chemical vapor deposition (CVD) method (pneumatic spray method) (figure 1) which is most commonly used because it is simple and has many advantages, such as it can produce homogeneous thin films with very regular crystallites sizes [5, 6]. It facilitates the control of the solution concentration, the control of temperature stabilization for glass substrates, the control of time for spraying, large area spraying, and control of composition. In addition, the morphology of films can be controlled; therefore, it is one of the most important method for the preparation of the Co_3O_4 thin films. The effect of manganese doping on the Co_3O_4 thin films crystallinity, transmittance, bandgap energy, and electrical conductivity of the Co_3O_4 is investigated.

The pneumatic spray technique is used to deposit the cobalt oxide (Co_3O_4) thin films have the shape and components shown in figure 1.

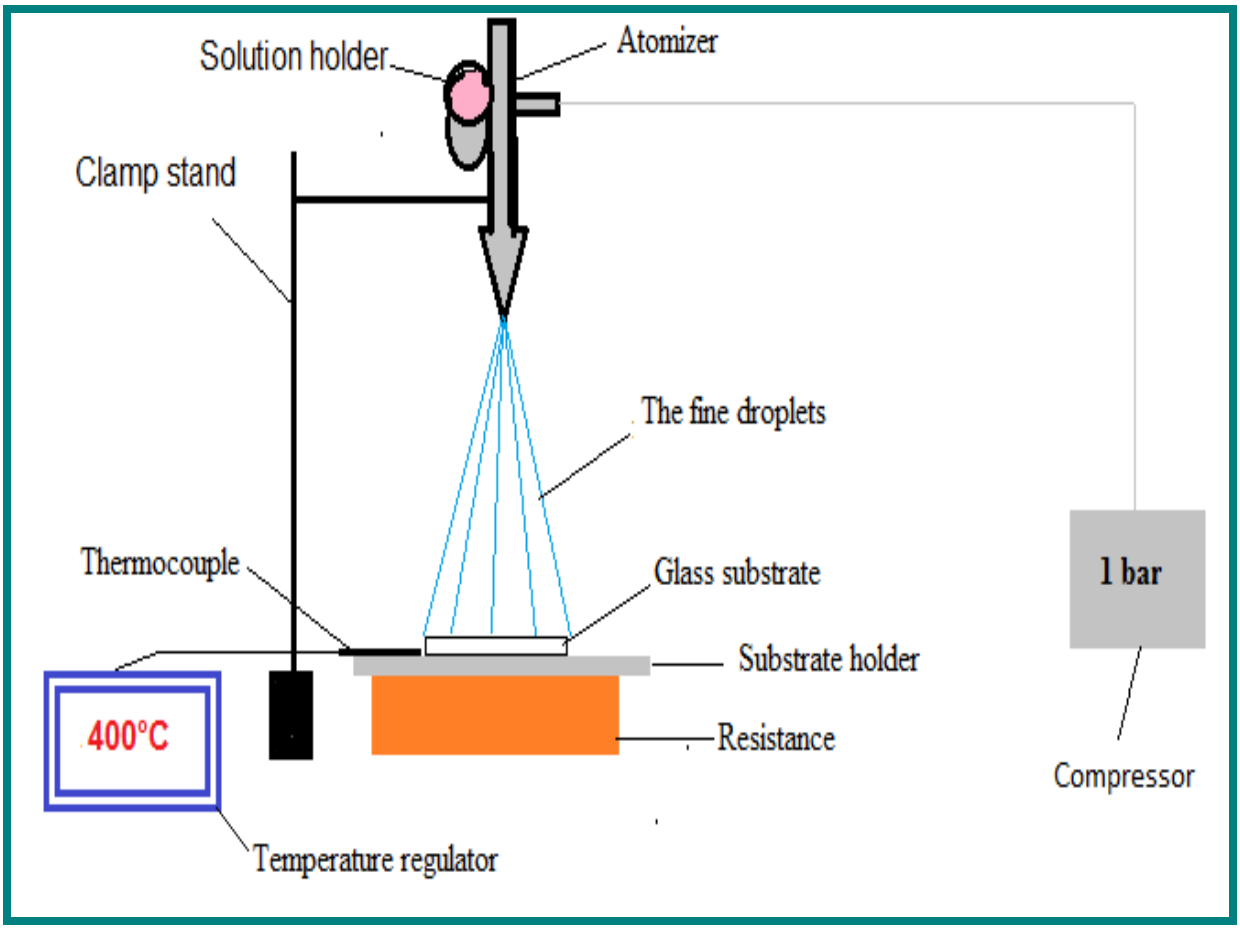

Figure 1. The experimental setup for pneumatic spray (PSM) deposition method.

I.4. Growth kinetics during for deposition

Thin films are deposited on a substrate by thermal evaporation, chemical decomposition, and/or the evaporation of source materials by the irradiation of energetic species or photons. Any thin-film deposition process involves three main steps:

1. Production of the appropriate atomic, molecular, or ionic species.
2. Transport of these species to the substrate.
3. Condensation on the substrate, either directly or via a chemical and/or electrochemical reaction, to form a solid deposit.

The unit species, on impacting the substrate, lose their velocity component normal to the substrate (provided the incident energy is not too high) and are physically adsorbed on the substrate surface. The adsorbed species are not, initially, in thermal equilibrium with the

substrate initially and move over the substrate surface. In this process, they interact among themselves forming bigger clusters.

The clusters or the nuclei, as they are called, are thermodynamically unstable and may tend to desorb in time, depending on the deposition parameters. If the deposition parameters are such that a cluster collides with other adsorbed species before getting desorbed, it starts growing in size. After reaching a certain critical size, the cluster becomes thermodynamically stable and the nucleation barrier is said to have been overcome. This step involving the formation of stable, chemisorbed, critical-sized nuclei is called the nucleation stage.

The critical nuclei grow in number as well as in size until a saturation nucleation density is reached. The nucleation density and the average nucleus size depend on a number of parameters such as the energy of the impinging species, the rate of impingement, the activation energies of adsorption, desorption, thermal diffusion, and the temperature, topography, and chemical nature of the substrate. A nucleus can grow both parallel to the substrate by surface diffusion of the adsorbed species, and perpendicular to it by direct impingement of the incident species. In general, however, the rate of lateral growth at this stage is much higher than the perpendicular growth. The grown nuclei are called islands. The next stage in the process of film formation is the coalescence stage, in which the small islands start coalescing with each other in an attempt to reduce the substrate surface area. This tendency to form bigger islands is termed agglomeration and is enhanced by increasing the surface mobility of the adsorbed species,

Larger islands grow together, leaving channels and holes of uncovered substrate. The structure of the films at this stage changes from discontinuous island type to porous network type. Filling of the channels and holes forms a completely continuous film [7].

I.4.1. Growth modes

In the early stage of research on thin films, it soon became clear that it was imperative to understand the mechanisms, which control and define the growth of thin films to achieve good control over these novel materials. Hence the huge effort of the scientific community to characterize, optimize and understand film growth.

Evidently, thin films are composed of atoms, which are their zero-dimensional building blocks. Extending this concept, nanoparticles (also termed 'nano-crystals') can also serve as zero-dimensional building blocks which by self-assembly may form two-dimensional

thin films or three-dimensional crystals (so-called 'nanoparticle super-lattices'), analogous to atomic films and crystal lattices [8].

Atomic thin film growth is understood to occur in form of three basic growth modes, which result from competing energy terms during the film deposition, i.e., Frank van der Merwe, Stranski-Krastanov, and Volmer-Weber growth. Various processes occur when atoms arrive at a substrate during thin film growth. That is adsorption, desorption, diffusion, finding or leaving of equilibrium positions. These processes occur simultaneously averaged over the ensemble of arriving atoms [9, 10, 11].

As in the case of atoms, the interplay of various free energy terms determines the way on how the nanoparticles (NPs)films will grow. These are in detail [12]: an entropic contribution E_{TS}, an inter-particle energy term E_p, summing up all relevant types of interactions between NPs [13], and a NP-to-substrate interaction energy E_s. A further important factor is the diffusion energy barrier, E_d, which can be overcome by 'thermal' energy $k_B T_s$. Hereby T_s is a quantity comparable to a substrate 'temperature', which precise physical meaning still needs to be understood for NP systems.

Depending on the relative magnitudes of E_d and $k_B T_s$ the NPs will either stay fixed at one place once they are attached to the substrate or move freely to seek energetically more favorable locations considering the two extreme cases.

From a comparison of these free energy terms one finds [11, 12] that three different growth modes follow: in the case where NP-to-substrate energy, Es, dominates a layer-by-layer growth is found, viz. the so-called Frank-van-der-Merwe growth mode (FvdM). Once a stable cluster (or 'nucleus') of NPs is formed, the following NPs prefer to attach at the periphery of the nucleus in contact with the substrate.

Accordingly, this leads to the advancement of planar film growth. Depending on the ratio of Ed and $k_B T_s$ (i.e., the mobility of NPs) one will either obtain polycrystalline or single-crystalline superlattices. In the first case, the immobility of NPs leads to the nucleation of many independent superlattice crystallites, while, in the other case, the large mobility enables the NPs to seek equilibrium positions and hence promotes single-crystal growth [8].

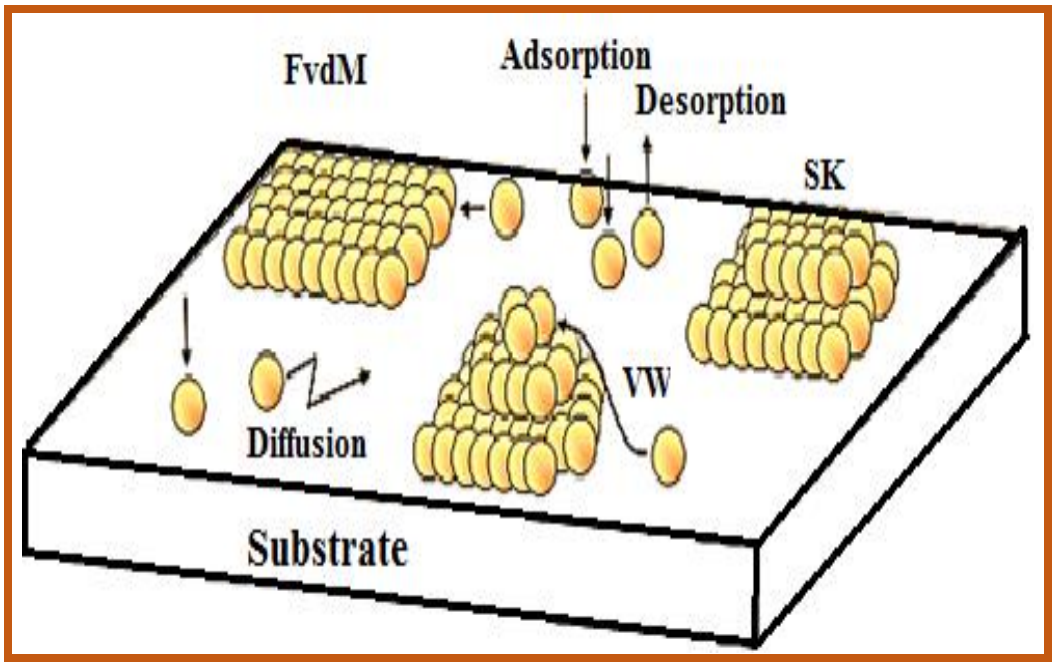

Figure 2. Schematic representation of the three known film growth modes [11].

II. Characterization methods

A measurement of thin-film properties is indispensable for the study of thin film materials and devices. The chemical composition, crystalline structure, and optical, electrical, and morphological properties must be considered in evaluating thin films.

II.1. X rays diffraction (XRD)

The X ray diffraction is carried out to study the crystalline quality of the Co_3O_4thin films (figure 3). It is a simple and non-destructive analysis technique, which provides means to identify different phases and their distribution in the sample, texture, evaluate average grain size, internal stress, etc[8].

Figure 3. Rigaku-Type MiniFlex600 X-ray diffractometer.

X-rays are electromagnetic waves with wavelength (0.5-50 Å) comparable to atomic separation distances. When propagating through a crystal, the X-rays interact with the lattice and are diffracted according to the Bragg's law [8]:

$$2d_{hkl}\sin\theta = n\lambda \quad \ldots\ldots\ldots\ldots\ldots\ldots\ldots\ldots\ldots\ldots\ldots\ldots\ldots\ldots (1)$$

d_{hkl}: The interplanar spacing.

n: The integer.

θ: The scattering angle.

λ: The wavelength.

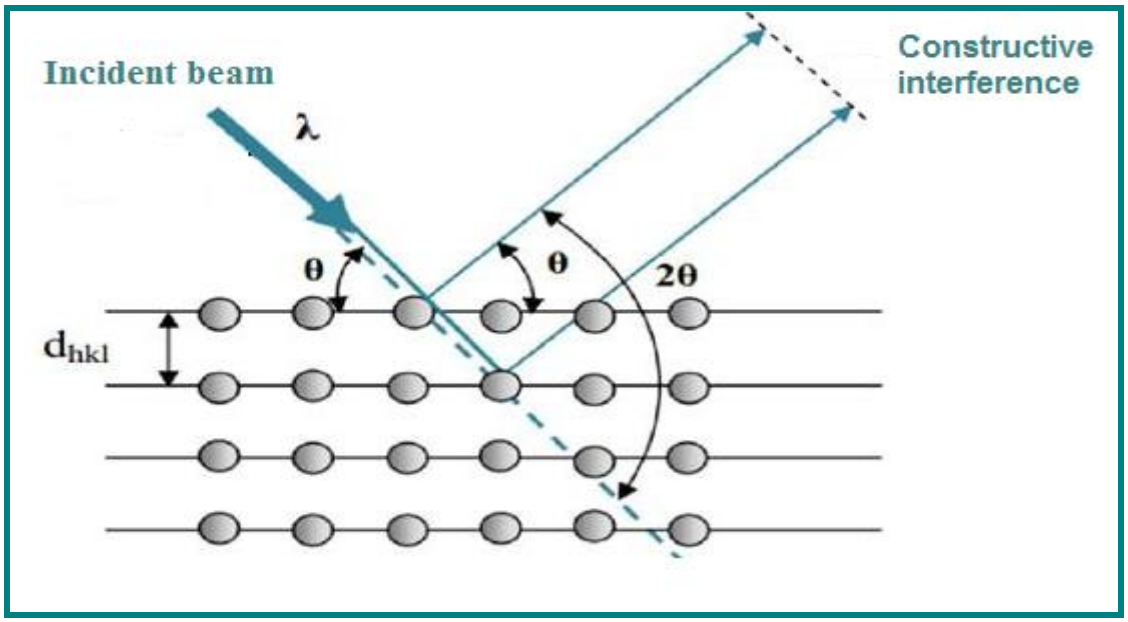

Figure 4. Schematic diagram of Bragg diffraction[3].

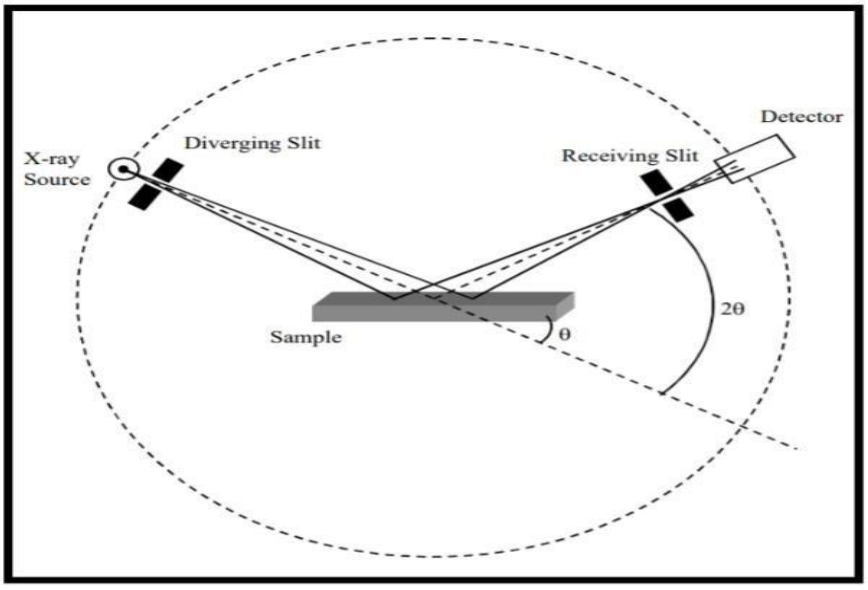

Figure 5. Schematics of X-ray diffractometer [8].

In this technique, the diffracted radiation is detected by the counter tube, which moves along the angular range of reflections. The intensities are recorded on a computer system. The X-ray diffraction data thus obtained is printed in tabular form on paper and is compared with Joint Committee Power Diffraction Standards (JCPDS) data to identify the unknown material. The sample used may be powder, single crystal or thin film. The crystallite size of the

elaborated sample is estimated from the full width at half maximum (FWHM) of the most intense diffraction line by Scherrer's formula as follows[8]:

$$D = \frac{0.9\,\lambda}{\beta\, cos\theta} \quad \ldots\ldots\ldots\ldots\ldots\ldots\ldots\ldots\ldots\ldots\ldots\ldots\ldots\ldots (2)$$

D: The crystallite size (nm).

λ : The wavelength of X-ray (nm).

β:The full width at half maxima of the peak (FWHM) in radians,

θ:TheBragg's angle (rd.).

It can be calculating the dislocations density using the grains size values according to the following relationship [8]:

$$\delta = \frac{1}{D^2} \ldots\ldots\ldots\ldots\ldots\ldots\ldots\ldots\ldots\ldots\ldots\ldots\ldots\ldots\ldots\ldots\ldots\ldots (3)$$

The micro-strain is calculated using, a Williamson-Hall plot method [14]

$$\beta * cos\theta = \frac{0{,}9 * \lambda}{D} + 4\varepsilon * sin\theta \ldots\ldots\ldots\ldots\ldots\ldots\ldots\ldots\ldots (4)$$

The lattice parameter values for Cubic system can be calculated from the following equations using the (hkl) parameters and the interplanar spacing d[2].

$$a = d_{hkl} * \sqrt{h^2+k^2+l^2} \ldots\ldots\ldots\ldots\ldots\ldots\ldots\ldots\ldots\ldots (5)$$

II.2. Scanning electron microscope (SEM)

The scanning electron microscope (SEM) is a type of electron microscope that images the sample surface by scanning it with a high-energy beam of electrons in a raster scan pattern. The electrons interact with the atoms to make the sample producing signals that contain information about the surface of the sample, composition and other properties of the Co_3O_4thin films. The SEM uses electrons instead of light to form an image. A beam of electrons is produced at the top of the microscope by heating of a metallic filament. The electron beam follows a vertical path through the column of the microscope. It makes its way through electromagnetic lenses which focus and direct the beam down towards the sample. Once it hits the sample, other electrons such as backscattered or secondary are ejected from the sample (see Figure 6). The SEM gives information on the surface morphology of the

sample, which can help us to check whether the growth has taken place or not. The SEM produces 2D images and reveals topographic features of the sample, which allows us to examine the diameter, length, shape and density of the TiO_2 nanostructures. However, the images from the SEM can not definitively prove that the obtained nanostructures actually consist of Co_3O_4[8].

In our case, SEM micrographs are recorded using aTESCAN-VEGA3 scanning electron microscope working at 20 kV (Figure 7).

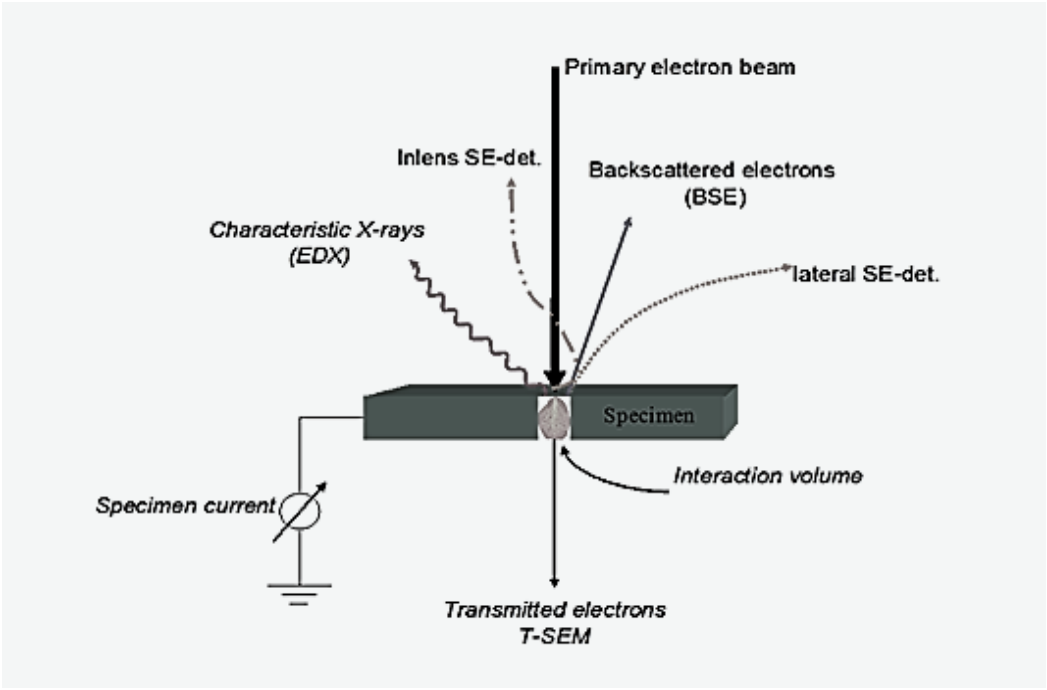

Figure 6. Illustration of electron-specimen interactions in SEM [8].

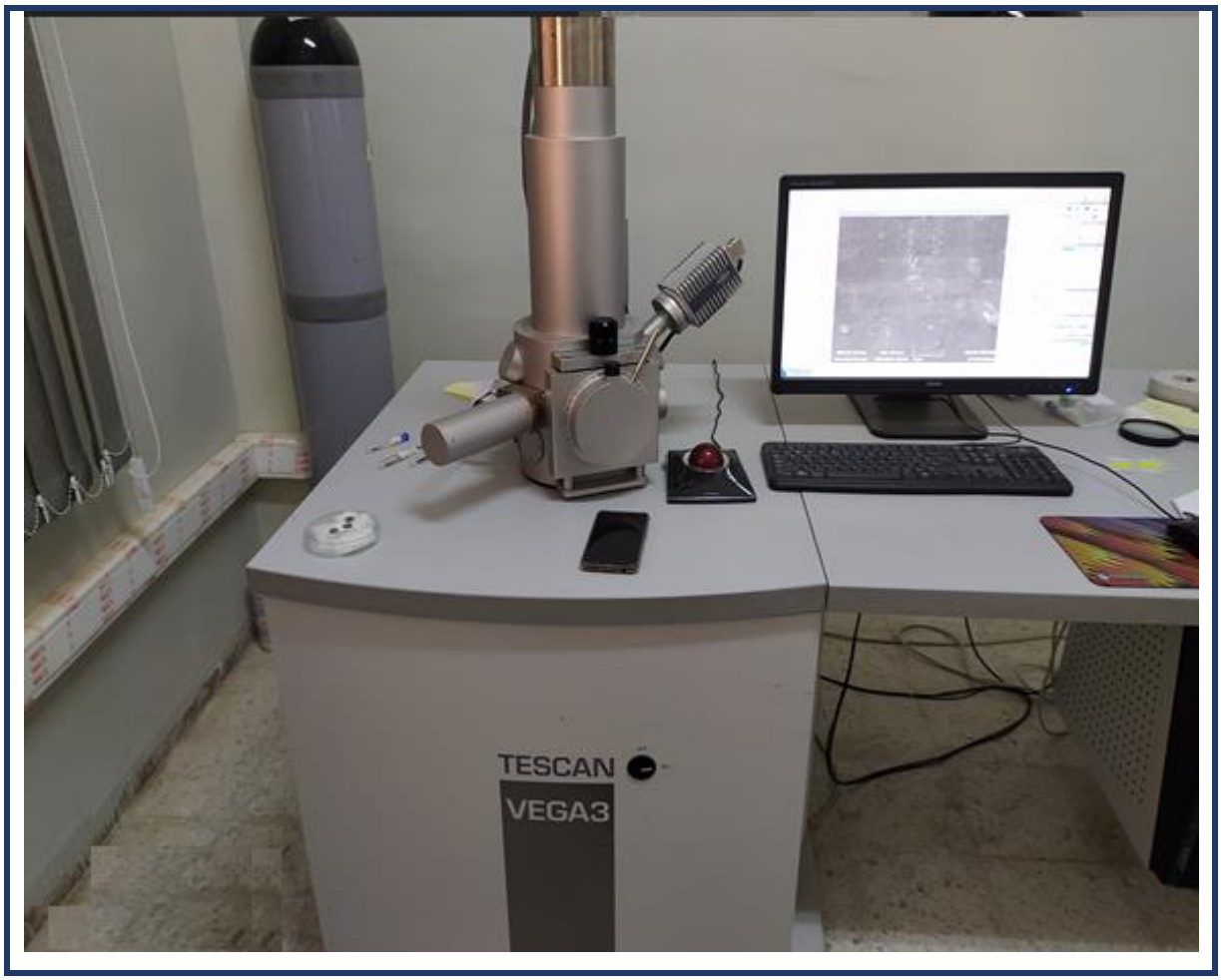

Figure 7. Scanning electron microscope "TESCAN-VEGA3".

II.3. Energy dispersive X-ray spectroscopy (EDS or EDX)

EDX is a chemical microanalysis technique which is used in conjunction with SEM. EDX can provide elemental analysis on areas as small as nanometer in diameter and it is used to determine the elemental composition of individual points or to map out the lateral distribution of elements from the imaged area. When an incident electron beam hits atoms of the sample, secondary and backscattered electrons are emitted from the sample surface. However, these are not the only signals emitted from the sample. When the incident beam bounces through the sample creating secondary electrons, it leaves thousands of the sample atoms with holes in the electron shells where the secondary electrons used to be. If these "holes" are in inner shells, the atoms are not in a stable state. To stabilize the atoms, electrons from outer shells will drop into the inner shells, however, because the outer shells are at a higher energy state, to do this the atom must lose some energy. It does this in the form of X-rays. The X-rays emitted from the sample atoms are characteristic in energy and wavelength

to, not only the element of the parent atom, but which shells lost electrons and which shells replaced them, this permits the elemental composition of the sample to be measured. An EDX spectrum not only identifies the element corresponding to each of its peaks, but also the type of X-ray to which it corresponds as well. For example, a peak corresponding to the amount of energy possessed by X-rays emitted by an electron in the L-shell going to the K-shell is identified as a K-alpha peak. The peak corresponding to X-rays emitted by M-shell electrons going to the K-shell is identified as K-beta peak [15] (figure 8).

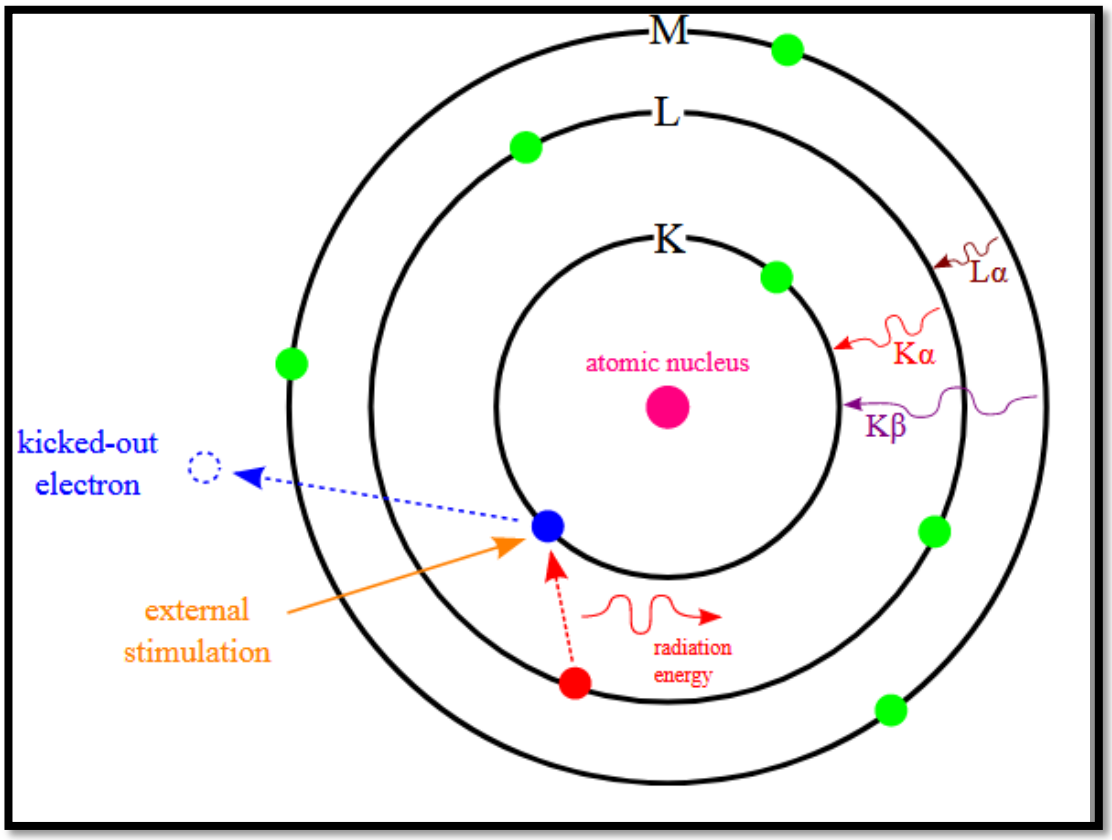

Figure 8. Scheme of X-ray excitations in EDX analysis[15].

II.4. Atomic force microscopy (AFM)

AFM is ideally suited for characterizing of nanoparticles (NPs) and nanomaterials (NMs). It offers both qualitative and quantitative information on many physical properties including size, morphology, surface texture and roughness. Statistical information, including size, surface area and volume distributions, can be determined as well. A wide range of particle sizes can be characterized in the same scan, from 1 nm to 8 µm. AFM offers high resolution and visualization in 3D images from the tip movement with high resolution. The vibration environment of the instrument limits resolution in the vertical, whereas resolution in

the horizontal is limited by the diameter of tip utilized for scanning. Typically, AFM instruments have vertical resolutions of less than 0.1 nm and X-Y resolutions of around 1 nm. In addition, the AFM can characterize NMs in multiple mediums including ambient air, controlled environments and even liquid dispersions. AFM is applied in air or liquid media and is based on the van der Waals forces between the NPs and the AFM tip [24].

The basic principle of non-contact 3D-AFM is that the cantilever rapidly oscillates just above the surface of the imaging sample. This offers a plethora of advantages, as compared to the traditional contact and intermittent modes. One of the most essential advantages is that there is no physical contact between the tip and the surface of the sample. Moreover, as depicted in figure 2, the Z-scanner, which moves the tip, is decoupled from the XY scanner, which solely moves the sample, thus, offering incredibly flat scanning and an additional benefit by improving its Z-scan bandwidth. Furthermore, by tilting the Z-scanner we can access the sidewall of the nanostructures and perform roughness measurements along the sidewall of photoresist lines while at the same time measure the critical dimensions of top, middle, and bottom lines (see figure 9).

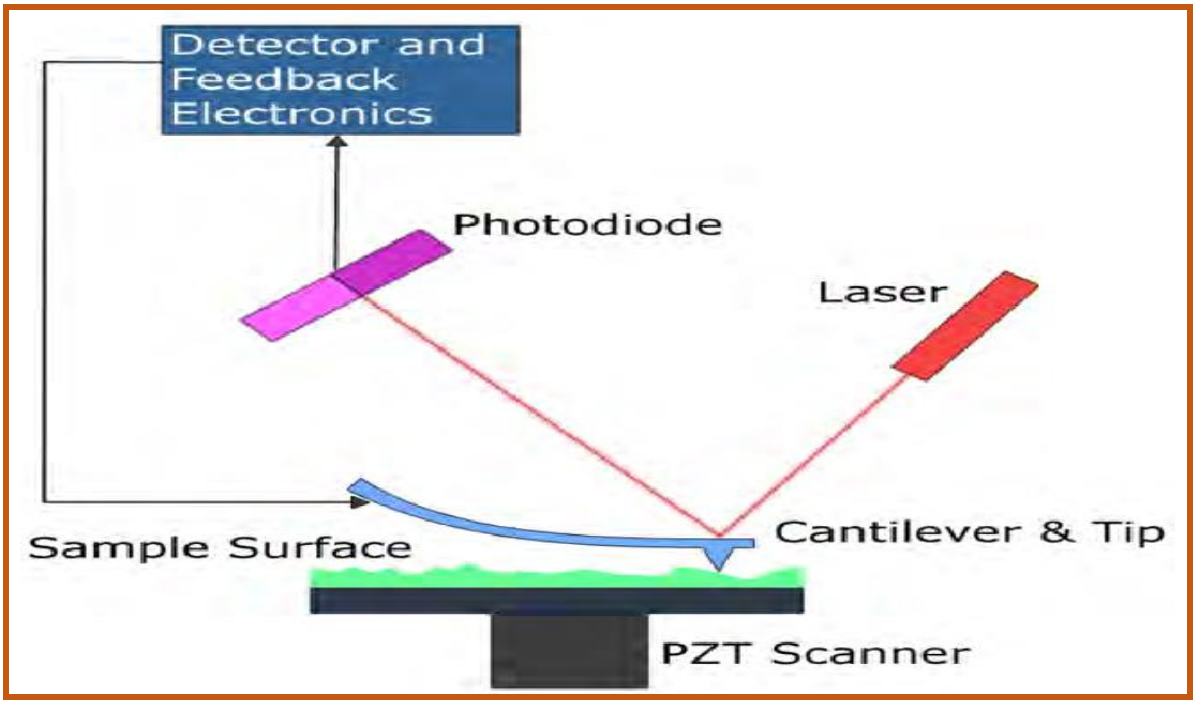

Figure 9. Schematic representation of the atomic force microscopy technique.

In our case,atomic force microscopyAFM are recorded using a“KLA-Tencor Stylus P7”(figure 10).

Figure 10. AFM: Atomic force microscopy “KLA-Tencor Stylus P7”.

II.5. Optical spectrophotometry

Optical spectrophotometry is a quick, an accurate and non-destructive technique that is used to determine the optical properties of materials. Thus, transmittance measurements are collected using wavelengths between 300 nm and 2000 nm and scan step of 0,5 nm. Ultraviolet-visible spectrophotometer involves the spectroscopy of photons in the ultraviolet region (200–400 nm) and visible region (400–800 nm). It is a type of absorption spectroscopy in which the excitation of the electrons takes place from ground state to excited state while fluorescence measures transitions from excited state to ground state. This method is most often used in a quantitative way to determine concentrations of an absorbing species in sample using the Beer-Lambert law. The principle is involved in UV-VIS-NIR Spectroscopy states in (figure 11), when a beam of monochromatic light is passed through a homogeneous medium of an absorbing substance, the rate of decrease in intensity of radiation with respect

to thickness of the absorbing medium is directly proportional to the intensity of incident radiation as well as the concentration of the medium [15].

$$I = I_0\, e^{-\alpha d} \ldots\ldots\ldots\ldots\ldots\ldots\ldots\ldots\ldots\ldots\ldots\ldots\ldots\ldots\ldots\ldots\ldots\ldots\ldots\ldots (6)$$

where $\alpha$is the absorption coefficient, d is the thickness of the film, I_0 and I are the intensity ofthe incident and the transmitted beams, respectively.

The absorption coefficient (α) can be calculated using the following expression:

$$\alpha = \frac{1}{d}\ln\frac{100}{T\,(\%)} \ldots\ldots\ldots\ldots\ldots\ldots\ldots\ldots\ldots\ldots\ldots\ldots\ldots\ldots\ldots\ldots\ldots\ldots\ldots\ldots (7)$$

where T(%) is the transmittance (quantity of the transmitted light), and can be directly measuredby [15]:

$$T\,(\%) = \frac{I}{I_0} \times 100 \ \ldots\ldots\ldots\ldots\ldots\ldots\ldots\ldots\ldots\ldots\ldots\ldots\ldots\ldots\ldots\ldots\ldots\ldots\ldots (8)$$

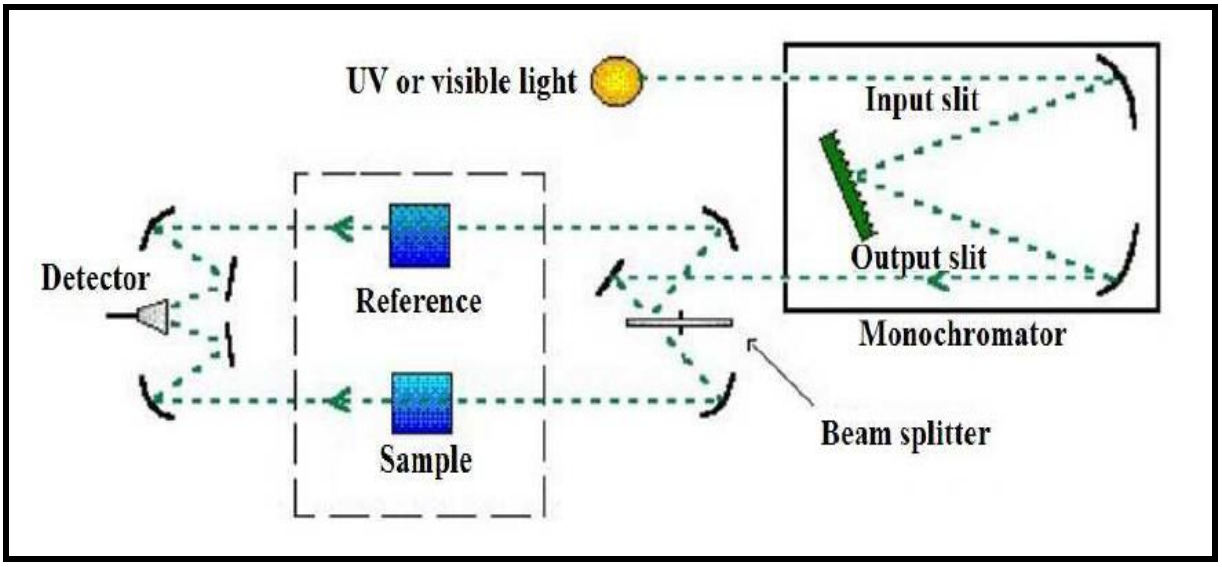

Figure 11. Schematic representation of constituent elements of a Spectrophotometer UV-VIS-NIR [3,17].

II.5.1. Film thickness d (Swanepoel method):

$$\mathrm{d} = \frac{\lambda_1\lambda_2}{2(\lambda_1 \mathrm{n}_2 - \lambda_2 \mathrm{n}_1)} \ldots\ldots\ldots\ldots\ldots\ldots\ldots\ldots\ldots\ldots\ldots\ldots\ldots\ldots\ldots\ldots\ldots\ldots\ldots (9)$$

Where: n_1 and n_2 are the refraction index of the film for the wavelength λ_1 and $\lambda_2$respectively, we can calculate n_1 and n_2 from the following relation:

$$n_{1,2} = \left[N_{1,2} + \left(N_{1,2}^2 + s^2\right)^{1/2}\right]^{1/2} \dots\dots\dots\dots\dots\dots\dots\dots\dots\dots\dots\dots (10)$$

Where: s is the refraction indexes of the substrate and $N_{1,2}$ can be obtained using thisrelation:

$$N_{1,2} = \frac{2s\left(T_M - T_{m1,2}\right)}{T_M T_{m1,2}} + \frac{s^2+1}{2} \dots\dots\dots\dots\dots\dots\dots\dots\dots\dots\dots\dots\dots\dots (11)$$

With: $T_{m1,2}$ is the minimum transmittance corresponds with $\lambda_1(\lambda_2)$ and $T_M$is the maximum transmittance confined between T_{m1} and T_{m2}[18].

II.5.2. Optical bad gap Eg

In high energy, absorption results from electronic transitions between wide states of band to band. It is usually described by Tauc law [19].

$$(\alpha h\nu)^n = A\left(h\nu - \mathrm{E_g}\right) \dots\dots\dots\dots\dots\dots\dots\dots\dots\dots\dots\dots\dots\dots (12)$$

Where: $h\nu$ is the photon energy, Eg is optical gap n and A are constants, n characterizes the optical type of transition and takes the values 2, 1/2 (2 for allowed direct transitions or 1/2 for allowed indirect transitions). In order to determine the nature of the transition from the films that are produced in this study, we will plot the curves $(\alpha h\nu)^2 = f(h\nu)$ [20]. We can obtain $E_g$value as it showing in figure 12:

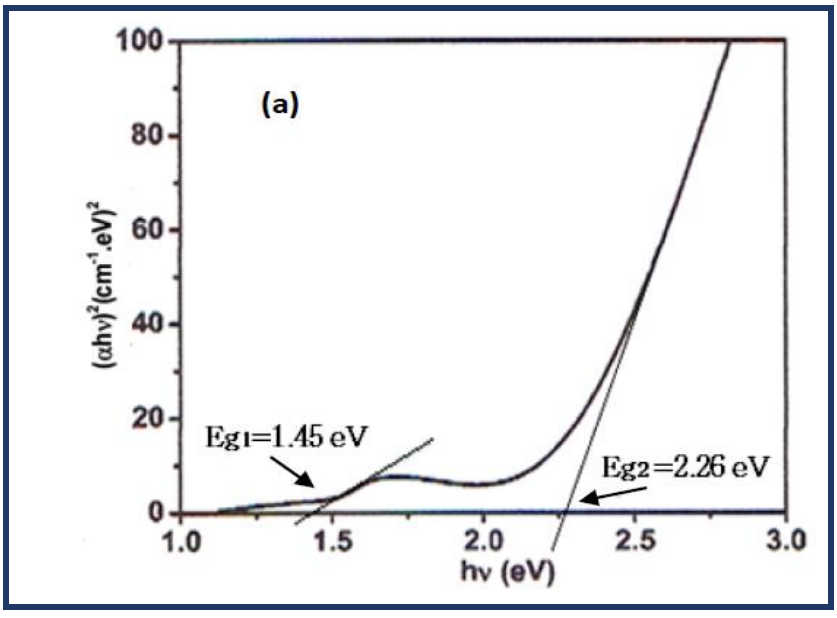

Figure 12. Curve represent the function $(\alpha h\upsilon)^2 = f(h\upsilon)$[8].

II.5.3. Urbach energy (E_u)

Urbach energy is usually used to describe the width of the localized states in the band gap (but not their positions). Pankove[21] has shown that the value of Eu is related to the impurity concentration. However, Redfield [22] has shown that all defects (point, line and planar defects) lead to local electric fields that cause band tailing. Thus, the Urbach energy can be considered a parameter that includes all possible defects. The relation between the Urbach energy and absorption coefficient is described by [23]:

$$\alpha = \alpha_0 exp\left(\frac{h\nu}{E_u}\right) \dots\dots\dots\dots\dots\dots\dots\dots\dots\dots\dots\dots\dots\dots\dots\dots (13)$$

where α_0 is a constant and E_u is Urbach energy.

By drawing (α) versus $h\nu$ we can determine Eu value as the reciprocal of the linear part slope (Figure 13) [15]:

$$Ln\ \alpha = Ln\ \alpha_0 + \frac{h\nu}{E_u} \dots\dots\dots\dots\dots\dots\dots\dots\dots\dots\dots\dots\dots\dots\dots\dots (14)$$

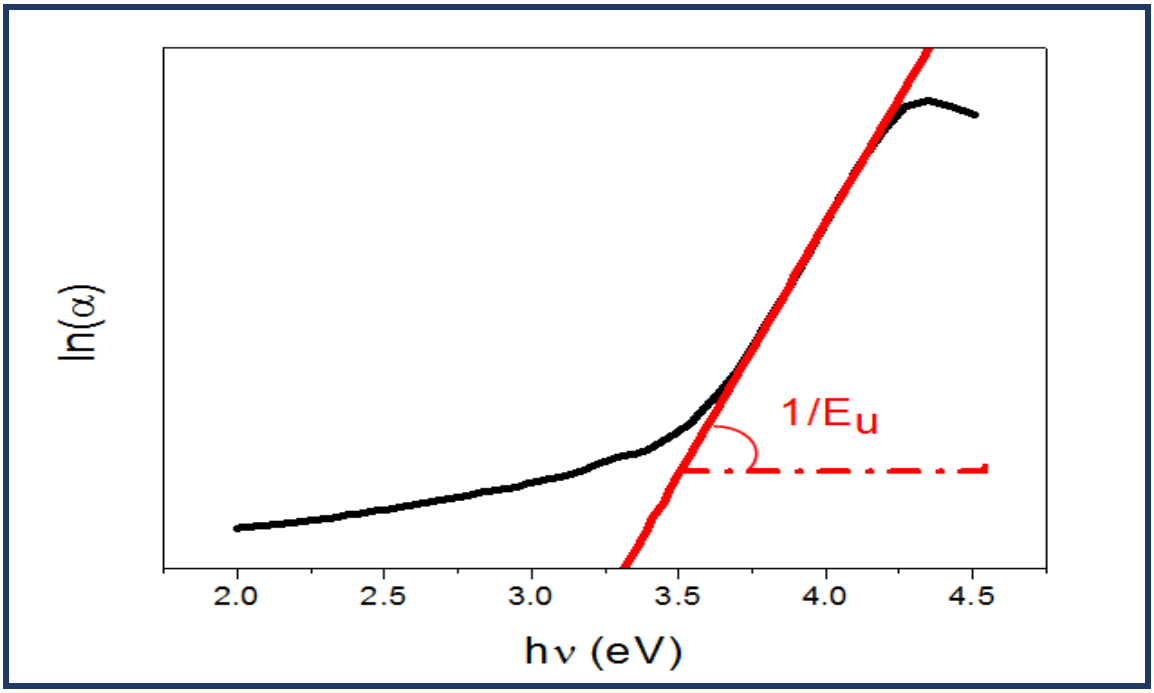

Figure 13. Determination of Urbach energy (Eu)[15].

II.6. Four-point probe resistivity measurements

Four-point probe measurements are made using four identical probes, equally spaced along the surface of the sample. A current is forced through the outer two probes while measuring the voltage across the inner two probes. Using a high-impedance voltmeter or electrometer, very little current flows through the inner probes, minimizing the contact resistance associated with the voltage measurement. Using only two-point measurements, the voltage is measured with current-carrying probes. As such, the probe and contact resistances become non-trivial. The more usual probe geometry configuration is when the four probes are placed in a line, as shown in figure 14. The voltage at probe 2, V_2, induced by the current flowing from probe 1 to probe 4 is given by:

$$V_2 = \frac{\rho I}{2\pi}.\left(\frac{1}{S_1} - \frac{1}{S_2 + S_3}\right) \dots\dots\dots\dots\dots\dots\dots\dots\dots\dots\dots\dots\dots\dots\dots\dots\dots\dots (15)$$

The voltage at probe 3 is:

$$V_3 = \frac{\rho I}{2\pi}.\left(\frac{1}{S_1 + S_2} - \frac{1}{S_3}\right) \dots\dots\dots\dots\dots\dots\dots\dots\dots\dots\dots\dots\dots\dots\dots\dots\dots\dots (16)$$

Then, by measuring $V = V_2 - V_3$, the voltage drop between probes 2and 3, and the current I through probes1 and 4, the resistivity can be determined usingfor equations(15) and (16) as:

$$\rho = \frac{2\pi V/I}{\left(\frac{1}{S_1} + \frac{1}{S_2} - \frac{1}{S_2+S_3} - \frac{1}{S_1+S_2}\right)} \dots\dots\dots\dots\dots\dots\dots\dots\dots\dots\dots\dots\dots\dots\dots\dots (17)$$

Thus, a direct measurement of the resistivity can be made using a high-impedance voltmeter and a current source. When the probe spacing are equal ($S_1 = S_2 = S_3 = S$),which is the most practical case, then equation(17) becomes:

$$\rho = 2\pi S.\frac{V}{I} \dots\dots\dots\dots\dots\dots\dots\dots\dots\dots\dots\dots\dots\dots\dots\dots\dots\dots\dots\dots\dots\dots\dots\dots\dots\dots\dots\dots (18)$$

Equations (17) and (18) are valid only for semi-infinite samples; that is, when both the thickness t and the sample surface are very large ($\rightarrow +\infty$), and the probes locations must be far from any boundary. Because these relations can be applied only to large ingots, then in many cases a correction factor f must be introduced in order to take into account the finite thickness and surface of the sample and its boundary effects. Further, for epitaxial layers, f must also consider the nature of the substrate-whether it is a conductor or an insulator. Thus, equation (18) becomes:

$$\rho = 2\pi S.\frac{V}{I}.f \dots\dots\dots\dots\dots\dots\dots\dots\dots\dots\dots\dots\dots\dots\dots\dots\dots\dots\dots\dots\dots\dots\dots\dots\dots\dots. (19)$$

For a thin semiconductor wafer or thin semiconducting layer deposited on an insulating substrate, and for the condition $t < S/2$, which represents most practical cases because the probe spacing S is usually on the order of a millimeter, then the correction factor due to the thickness is:

$f = \frac{t/S}{2ln2}$ So that:

$$\rho = 4.532.t.\frac{V}{I} \dots\dots\dots\dots\dots\dots\dots\dots\dots\dots\dots\dots\dots\dots\dots\dots\dots\dots\dots. (20)$$

Figure 14. Linear four-point probe configuration[4].

III. Conclusion

The pneumatic spray deposition method (PSM) and the deposition process of Co_3O_4 thin films are illustrated in this chapter. Different characterization techniques are employed to study our films; these techniques are described briefly.

References

[1] A. Aldrin, Preparation and characterization of certain II-VI, I-III-VI2 semiconductor thin films and transparent conducting oxides, PhD thesis, Cochin University of Science and Technology, Kerala, India, 2004.

[2] M. Dahnoun**,** Preparation and characterization of Titanium dioxide and Zinc oxide thin films via Sol-Gel (spin coating) technique for optoelectronic applications, Doctorate these, University of biskra,2020.

[3] Nabila Kouidri. Contribution à l'étude de couches minces d'oxydes transparents conducteurs à base de zinc et cobalt par spray pneumatique, Doctorat thesis, University Mohamed Khider of Biskra, 2019.

[4] Adel Bouhdjer, Study of Thin Layers of Indium Oxide (In2O3) Elaborated by Chemical Means, Doctorat thesis, University Mohamed Khider of Biskra, 2016.

[5] W. Daranfed, N. Guermat and K. Mirouh, Experimental Study of Precursor Concentration the Co3O4 Thin Films Used as Solar Absorbers, Annales de Chimie - Science des Mat´eriaux 44 (2020), 121–126.

[6] S. Salman Chiad, H. Ali Noor, O. MazinAbdulmunem and N. FadhilHabubi, Optical and Structural properties of Ni-doped Co3O4 Nanostructure Thin Films Via CSPM, Journal of Physics: Conference Series 1362 (2019), 012115.

[7] Messemche Radhia, Elaboration and characterization of undoped and doped titanium dioxide thin layers by sol gel (spin coating) for photocatalytic applications, Doctorat thesis, University Mohammad Khider of Biskra, (2021).

[8] Y. Benkhetta, Elaboration and characterization of thin layers of zinc oxide (ZnO) deposited by ultrasonic spray for photovoltaic and optoelectronic applications,Thesis,Doctorate, University Biskra, 2019.

[9] Venables, J. A. Introduction to Surface and Thin Film Processes; Cambridge University Press, 2000.

[10] Pimpinelli, A.; Villain, J. Physics of Crystal Growth; Cambridge University Press, 1999

[11] Freund, L. B.; Suresh, S. Thin Film Materials: Stress, Defect Formation and Surface Evolution; Cambridge University Press, 2003.

[12] Bishop, K. J. M.; Wilmer, C. E.; Soh, S.; Grzybowski, B. A. Nanoscale Forces and Their Uses in Self-assembly. Small 2009, 5, 1600–30.

[13] S. Brochen, electrical properties of ZnO single crystale, doctoral thesis, Grenoble University (2006).

[14] A.K. Zak, W.H. Majid, M.E. Abrishami, R. Yousefi, X ray analysis of ZnO nanoparticles by Williamson-Hall and size-strain plot methods, Solid State Sci. 13 (2011) 251–256.

[15] A. Yahia**,**Optimization of indium oxide thin films properties prepared by sol gel spin coating process for optoelectronic applications, Doctorate these, University of biskra,2020.

[16] J. Solé, L. Bausa, D. Jaque, An introduction to the optical spectroscopy of inorganic solids, John Wiley & Sons, 2005.

[17] A. Jrad, Elaboration, characterization and design of ZnS thin films for optoelectronic application,Doctorate these, University of El-Manar in Tunis (2017).

[18] R. Swanepoel, "Determination of the thickness and optical constants of amorphous silicon", Journal of Physics E: scientific instruments, 16(12), (1983) 1214.

[19] J. Tauc., R. Grigorovici., and A. Vancu, *"Optical properties and electronic structure of* amorphous germanium", Physica Status Solidi (B), 15(2), (1966) 627- 637.

[20] Z. Bencharef, A. Chala, R. Messemeche, Y. Benkhetta, The physical properties of spinel cupic Co_3O_4 thin films prepared by a PSM, Main Group Chemistry 21(2022) 329-340.

[21] J.I. Pankove, Absorption edge of impure gallium arsenide, Phys. Rev. 140 (1965) A2059.

[22] D. Redfield, Electric fields of defects in solids, Phys. Rev. 130 (1963) 914.

[23] T.P. Rao, M.S. Kumar, Physical properties of Ga-doped ZnO thin films by spray pyrolysis, J. Alloys Compd. 506 (2010) 788–793.

[24] Marinella. Farré,Damià. Barceló,Chapter 1 - Introduction to the Analysis and Risk of Nanomaterials in Environmental and Food Samples, Comprehensive Analytical Chemistry 59 (2012) 1-32.

CHAPTER THREE

Structural, Compositional and Morphological Study of Co_3O_4:N (N= Mn, La, Sn and Zn) Thin Films.

Chapter III describes the structural, chemical composition and surface morphology of the chemical vapor deposited(pneumatic spray method)Co_3O_4:N (N= Mn, Sn, La and Zn) thin films, grown on heated glasses substrates (at 400°C), using an aqueous solution with concentration 0,1M and deposition time is 4 min. In particular, the effect of the doping percentage on the crystallite size (D), lattice strain (ε)and structural parameters is checked.

I. Structural properties

I.1. XRD analysis

The effect of manganese, lanthanum, tin and zinc doping on the cobalt oxide thin films structure is studied by X-ray diffraction (DRX). The different weight percentages of Mn, La, Sn and Zn (WPM, WPL, WPS and WPZ) were exclusively fixed to 0,2,4,6,8 and 10 wt % for this investigation. The logged XRD patterns are given in figure 1.From the DRX patterns of all cases, the diffraction peaks at about 19,06; 31,5; 36,8; 44,2; 59,6 and 65,5 correspond to (111);(220); (311); (222); (400); (511) and (440) planes of cubic spinel Co_3O_4 structure according to(JCPDS 42-1467; space grope Fd-3m)[1]; these results are in agreement with other studies [2-3].It has the cubic spinel Co_3O_4 structure without additional crystalline influence for Mn, Sn, La and Zn, they do not indicate an additional phase in the thin films. Typically, the patterns of Co_3O_4thin films deposited by different weight percentages of Mn, La, Sn and Zn (WPM, WPL, WPS and WPZ) are noticed the presence of broad peak. This indicate to the contribution of the amorphous glass substrate appears as a large band around 20°-29° in the collected patterns. The patterns of the thin films which are prepared with a WPL are lower intensity compared to other patterns. On the other hand, we notice that the patterns of thin films are prepared with a WPS are a higher intensity. As can be see for all these films, the Co_3O_4phase grows in its cubic spinel structure with a preferential crystallographic orientation along the (111) peak, Manickam et al. [4],Manogowri et al. [5], Louardi et al. [6],and Kouidri et al [2] have obtained the same result for the Co_3O_4 thin films prepared by spray method.

They established that Sn, Mn and Zn ions are successfully incorporated into the hosting blende lattice for all the investigated doping concentration, while the La solubility limit into Co_3O_4 thin films be smaller, 6wt%.

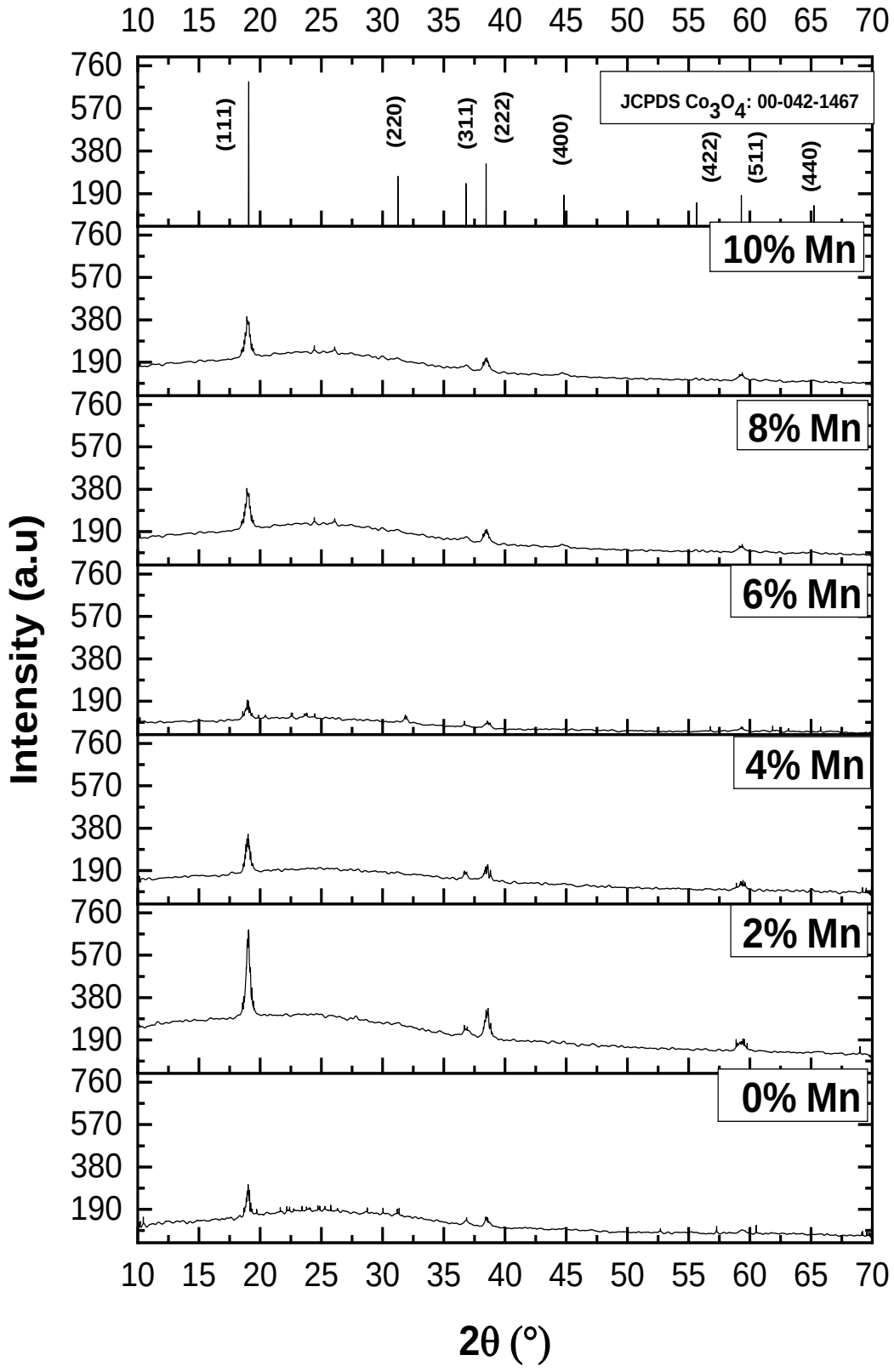
JCPDS Co_3O_4: 00-042-1467
(111)
(220)
(311)
(222)
(400)
(422)
(511)
(440)
10% Mn
8% Mn
6% Mn
4% Mn
2% Mn
0% Mn
Intensity (a.u)
2θ (°)

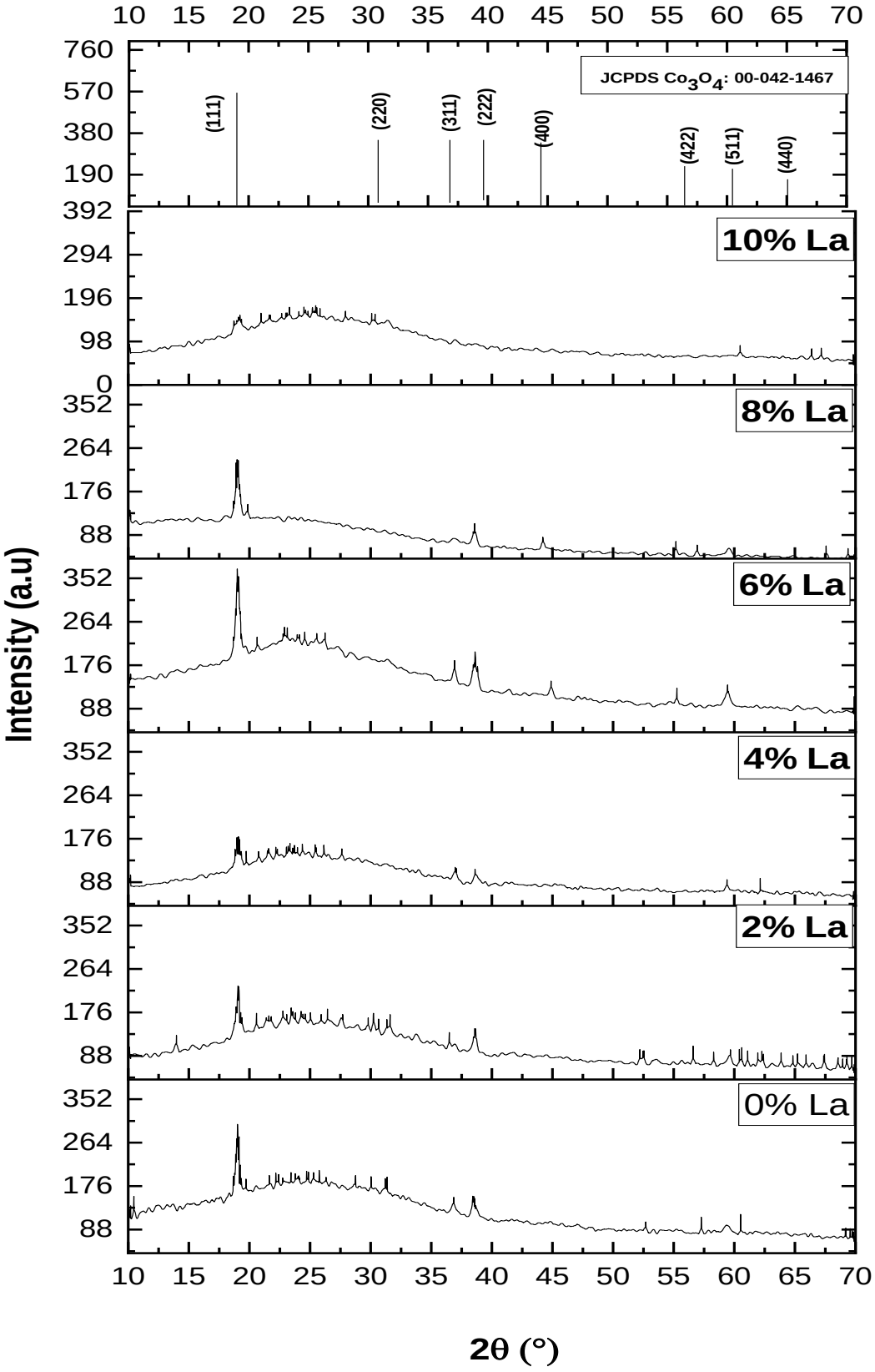
JCPDS Co_3O_4: 00-042-1467
(111)
(220)
(311)
(222)
(400)
(422)
(511)
(440)
10% La
8% La
6% La
4% La
2% La
0% La
Intensity (a.u)
2θ (°)

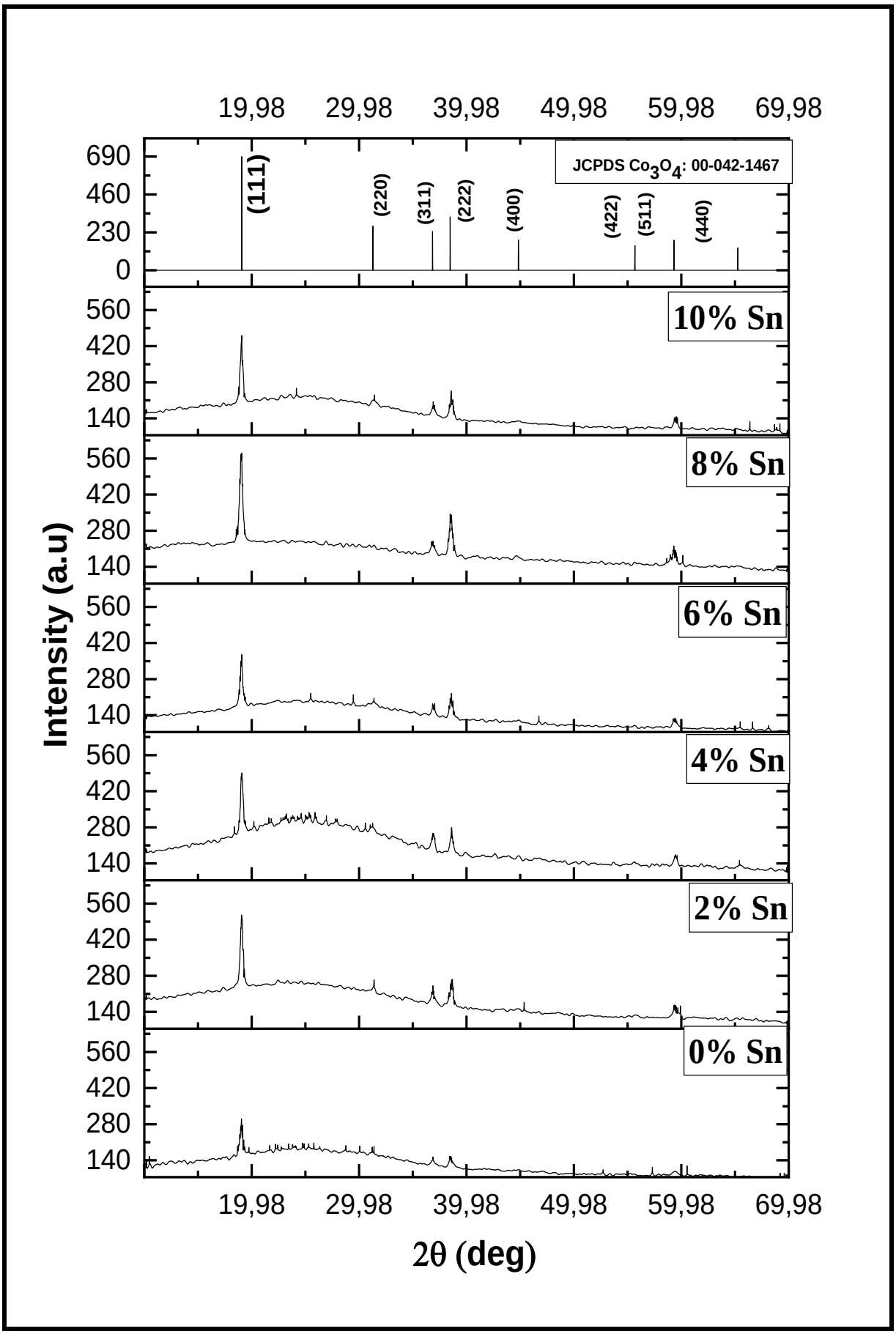
19,98
29,98
39,98
49,98
59,98
69,98
JCPDS Co_3O_4: 00-042-1467
(111)
(220)
(311)
(222)
(400)
(422)
(511)
(440)
690
460
230
0
10% Sn
8% Sn
6% Sn
4% Sn
2% Sn
0% Sn
560
420
280
140
Intensity (a.u)
2θ (deg)

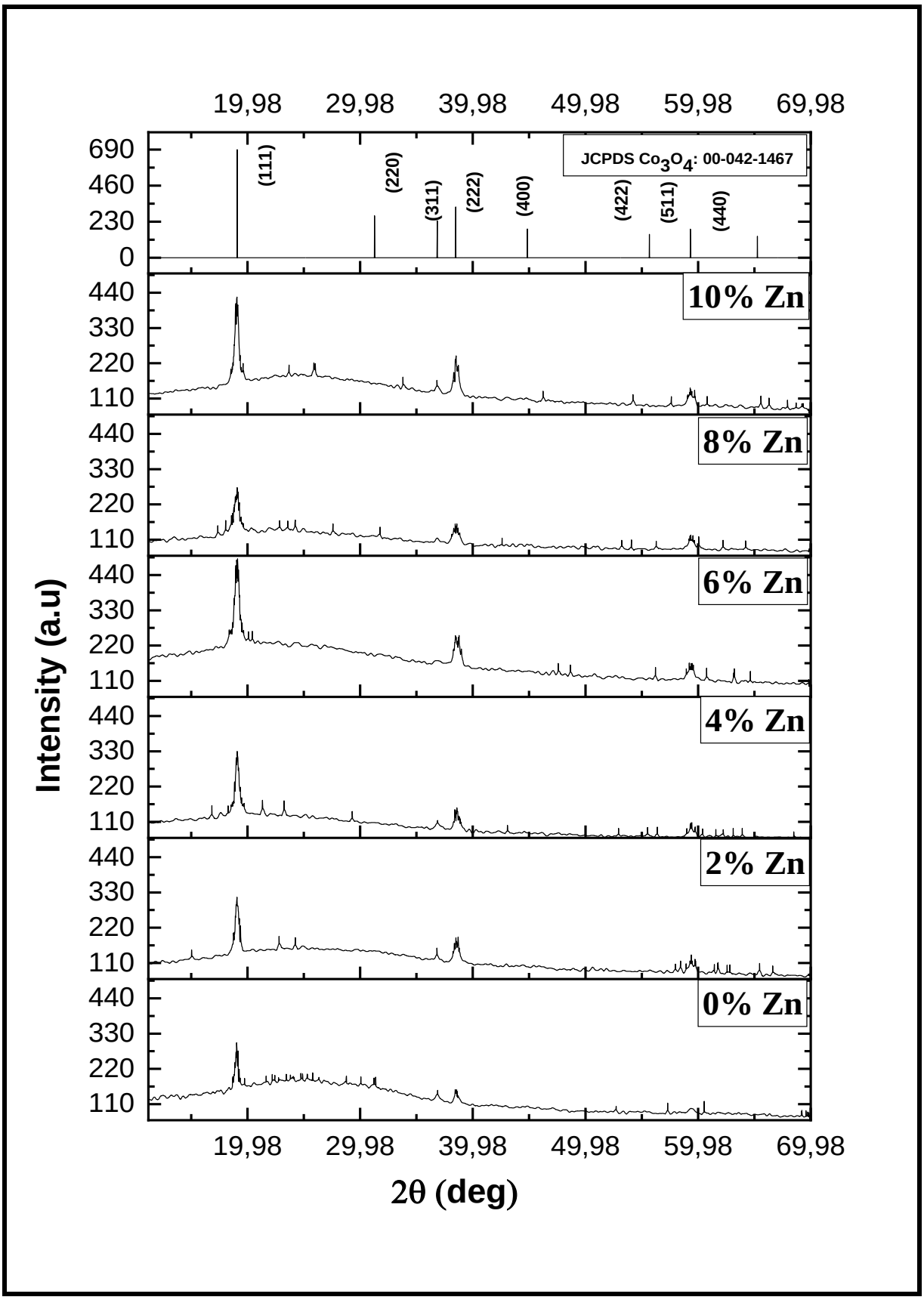

Figure 1.DRX patterns of Co3O4: N thin films deposited by different WPN (N= M, L, S and Z).

I.1.1 Crystallite size D and dislocation (δ_{dislo}) lines

The crystallite size D is calculated using the Williamson-Hall formula [7-9], focusing on all they peaks diffraction (see table 1for Mn doping). As seen from figure 3(the conclusion of the figure 2), the crystallite size for Mn doping increases slightly when the WPM increases and reaches a value of 35.47 nm for the film with a WPM concentration of 2wt%. For higher WPM content it starts decreasing down to 24.13 nm for a WPM of 6wt% and continues increasing up to 25.8 nm for a WPM of 8wt%. Besides, the lattice strain (ε) range between 0.029% and 0.275% for all the Mn doped sample series except for that corresponding to a WPM content of 2wt%. In this case, they reach an average value of about 0.275%.

Table.1 Williamsson-Hall XRD analysis of Mn-doped Co_3O_4 for cubic spinel structure.

(hkl)		%0	2%	4%	6%	8%	10%
111	$4\sin\theta/\lambda$	4,284334	4,286396	4,282140	4,277017	4,278158	4,278534
	$\beta\cos\theta/\lambda$	0,0341223	0,041662	0,044905	0,054003	0,046282	0,049922
220	$4\sin\theta/\lambda$	6,975272	-	-	7,122787	-	-
	$\beta\cos\theta/\lambda$	0,0496311	-	-	0,038893	-	-
311	$4\sin\theta/\lambda$	8,195901	8,197707	8,180243	8,1564149	8,183030	8,188084
	$\beta\cos\theta/\lambda$	0,04034	0,05256	0,031759	0,049207	0,039036	0,032692
222	$4\sin\theta/\lambda$	8,555871	8,560096	8,551267	8,5641499	8,562878	8,543538
	$\beta\cos\theta/\lambda$	0,0378099	0,045747	0,056475	0,049207	0,051553	0,050556
511	$4\sin\theta/\lambda$	12,851565	12,83506	12,841683	12,827709	12,834534	12,834636
	$\beta\cos\theta/\lambda$	0,0492499	0,065345	0,063590	0,0568862	0,047879	0,0512542
Crystallite size D (nm)		32,42	35,47	32,10	24,13	25,82	22, 90
Lattice strainε (x 10^{-3})		1,39	2,75	2,38	0,737	0,754	0,288

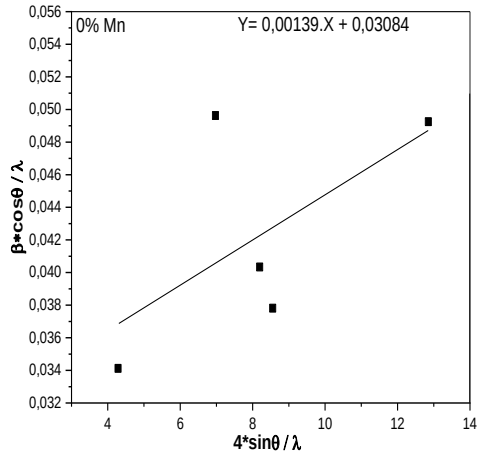
0% Mn
Y= 0,00139.X + 0,03084
β*cosθ / λ
4*sinθ / λ

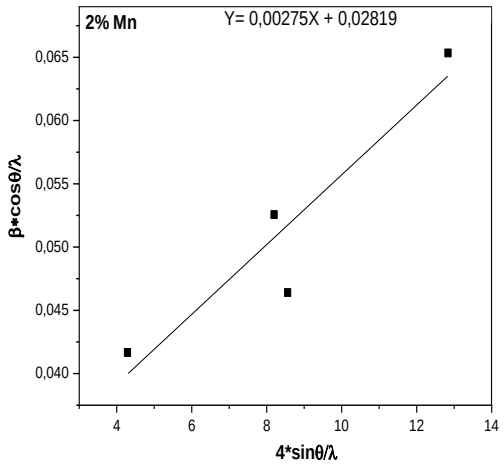
2% Mn
Y= 0,00275X + 0,02819
β*cosθ/λ
4*sinθ/λ

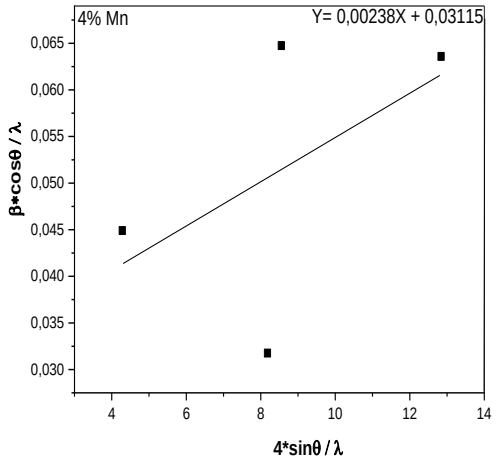
4% Mn
Y= 0,00238X + 0,03115
β*cosθ / λ
4*sinθ / λ

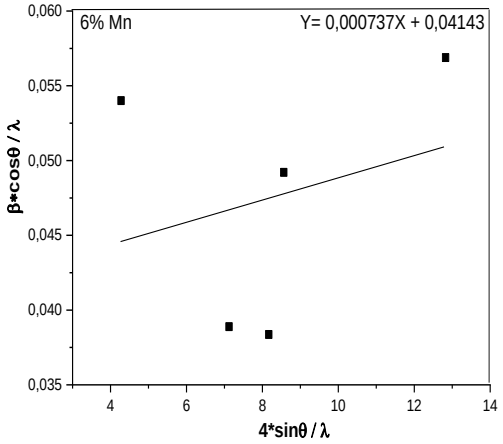
6% Mn
Y= 0,000737X + 0,04143
β*cosθ / λ
4*sinθ / λ

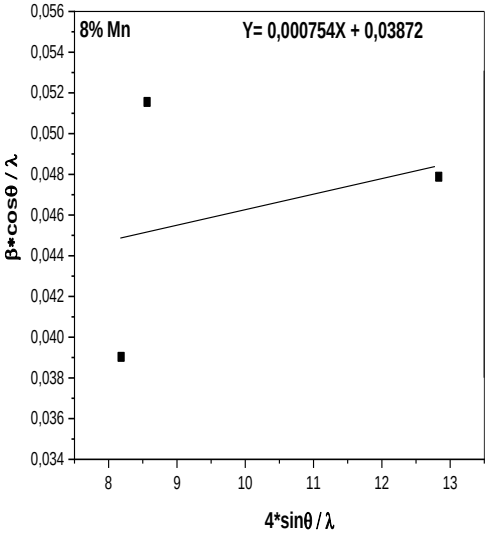
8% Mn
Y= 0,000754X + 0,03872
β*cosθ / λ
4*sinθ / λ

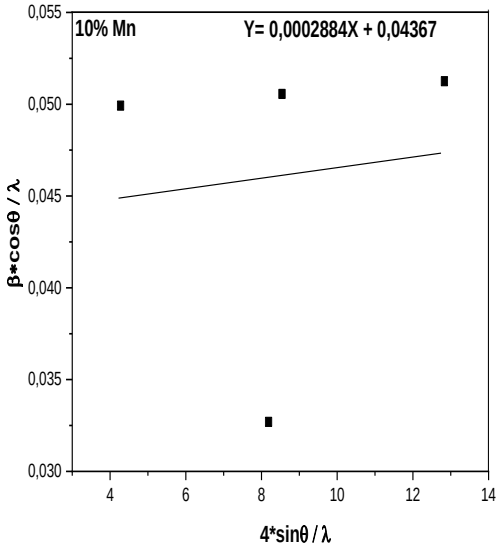
10% Mn
Y= 0,0002884X + 0,04367
β*cosθ / λ
4*sinθ / λ

Figure 2. Williamson-Hallplots of Mn-doped Co_3O_4 for cubic spinel structure.

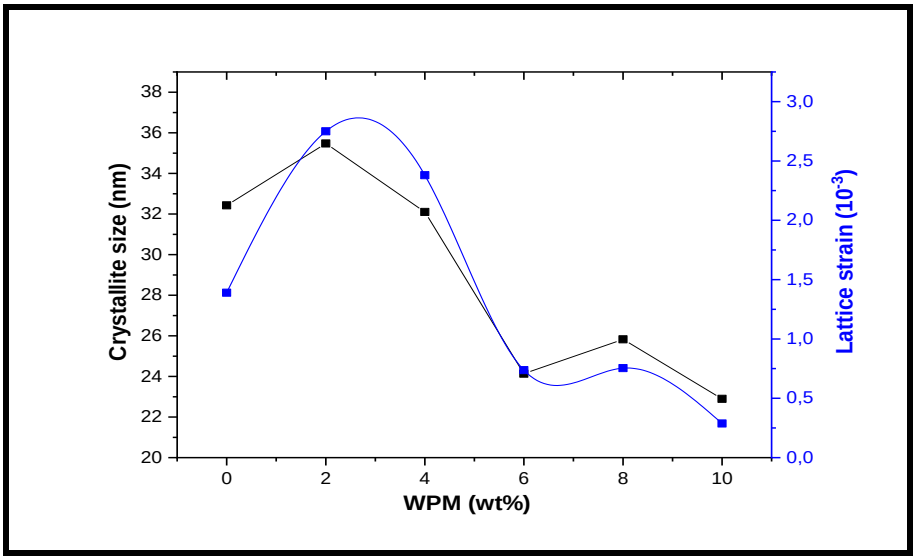

Figure 3. Lattice strain and crystallite size of Mn-doped Co_3O_4 from Williamson-Hall plots.

From figure 5 (the conclusion of the figure 4) of La doping, the crystallite size decreases from 32.4 nm to 20 nm when WPL concentration increases from 0 to 2wt% and continues increasing up to 33nm for a WPL of 10wt%. The lattice strain (ε) decreases from $1{,}39.10^{-3}$ to $0{,}12.10^{-3}$when the WPL increases from 0 to 2wt% and continues increasing up to $1{,}55.10^{-3}$for a WPL of 10wt%. As seen, the higher value of grain size is found at 2wt% of Mn doping. This indicates an improvement in the crystalline state of the thin films of cobalt oxide. In addition, the lower value of the grain size is found in the 6wt%of Mn doping. Therefore, when doping with Mn, it is advisable to use lower values.

Table 2. Williamsson-Hall XRD analysis of La-doped Co_3O_4 for cubic spinel structure.

(hkl)		%0	2%	4%	6%	8%	10%
111	$4\sin\theta/\lambda$	4,284334	4,29529	4,29992	4,29156	4,28691	4,31449
	$\beta\cos\theta/\lambda$	0,0341223	0,04296	0,04246	0,04441	0,03596	0,06977
220	$4\sin\theta/\lambda$	6,975272	7,04204	-	-	-	-
	$\beta\cos\theta/\lambda$	0,0496311	0,05958	-	-	-	-
311	$4\sin\theta/\lambda$	8,195901	8,19133	8,22026	8,21158	8,21203	-
	$\beta\cos\theta/\lambda$	0,04034	0,05876	0,04974	0,031824	0,035713	-
222	$4\sin\theta/\lambda$	8,555871	8,57371	8,57371	8,57448	8,56531	-

	$\beta\cos\theta/\lambda$	0,0378099	0,04581	0,04581	0,05200	0,04958	-
400	$4\sin\theta/\lambda$	-	-	-	9,90259	9,76438	-
	$\beta\cos\theta/\lambda$	-	-	-	0,036996	0,048224	-
511	$4\sin\theta/\lambda$	12,851565	12,89498	12,85422	12,86075	12,881074	-
	$\beta\cos\theta/\lambda$	0,0492499	0,04785	0,047161	0,04992	0,047798	-

Crystallite size D (nm)		32,42	20,00	23,87	25,97	33,44	-
Lattice strainε (x 10^{-3})		1,39	0,12	0,515	0,512	1,55	-
Crystallite size D (nm) of Scherrer's formula		-	-	-	-	-	14,33
Lattice strainε (x 10^{-3})		-	-	-	-	-	17,44

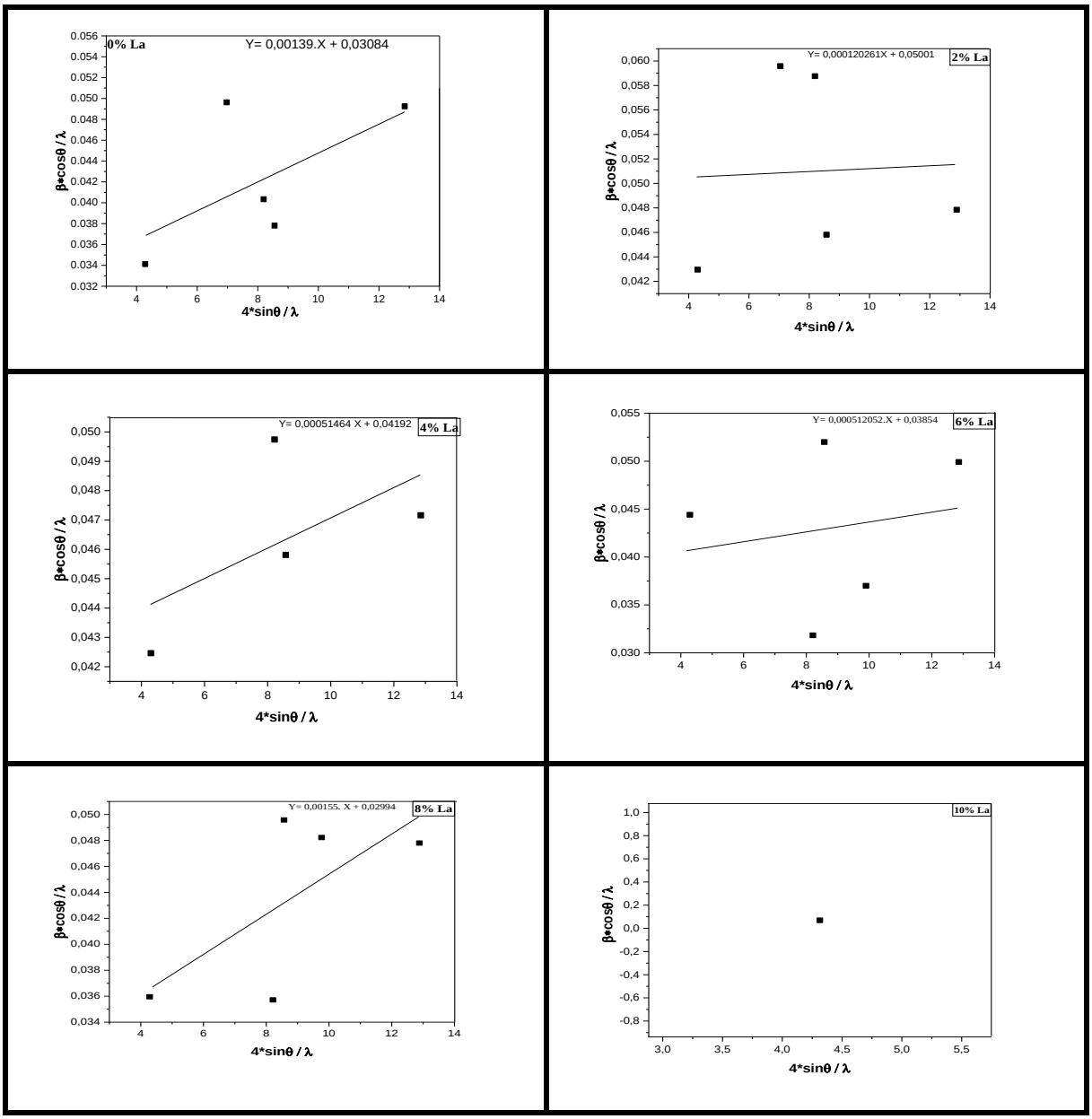

Figure 4. Williamson-Hallplots of La-doped Co_3O_4 for cubic spinel structure.

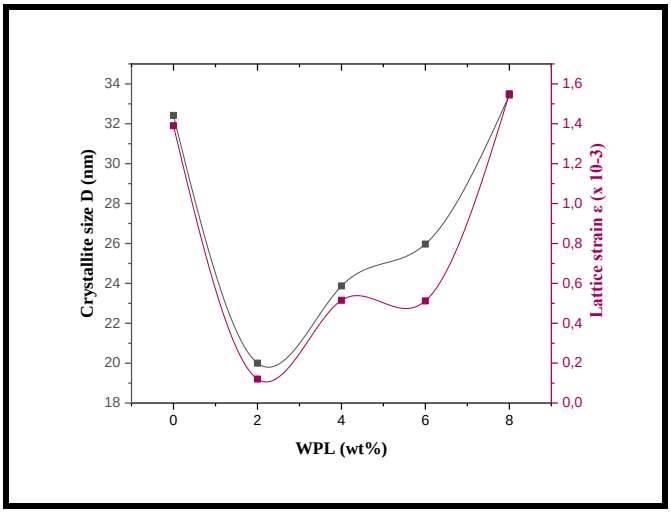

Figure 5. Lattice strain and crystallite size of La-doped Co_3O_4 from Williamson-Hall plots.

From figure 7 (the conclusion of the figure 6) of Sn doping, the crystallite size range between 32.4 nm to 41.91 nm for all the Sn doped sample series except for that corresponding to a WPS of 2 wt%. In this case, average value is about 100 nm. The lattice strain (ε) range between $0{,}313.10^{-3}$and $1{,}41.\ 10^{-3}$for all the Sn doped sample series except for that corresponding to a WPS of 2 wt%. In this case, average value is about $3{,}37.10^{-3}$.As seen, the higher value of grain size is found at 8wt% of La doping. This indicates an improvement in the crystalline state of the thin films of cobalt oxide. In addition, the lower value of the grain size is found in the 2wt%of La doping. Therefore, when doping with La, it is advisable to use higher values.

Table 3. Williamsson-Hall XRD analysis of Sn-doped Co_3O_4 for cubic spinel structure.

(hkl)		%0	2%	4%	6%	8%	10%
111	$4\sin\theta/\lambda$	4,284334	4,291118	4,29536	4,285992	4,28034	4,28838
	$\beta\cos\theta/\lambda$	0,0341223	0,030539	0,0289989	0,031113	0,032887	0,030058
220	$4\sin\theta/\lambda$	6,975272	-	-	7,00749	-	7,01993
	$\beta\cos\theta/\lambda$	0,0496311	-	-	0,03181	-	0,031136
311	$4\sin\theta/\lambda$	8,195901	8,19644	8,20237	8,2074	8,19456	8,20813
	$\beta\cos\theta/\lambda$	0,04034	0,02955	0,03198	0,03729	0,041376	0,038467
222	$4\sin\theta/\lambda$	8,555871	8,57042	8,57256	8,564184	8,55828	8,568193

	$\beta\cos\theta/\lambda$	0,0378099	0,03538	0,02726	0,034298	0,033496	0,033563
511	$4\sin\theta/\lambda$	12,851565	12,86266	12,86218	12,85043	12,83335	12,860663
	$\beta\cos\theta/\lambda$	0,0492499	0,05867	0,031861	0,04266	0,04057	0,037697
Crystallite size D (nm)		32,42	100	36,55	41,91	33,49	37, 66
Lattice strainε (x 10^{-3})		1,39	3,37	0, 313	1, 41	0,853	0,932

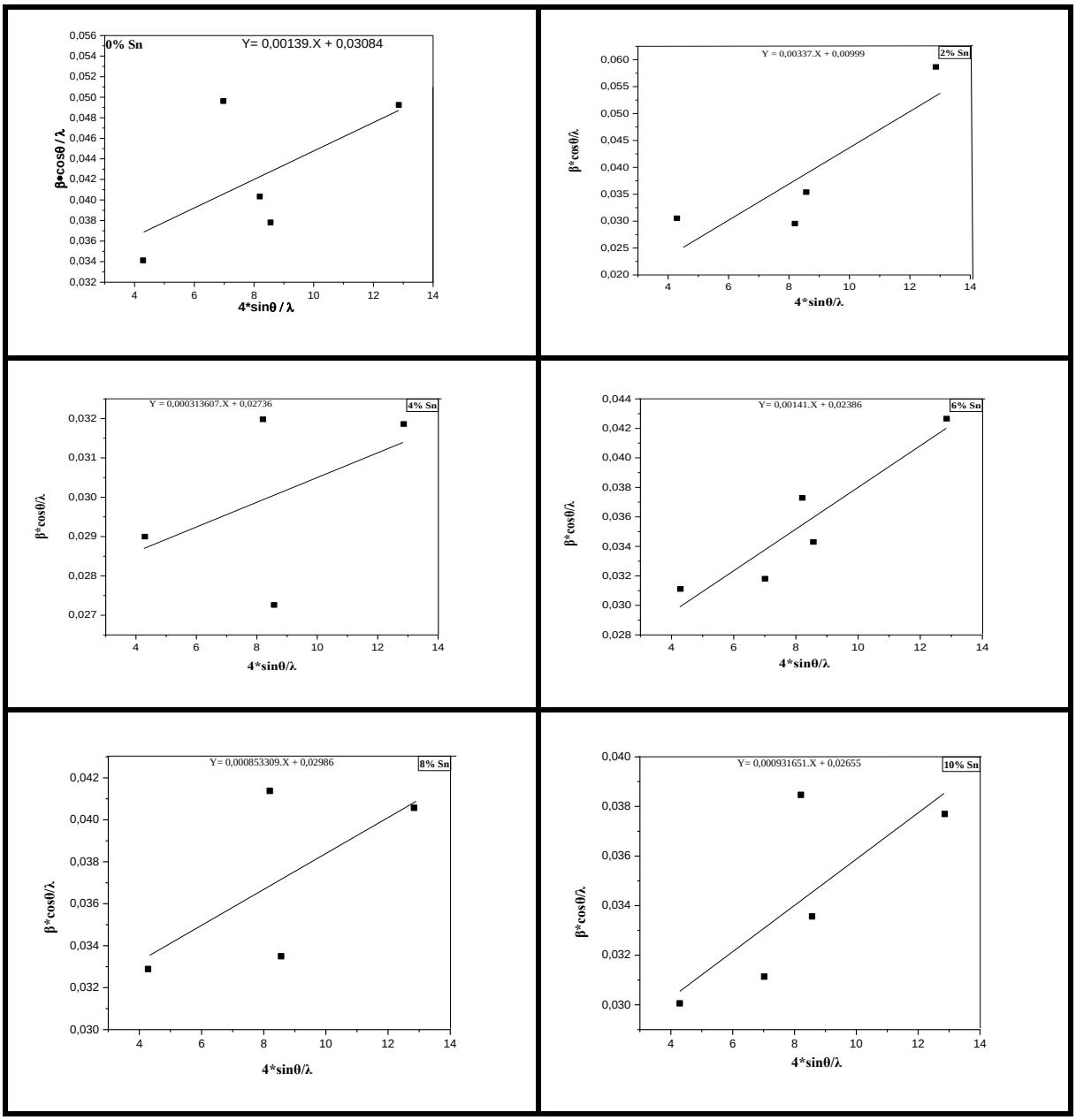

Figure 6. Williamson-Hallplots of Sn-doped Co_3O_4 for cubic spinel structure.

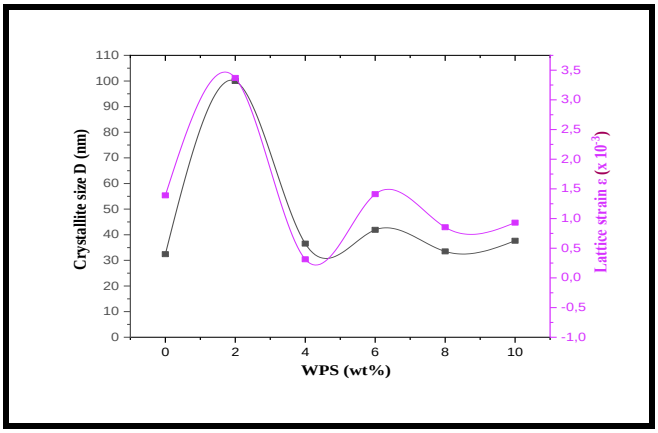

Figure 7. Lattice strain and crystallite size of Sn-doped Co_3O_4 from Williamson-Hall plots.

From figure 9 (the conclusion of the figure 8)of Zn doping, the crystallite size decreases from 32.4 nm to 16.2 nm when WPZ concentration increases from 0 to 6wt% and continues increasing up to 31.15 nm for a WPZ of 10wt%.The lattice strain (ε) of Zn doping increases from $1{,}39.10^{-3}$ to $2{,}03.10^{-3}$ when WPZ concentration increases from 0 to 2wt%, continues decreasing to $0{,}94.10^{-3}$ when WPZ concentration increases from 6wt% and after this content decrease of lattice strain to 1.88 % for a WPS of 10 wt%.. As seen, the higher value of grain size is found at2wt% of Sn doping. This indicates an improvement in the crystalline state of the thin films of cobalt oxide. In addition, the lower value of the grain size is found in the 4wt%ofSn doping. Therefore, when doping with Sn, it is advisable to use lower values.

Table 4. Williamsson-Hall XRD analysis of Zn-doped Co_3O_4 for cubic spinel structure.

(hkl)		%0	2%	4%	6%	8%	10%
111	$4\sin\theta/\lambda$	4,284334	4,2942	4,297	4,29277	4,299	4,28723
	$\beta\cos\theta/\lambda$	0,0341223	0,05048	0,051101	0,06885	0,07112	0,051002
220	$4\sin\theta/\lambda$	6,975272	-	-	-	-	-
	$\beta\cos\theta/\lambda$	0,0496311	-	-	-	-	-
311	$4\sin\theta/\lambda$	8,195901	-	8,2067	-	-	8,19305
	$\beta\cos\theta/\lambda$	0,04034	-	0,05069	-	-	0,036998
222	$4\sin\theta/\lambda$	8,555871	8,5675	8,57115	8,56974	8,5489	8,55707
	$\beta\cos\theta/\lambda$	0,0378099	0,05681	0,06439	0,063588	0,05984	0,051564

511	$4\sin\theta/\lambda$	12,851565	12,8575	12,85086	12,8422	12,85685	12,8439
	$\beta\cos\theta/\lambda$	0,0492499	0,06784	0,061395	0,07688	0,08763	0,07025
Crystallite size D (nm)		32,42	24,40	21,65	16,20	17,78	26,21
Lattice strainε (x 10^{-3})		1,39	2,03	1,26	0,94	1,94	1,88

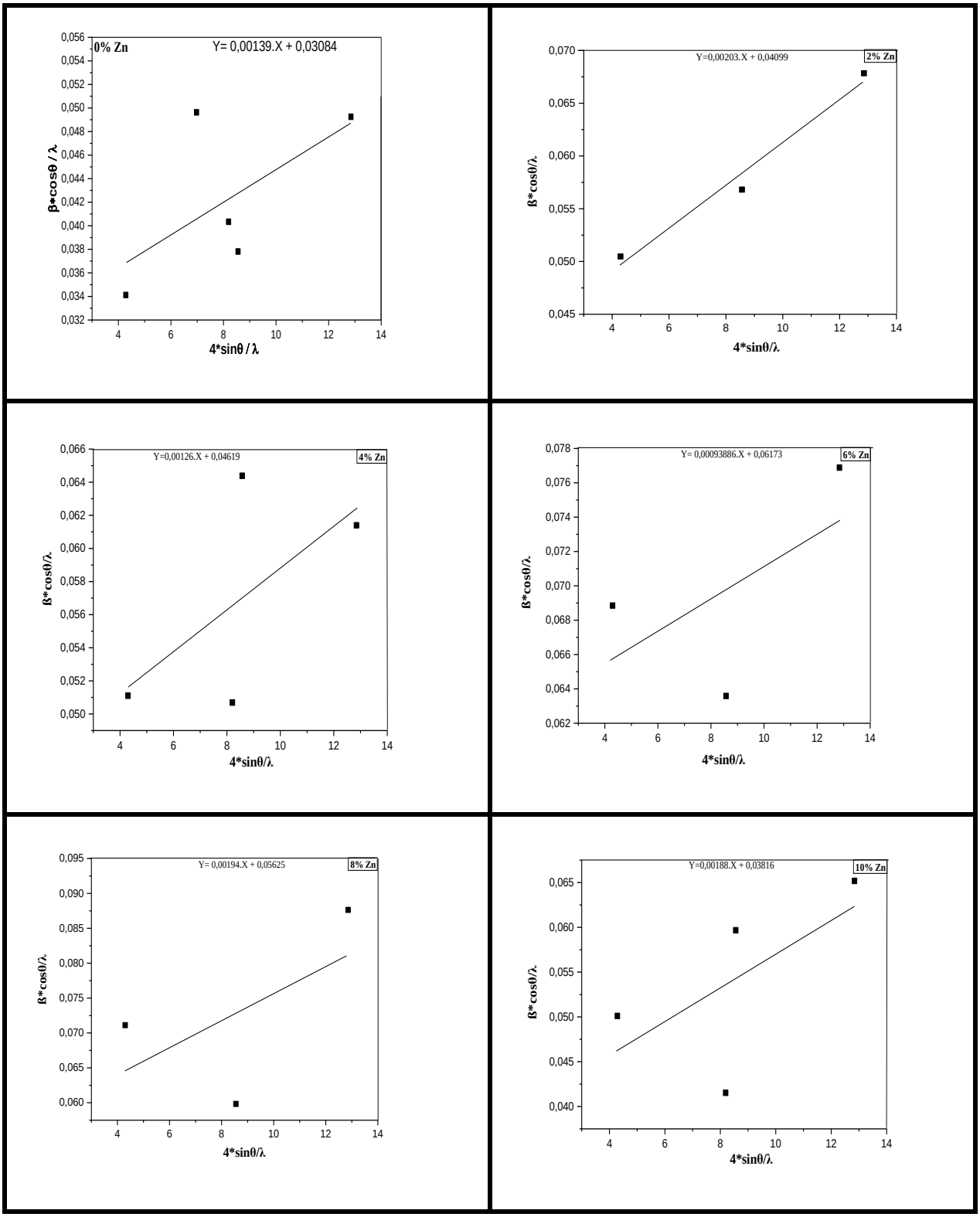

Figure 8. Williamson-Hall plots of Zn-doped Co_3O_4 for cubic spinel structure.

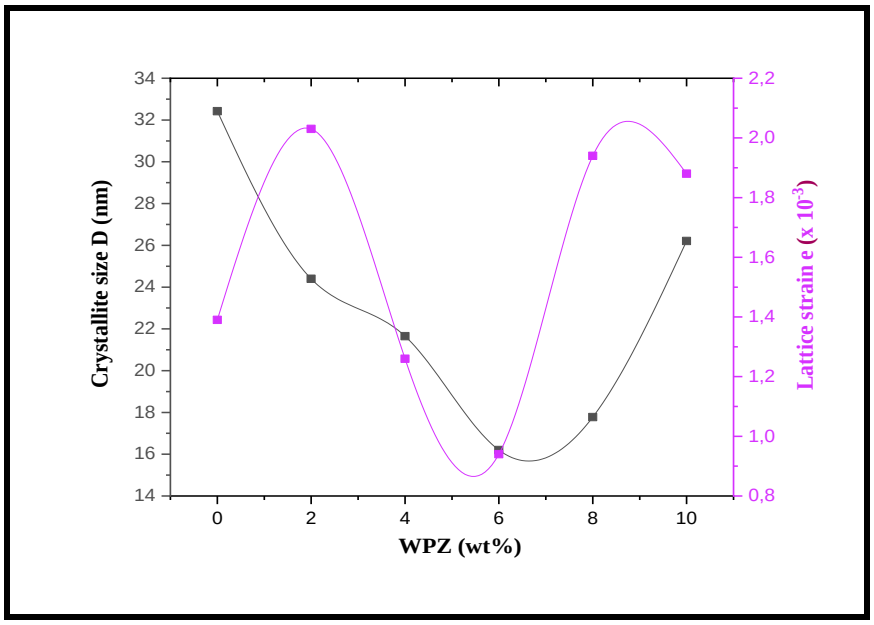

Figure 9. Lattice strain and crystallite size of Zn-doped Co_3O_4 from Williamson-Hall plots.

Using the crystal size, the dislocation (δ_{dislo}) lines per unit volume of the crystal is calculated by using the Williamson and Smallman (equation III.8). (see chapter II). It is plotted as a function of the WPN (N=Mn, La, Sn and Zn) doping concentration for all the formed thin films (Figure 10). It is found to slightly decrease from $7{,}948 \times 10^{+14}$line/ $m^2$with WPM doping content increment up to 2 wt%. Then, it increases with further increase of WPM doping reaching $19{,}069 \times 10^{+14}$line/ $m^2$for 10 wt%. As seen, the higher value of grain size is found at 10wt% of Zn doping. This indicates an improvement in the crystalline state of the thin films of cobalt oxide. In addition, the lower value of the grain size is found in the 6wt%ofZn doping. Therefore, when doping with Zn, it is advisable to use higher values.

Finally, comparing the measured crystallite size values on all the studied Co_3O_4:N thin films to those previously obtained on others doped CVD and sol-gel made Co_3O_4 on , it find that they are of the same range order [2;10-12].

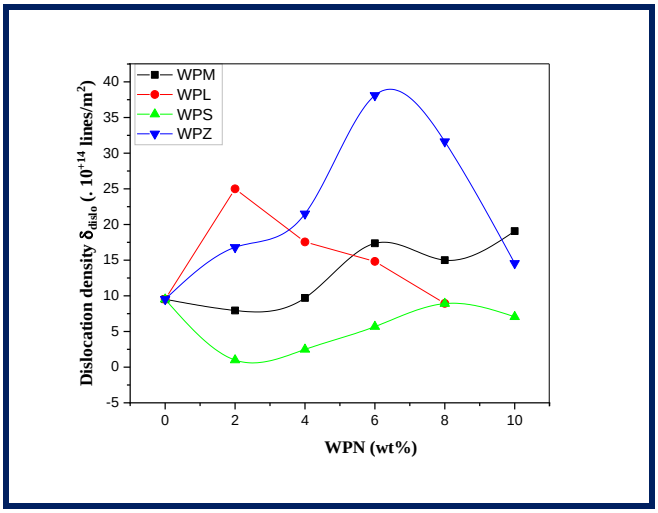

Figure 10. The dislocation density (δ_{dislo}) of Co_3O_4:N (N= Mn, La, Sn and Zn) thin films for different N doping.

Table 5. The calculated values of crystallite size(D), lattice strain (ε) and dislocation density (δ_{dislo}) in Co_3O_4:N thin films.

	WPN (wt%)	D (nm)	ε(.10^{-3})	δ_{dislo}(.10^{14} lines/m^2)
Co_3O_4	0	32,4254	1,39	9,51
Co_3O_4:Mn	2	35,4736	2,75	7,948
	4	32,1027	2,38	9,705
	6	24,1371	0,737	17,361
	8	25,8264	0,754	15
	10	22,899	0,288	19,069
Co_3O_4:La	2	20	0,12	25
	4	23,87	0,515	17,55
	6	25,97	0,512	14,82
	8	33,44	1,55	8,94
	10	-	-	-
Co_3O_4:Sn	2	100	3,37	1,00
	4	36,55	0,3136	2,48
	6	41,91	1,41	5,69
	8	33,49	0,8533	8,916
	10	37,665	0,9316	7,05
Co_3O_4:Zn	2	24,4	2,03	16,8
	4	21,65	1,26	21,51
	6	16,2	0,94	38,1
	8	17,78	1,94	31,63
	10	26,21	1,88	14,56

In the Co_3O_4:La thin films, the dislocation density (δ_{dislo}) increases from $25 \times 10^{+14}$line/ m^2 with La doping content increment up to 2 wt%. Then, it decreases with further increase of La doping concentration reaching $8{,}94 \times 10^{+14}$line/ m^2 for 8wt%. This behavior can be connected to the observed crystallite size increasng with the doping content.

In the Co_3O_4:Sn thin films, the dislocation density (δ_{dislo}) decreases from $1{,}0 \times 10^{+14}$line/ m^2 with Sn doping content increment up to 2 wt%.Then, it increases with further increasing of Sn doping concentration reaching $7{,}05 \times 10^{+14}$line/ m^2 for 10 wt%, suggesting that the resultant thin films, in particular, exhibits the best crystalline quality.

In the Co_3O_4:Zn thin films, the dislocation density (δ_{dislo}) increases from $38{,}1 \times 10^{+14}$line/ m^2 with Zn doping content increment up to 6 wt%. Then, it decreases with further increasing of Zn doping concentration reaching $14{,}56 \times 10^{+14}$line/ m^2 for 8wt%. This indicates that the resulted thin films, exhibits the lower crystalline quality.

I.1.2. Lattice parameters and d-spacing

Co_3O_4:Mn has a cubic structure with cell parameters are calculated (equation 5 in the chapter 2)TableIII.2 shows the cell parameters a and d-spacing experimental and theoretical (see table 6). It is noted that the experimental cell parameters are larger than the theoretical cell parameters, which indicates the presence of expansion in the cell.

Table 6. Structural parameter of Co_3O_4:Mn thin films.

WPM (wt%)	**d_{hkl} (nm)**		**a (nm)**		
	(111)	**(222)**	**(111)**	**(222)**	
0	0.4668	0.2337	0.80855	0.8097	
2	0.4666	0.2336	0.80816	0.8093	$d_{theo}(111) = 0{,}466700$Å
4	0.4670	0.2339	0.808963	0.8102	$d_{theo}(222) = 0{,}233400$Å
6	0.4676	0.2335	0.8099	0.8089	$a_{theo} = 0{,}80837$ Å
8	0.4674	0.2335	0.8096	0.8090	
10	0.4674	0.2340	0.8096	0.8109	

In the Co_3O_4:La thin films, Lattice parameters is noted that the experimental cell parameters are less than the theoretical cell parameters (see table 7), which indicates the presence of expansion in the cell.

Table 7. Structural parameter of Co_3O_4:La thin films

WPM (wt%)	d_{hkl} (nm)		a (nm)		
	(111)	(222)	(111)	(222)	
0	0.4668	0.2337	0.80855	0.8097	
2	0.4656	0.2333	0.80649	0.80808	$d_{theo}(111) = 0{,}466700$Å
4	0.4651	0.2333	0.80562	0.80808	$d_{theo}(222) = 0{,}233400$Å
6	0.4660	0.2325	0.80719	0.80800	$a_{theo} = 0{,}80837$ Å
8	0.4665	0.2335	0.80806	0.80887	
10	0.4635	-	0.80290	-	

In the Co_3O_4:Sn thin films, Lattice parameters is noted that the experimental cell parameters are less than the theoretical cell parameters (see table 8), which indicates the presence of compression in the cell.

Table 8. Structural parameter of Co_3O_4:Sn thin films

WPM (wt%)	d_{hkl} (nm)		a (nm)		
	(111)	(222)	(111)	(222)	
0	0.4668	0.2337	0.80855	0.8097	
2	0.4661	0.2334	0.80727	0.8084	$d_{theo}(111) = 0{,}466700$Å
4	0.4656	0.2333	0.80648	0.8082	$d_{theo}(222) = 0{,}233400$Å
6	0.4666	0.2335	0.80824	0.8090	$a_{theo} = 0{,}80837$ Å
8	0.4672	0.2337	0.80930	0.8095	
10	0.4644	0.2334	0.80779	0.8109	

Table 9. Structural parameter of Co_3O_4:Zn thin films

WPM (wt%)	d_{hkl} (nm)		a (nm)		
	(111)	(222)	(111)	(222)	
0	0.4668	0.2337	0.80855	0.8097	

2	0.4657	0.2334	0.80669	0.8087	$d_{theo}(111) = 0{,}466700Å$ $d_{theo}(222) = 0{,}233400Å$ $a_{theo} = 0{,}80837$ Å
4	0.4654	0.2333	0.80617	0.8083	
6	0.4659	0.2334	0.8069	0.8084	
8	0.4652	0.2339	0.80579	0.81042	
10	0.4665	0.2337	0.80800	0.809	

In the Co_3O_4:Zn thin films, Lattice parametersis note that the experimental cell parameters are less than the theoretical cell parameters (see table 9), which indicates the presence of compression in the cell.

II. Morphological properties

II.1. Surface morphology

II.1.1. Mn doping

The scanning electron microscopy images ofCo_3O_4: Mn thin films are deposited at 400°C with different PWM are shown in figure 11. The images of thin films are almost homogeneous and well covered without any pinholes and cracks on the glass substrates. The density and distribution of the material deposited clearly depend on the PWM; on higher percentages of Mn, as can see surface of the Co_3O_4 film has changed to granular surface. The evolution of the surface in Co_3O_4: Mn as a function of the PWM as a function of the deposition percentage can be explained as follows; at low deposition percentage, this means that a few amounts of Co_3O_4:Mn are deposited, a smooth surface is then formed. Increasing of Mn amount leads to decrease in the smooth surface is then formed, which incite the increase in thickness of thin films.

The chemical composition of elements present in the Mn-doped Co_3O_4thin films is determined using EDS spectra with the scanning electron microscopy (SEM).figure 6 shows the atomic percentages of elements present in the Mn-doped Co_3O_4. The oxygen and manganese density increases, but the cobalt density decreases in thin films. From the EDS spectra, from percentages for chemical compositions of the films are obtained near to the stoichiometric in nature. Such surface morphology may offer expanded surface area, beneficial for gas sensing [11] and electrochromic applications [13].

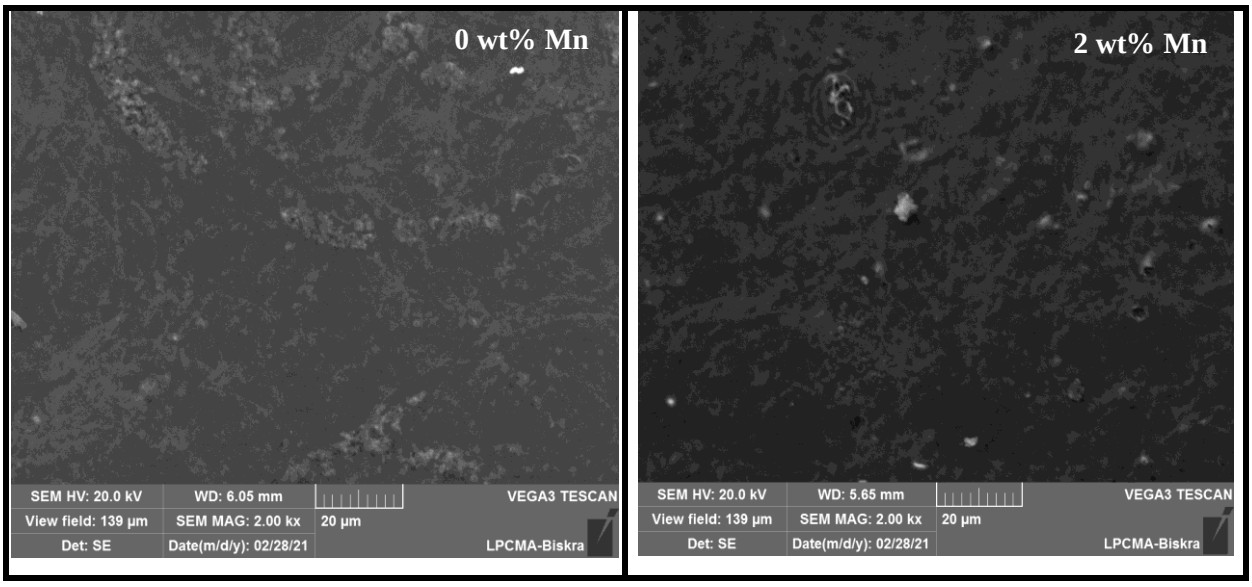
0 wt% Mn
SEM HV: 20.0 kV
WD: 6.05 mm
VEGA3 TESCAN
View field: 139 µm
SEM MAG: 2.00 kx
20 µm
Det: SE
Date(m/d/y): 02/28/21
LPCMA-Biskra
2 wt% Mn
SEM HV: 20.0 kV
WD: 5.65 mm
VEGA3 TESCAN
View field: 139 µm
SEM MAG: 2.00 kx
20 µm
Det: SE
Date(m/d/y): 02/28/21
LPCMA-Biskra

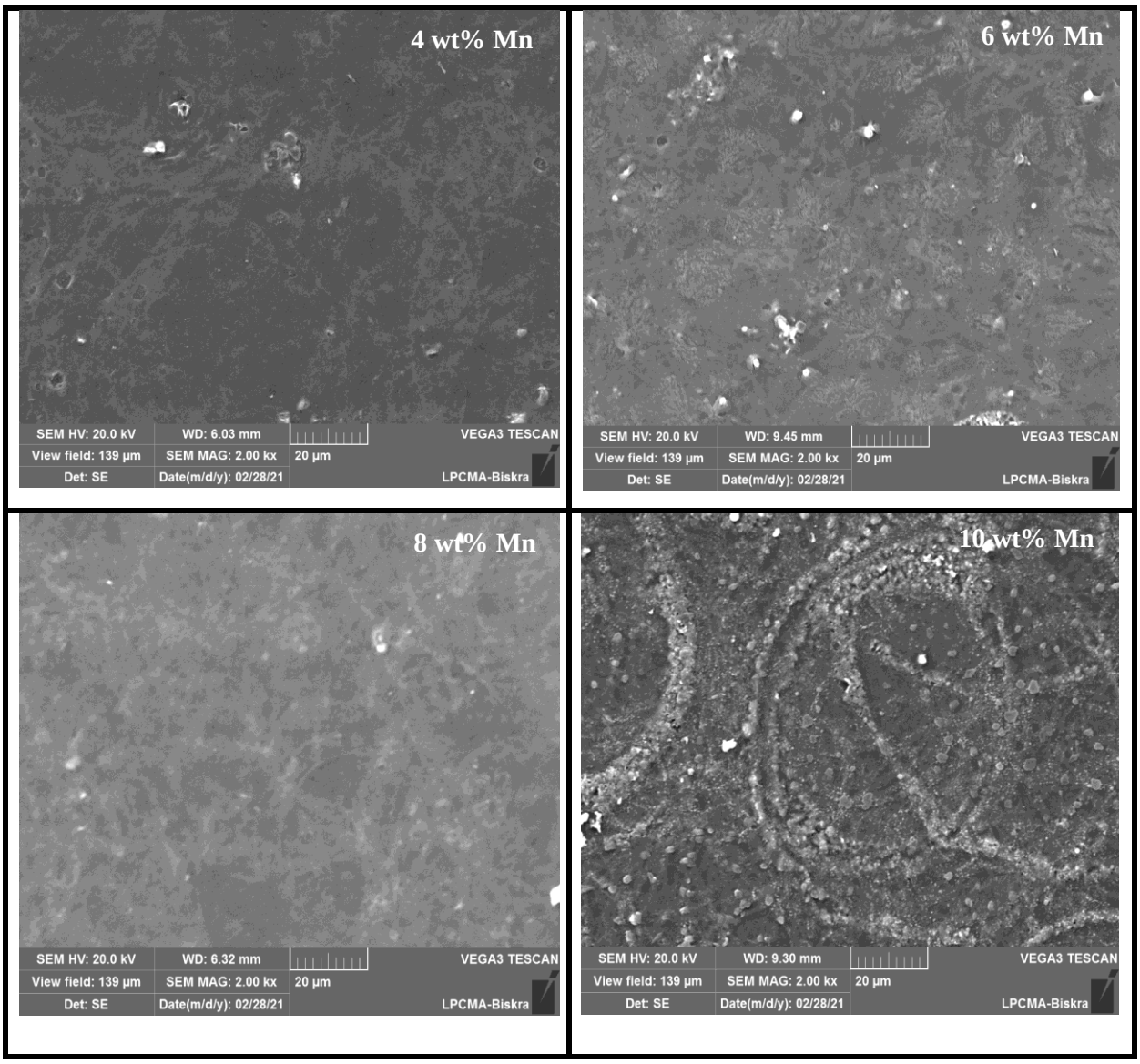

Figure 11. Top view SEM images of Co3O4:Mn thin films deposited on glass at 400°C.

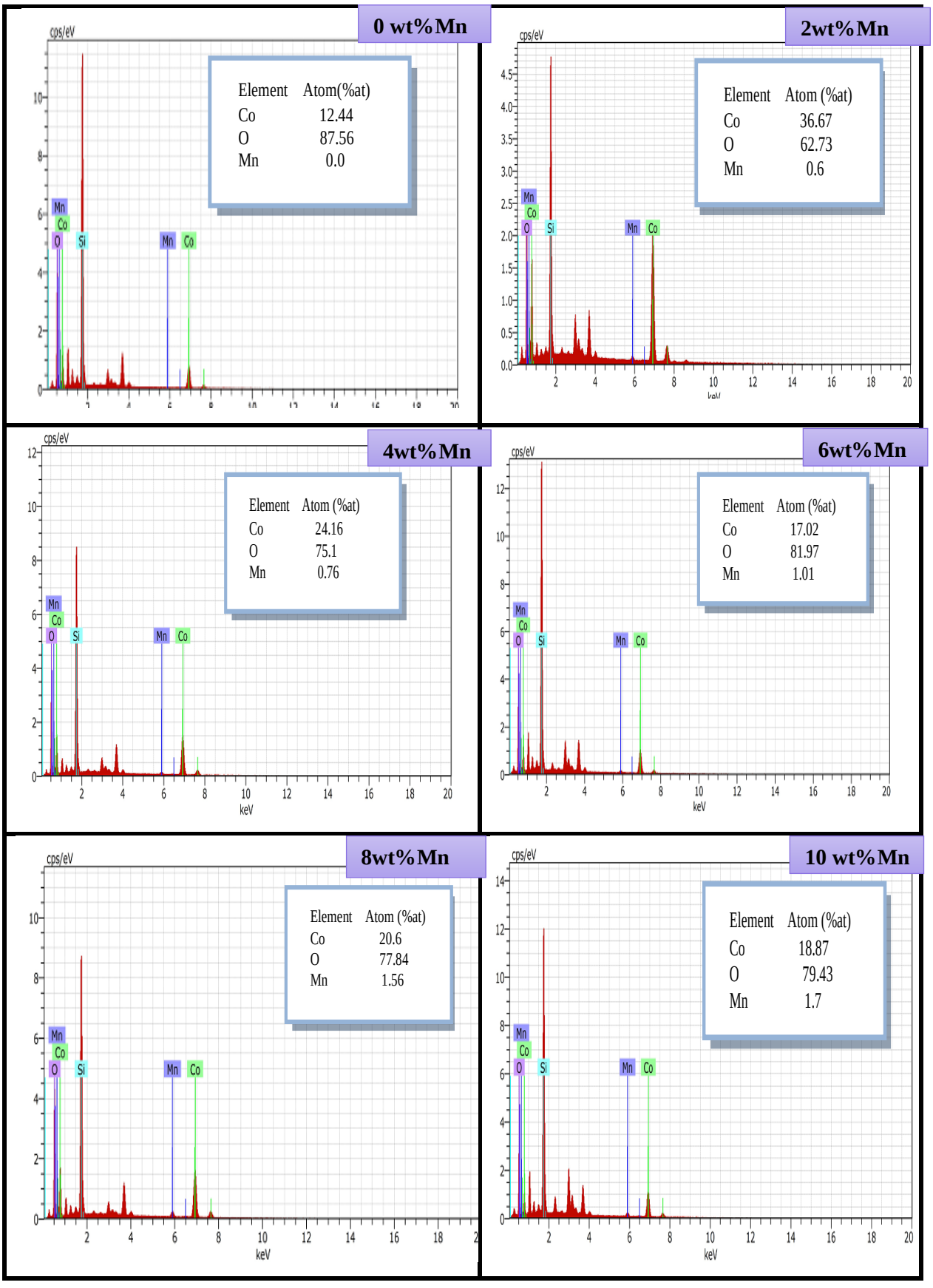

Figure 12. EDS analysis of Co_3O_4:Mn thin films deposited on glass at 400°C.

The morphological arrangement of the Mn-doped Co_3O_4 thin films are deposited at 400°C with different weight percentage of manganese (WPM) is analyzed using atomic force microscopy (AFM) with three dimensional (3D) and is presented in figure 13. From AFM micrographs it is shown that the straight acicular nanorods (SANRs) is consistent with the results reported elsewhere [14], whereas, thin films of lower WPM, it shows fewer the SANR compared to the films with a higher WPM. A quantitative analysis of surface roughness upon small-scale image using the roughness function of the weight percentage of Mn led to Rms values nm of 217 and 566 nm for lower WPM and higher WPM, respectively. The evolution of film surface as a function of the WPM as a function of the deposition rate can be explained as follows; at low percentage rat, this means that a few amounts of the Mn-doped Co_3O_4 are deposited; therefore, fewer SANRs appear, so the surface is less rough. Increasing the WPM leads to an increase in the number of SANRs , and thus is increased roughness.

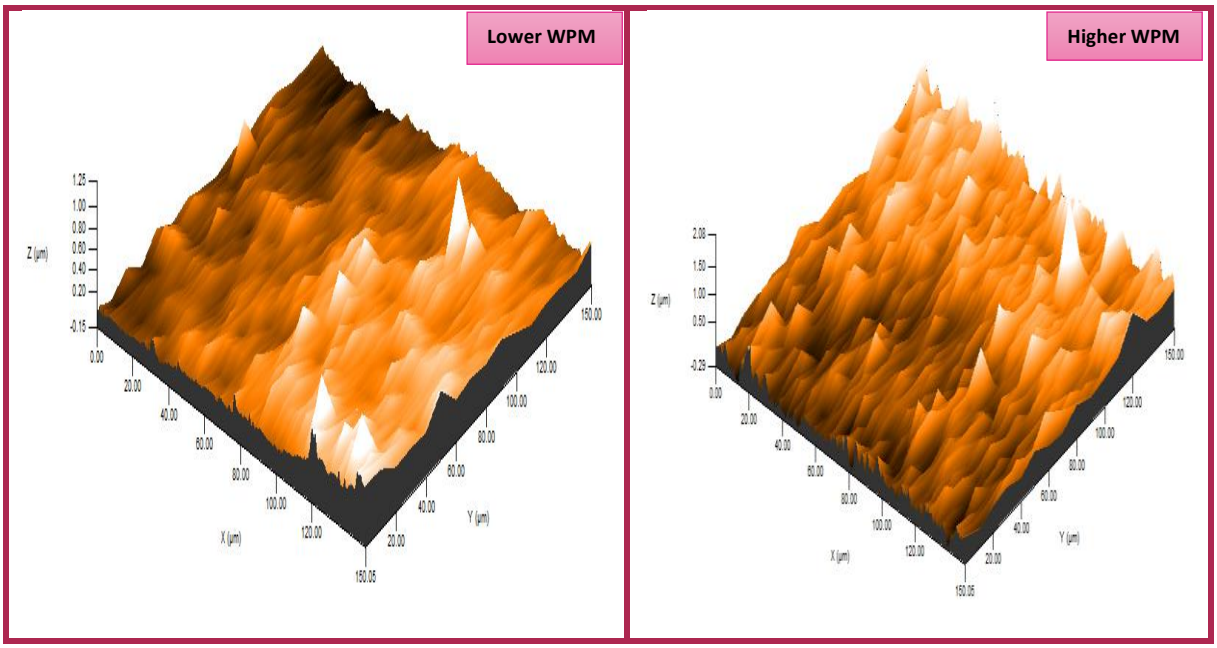

Figure 13. 3DAFM images of Co3O4: Mn thin films with different WPM.

II.1.2. La doping

The morphological arrangement of the La-doped Co_3O_4 thin films deposited at 400°C with different weight percentage of manganese (WPM) was analyzed using atomic force microscopy (AFM) with three dimensional (3D) and is presented in figure 14. From AFM micrographs it is shown that the straight acicular nanorods (SANRs)is consistent with the results reported elsewhere [14], whereas, thin films of lower WPL, it shows fewer the SANR

compared to the films with a higher WPL. The evolution of film surface as a function of the WPM as a function of the deposition rate can be explained as follows; at low percentage rat, this means that a few amounts of the Mn-doped Co_3O_4 are deposited; therefore, fewer SANRs appear, so that the surface is less rough. Increasing the WPM leads to an increase in the number of SANRs, and thus increased roughness.

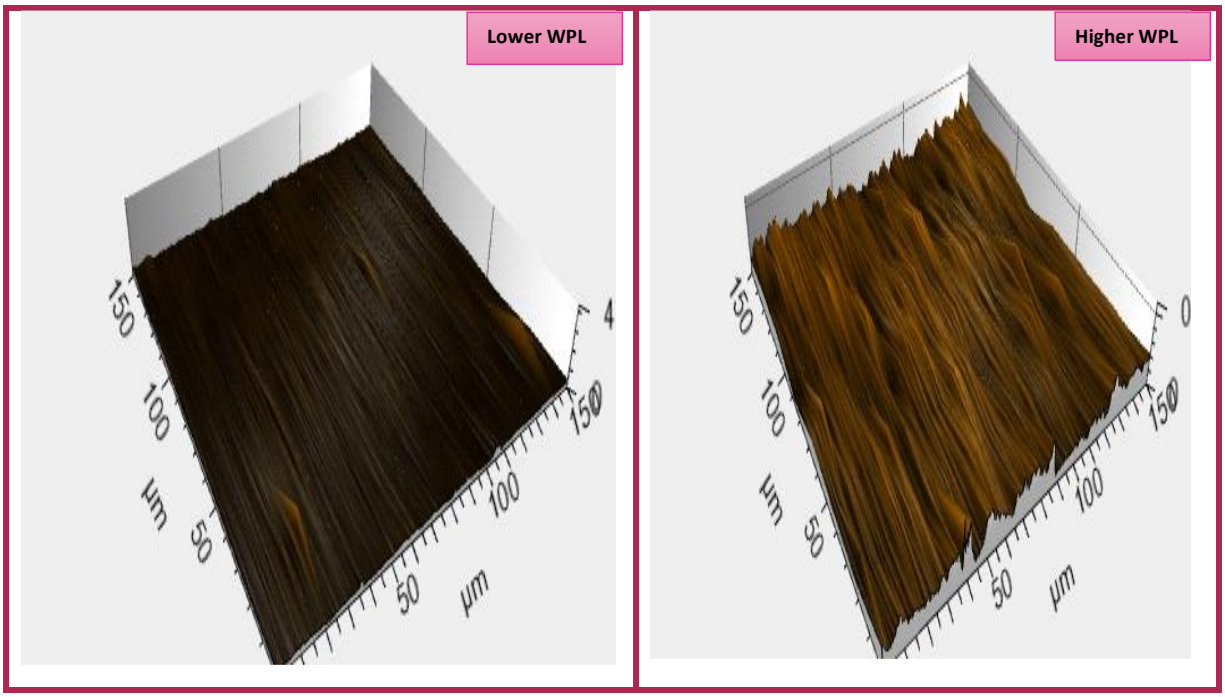

Figure 14. 3DAFM images of Co3O4: La thin films with different WPL.

II.1.3. Sn doping

The SEM images of lower WPS and higher WPS thin films are shown in figure 15**.** It is confirmed from SEM images, the spray pneumatic technique can deliver thin films with smooth surface morphology. The images show that Sn doping does not affect significantly the surface morphology of Co_3O_4 thin films.

The Study of the composition analysis of the coated films by EDS spectrum is shown in figure 15.Through the EDS spectrum confirms the presence of the required elements such as Sn, Co and O. We note that atomic ratio Sn increased with a linear decrease in O and Co.

Which indicates that the pneumatic spraying method can provide a thin film with good stoichiometry nature.

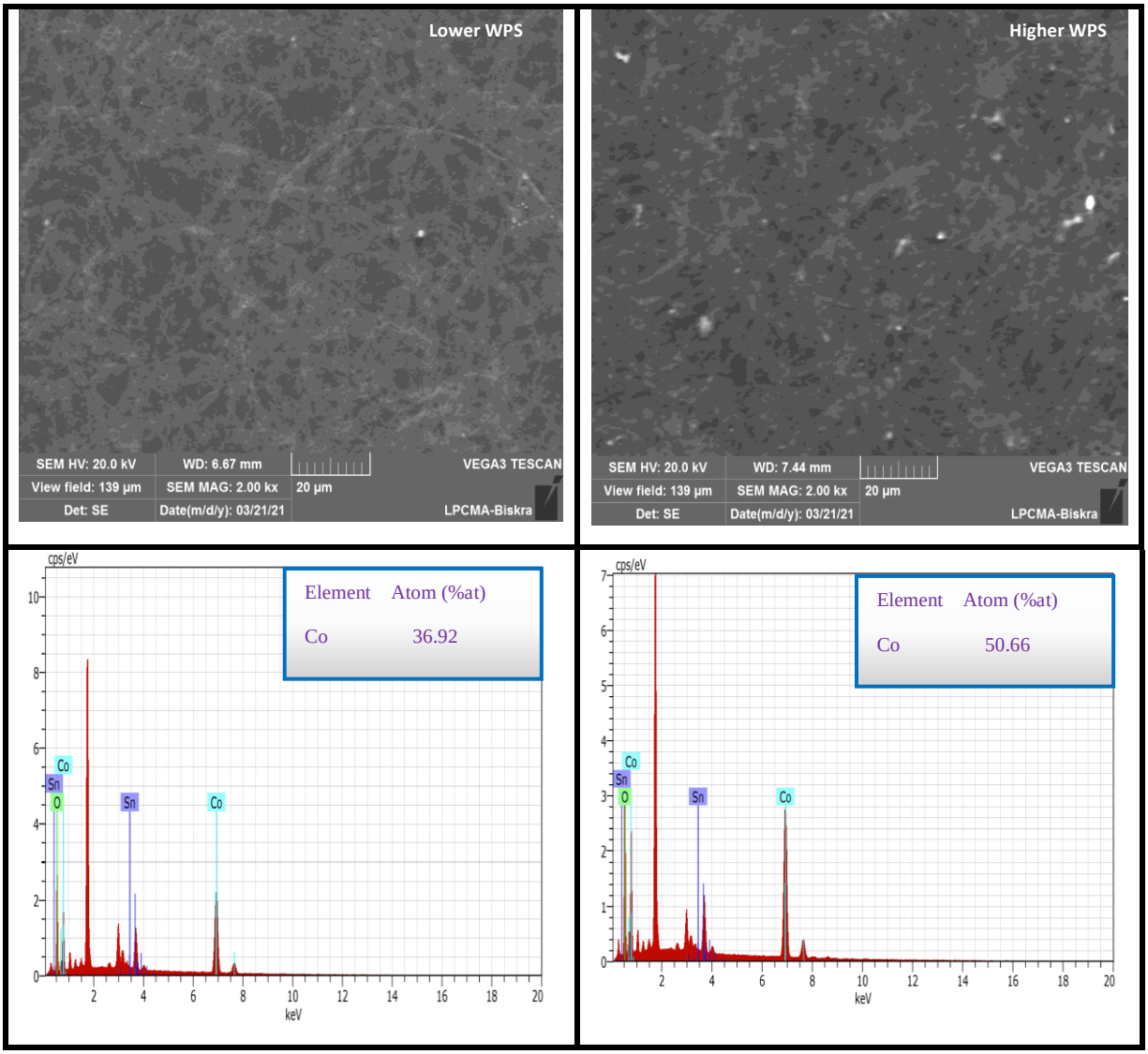

Figure 15. SEM images and EDS spectra of Co3O4:Sn thin films.

III. Conclusion

This chapter focuses on the effect of manganese, Lanthanum, tin and zinc doping on the structural, morphological and compositional properties of cobalt oxide thin films are deposited by pneumatic spray on glass substrates at 400°C temperature. According to DRX study, Co_3O_4:N (N= Mn, La, Sn and Zn)thin films show cubic spinel crystalline structure which oriented along to (111) plane. Thus, batter crystalline quality is obtained for doping weight percent Mn (2 wt%), La (8wt%), Sn (2wt%) and Zn (10 wt%).

Top view SEM images of the thin films show that they are nearly homogeneous and well covered without any holes and cracks. Also, the top view SEM images do not show any modification in the surface morphology of the thin films produced after doping. From the three dimensional (3D) AFM micrographs, it is evident that the straight acicular nanorods (SANRs). Also show that the films have a rough surface.

References

[1] R.C. Ambare, S.R. Bharadwaj, B.J. Lokhande,Electrochemical characterization of Mn: Co_3O_4 thin films prepared by spray pyrolysis via aqueous route, Current Applied Physics, 14(2014) 1582-1590.

[2] Nabila Kouidri . Saâd Rahmane. Abdelkrim Allag, Substrate temperature-dependent properties of sprayed cobalt oxide thin films, Journal of Materials Science: Materials in Electronics30 (2019) 1153–1160.

[3] R. Venkatesha, C. Ravi Dhasa, R. Sivakumarb, T. Dhandayuthapanib, P. Sudhagarc, C. Sanjeevirajad , A. Moses Ezhil Raje. Analysis of optical dispersion parameters and electrochromic properties of manganese-doped Co3O4 dendrite structured thin films. Journal of Physics and Chemistry of Solids 122 (2018) 118–129.

[4] M. Manickam, V. Ponnuswamy, C. Sankar, R. Mariappan, R. Suresh, Influence of Substrate Temperature on the Properties of Cobalt Oxide Thin Films Prepared by Nebulizer Spray Pyrolysis (NSP) Technique, Silicon 8 (2016) 351–360.

[5] R. Manogowri, R. Mary Mathelane, S. Valanarasu, I. Kulandaisamy, A. Benazir Fathima, A. Kathalingam, Effect of annealing temperature on the structural, morphological, optical and electrical properties of Co_3O_4 thin film by nebulizer spray pyrolysis technique *Journal of Materials Science: Materials in Electronics*volume 27 (2016) 3860–3866.

[6] A. Louardi, A. Rmili, F. Ouachtari, A. Bouaoud, B. Elidrissi,H. Erguig, Characterization of cobalt oxide thin films prepared by a facile spray pyrolysis technique using perfume atomizer, Journal of Alloys and Compounds,509 (2011) 9183–9189.

[7] Z. Bencharef, A. Chala, R. Messemeche, Y. Benkhetta, The physical properties of spinel cupic Co_3O_4 thin films prepared by a PSM, Main Group Chemistry 21(2022) 329-340.

[8] Abdelhakim. Mahdjoubi, Abdaali. Hafid, Mohammed. Salah Aida, Abdelhamid Benhaya, An original way to obtain porous $Zn_{(1-x)}Mg_xO$ thin films by spray pyrolysis technique, Semiconductor Physics Quantum Electronics & Optoelectronics (2017)55-63.

[9] Messemche Radhia,Elaboration and characterization of undoped and doped titanium dioxide thin layers by sol gel (spin coating) for photocatalytic applications, Doctorat thesis, University Mohammad Khider of Biskra, (2021).

[10] C. Ravi Dhas, R.Venkatesh, R.Sivakumar,T. Dhandayuthapani, B.Subramania, C.Sanjeeviraja, A. Moses Ezhil Raj, Electrochromic performance of chromium-doped Co_3O_4 nanocrystalline thin films prepared by nebulizer spray technique, Journal of alloys and Compounds 784(2019)49-59.

[11] R. Venkatesh, C. Ravi Dhas, R. Sivakumar, T. Dhandayuthapani, B. Subramania, C. Sanjeeviraja, A. Moses Ezhil Raj, Tailoring the physical properties and electrochromic performance of nebulizer spray coated Co_3O_4 films through copper doping, Solid State Ionics 334 (2019)5-13.

[12] Sahar Soltani, Seyde Mohammad Rozati, Mohammad Bagher Askari, Optical and electrochemical properties of spinal cubic nanostructured thin film Co_3O_4prepared by spray pyrolysis, Physica B: physics of Condensed Matter 625(2022)413464.

[13] C. RaviDhas, R.Venkatesh, R.Sivakumar, A. Moses EzhilRaj, C.Sanjeeviraja, Effect of solution molarity on optical dispersion energy parameters and electrochromic performance of Co_3O_4 films, Optical Materials, 72 (2017) 717-729.

[14] Ouahiba Herzallah, Hachemi Ben Temam, Asma Ababsa, Abderrahmane Gana, Electrodeposited Ni-Co Films from Electrolytes with Different Co Contents, Defect and Diffusion Forum 406 (2021) 219-228.

CHAPTER FOUR

Optical and electrical study ofCo$_3$O$_4$:N (N= Mn, La, Sn and Zn) Thin Films.

I. Introduction

It is known that the properties of the Co_3O_4 thin films are obtained by pneumatic spray method which is related to the deposition parameters of this technique. Therefore, deposition conditions have been extensively studied in order to improve these properties of Co3O4 fine sprays. The most studied parameters are: substrate temperature [1-2], deposition time [3], precursor molarity [4] and doping [5-9].

This chapter, the effect of incorporating different doping on the optical and electrical properties of Co_3O_4:N (N= Mn, Sn, La and Zn) thin films deposited by pneumatic spray method on glasses substrates annealing at 400°C is studied. An aqueous solution with a concentration 0,1M and a precipitation time of 4minutes is used. These properties are studied by photo spectrophotometry and four-point probe measurements.

II. Optical properties

II.1. Transmittance properties

In order to investigate the effect of doping on the optical properties of Co_3O_4 thin films, UV-Vis-NIR studies are performed. In fact, we remark, from figure 1, that the presence of the same shape in the visible region reflects the homogeneity of the grown films. Moreover, a significant decrease of transmittance in both visible and infrared regions after Mn, Sn, La and Zn doping. From the same figure, we can note that the transmittance of the films increases only when doped with Mn for 2wt%in visible region and for 2,8 and 10wt% in infrared region. The optical transmittance of the film is influenced by several factors such as surface roughness, structural defects in the film, porosity, film thickness, crystallinity, color of the film and surface structure [10-18]. This reduction is very probably related to the spinel phase have low crystalline size and dark color of the film which increasing light scattering and absorption. This leads to minimum transmittance in the films. Similar observation has been found by others researchers [1,5-9]. These films are allowed to be use in solar cells and the PN junction [19-21].

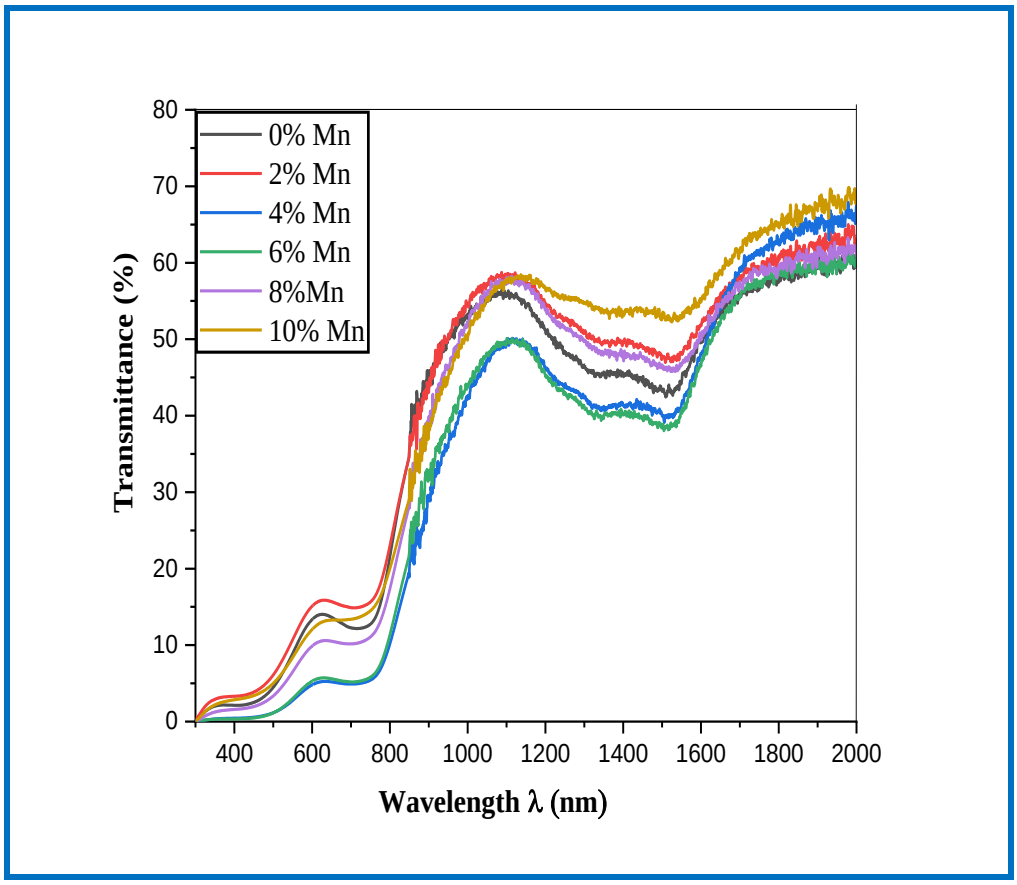
0% Mn
2% Mn
4% Mn
6% Mn
8%Mn
10% Mn
Transmittance (%)
Wavelength λ (nm)
0
10
20
30
40
50
60
70
80
400
600
800
1000
1200
1400
1600
1800
2000

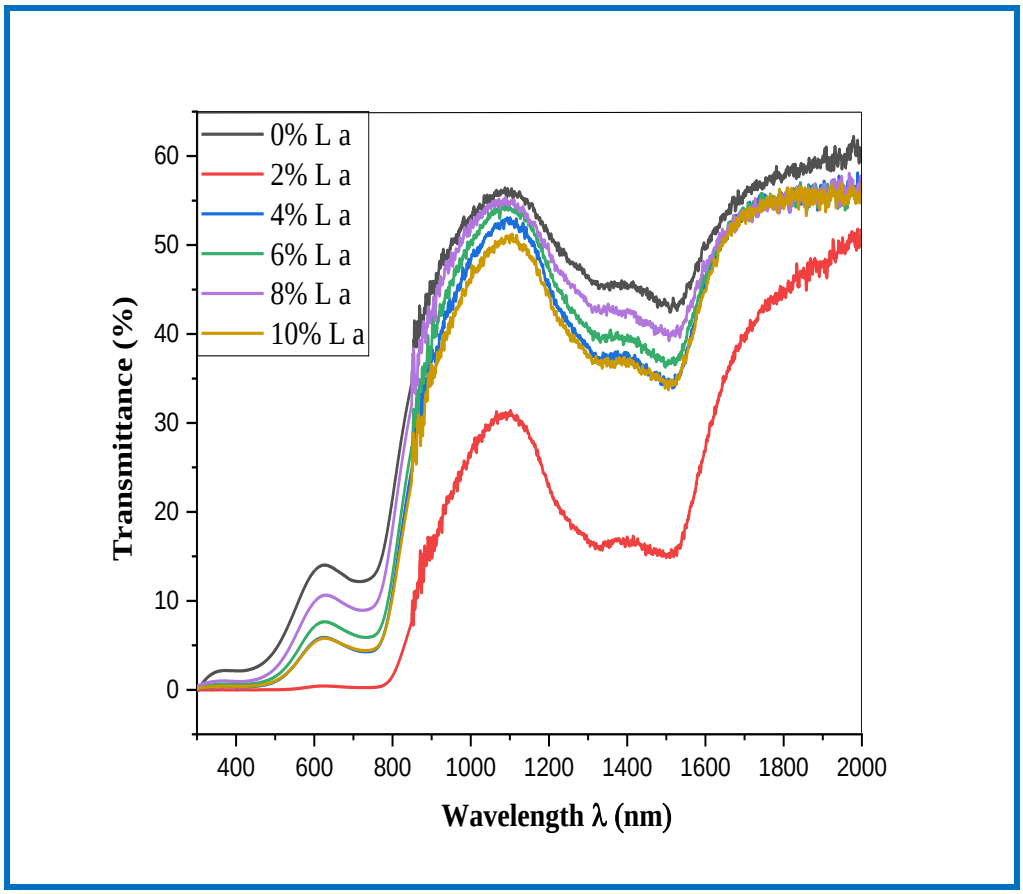
0% L a
2% L a
4% L a
6% L a
8% L a
10% L a
Transmittance (%)
Wavelength λ (nm)
0
10
20
30
40
50
60
400
600
800
1000
1200
1400
1600
1800
2000

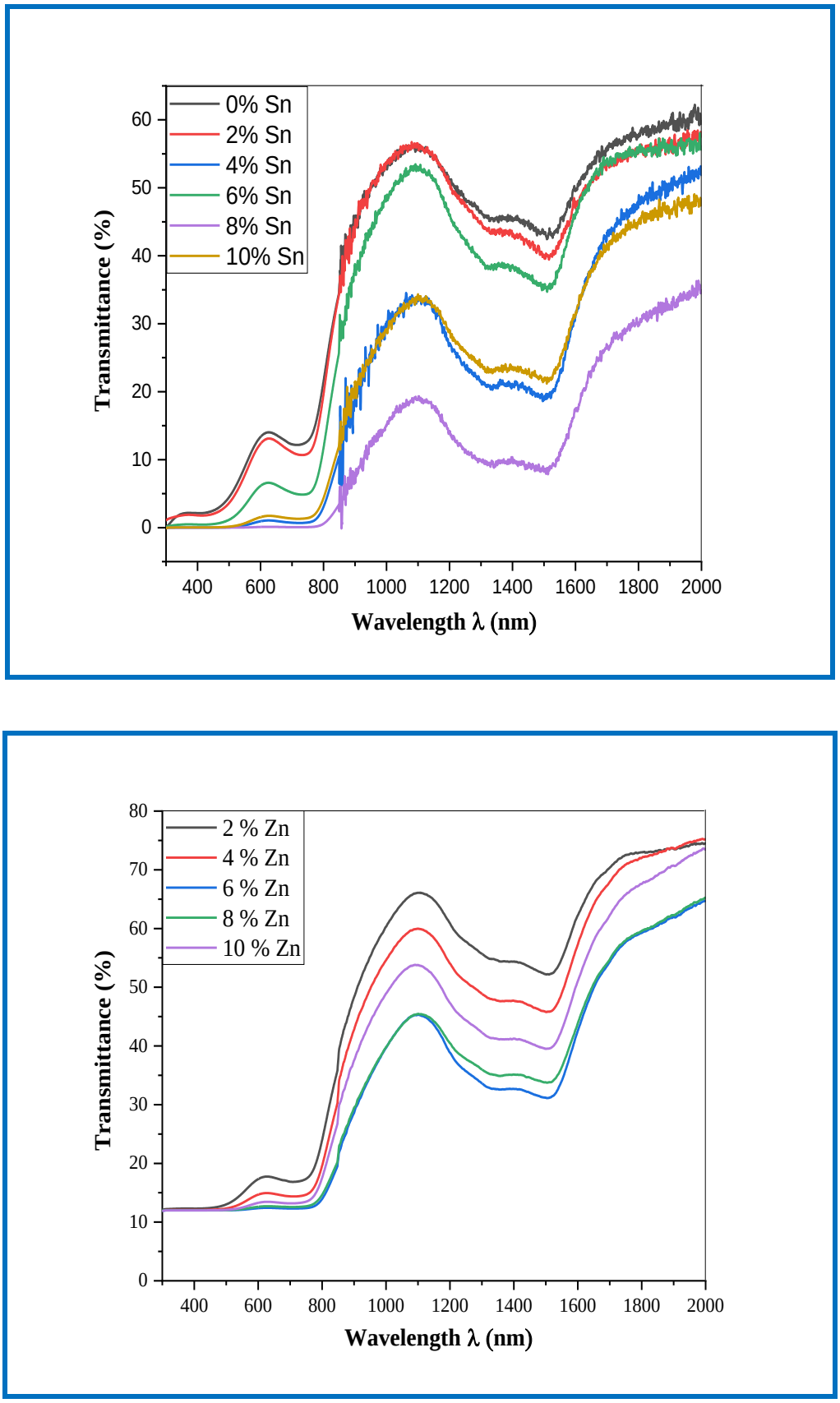

Figure 1. Optical transmittance spectra of pneumatic spray method (CVD) made Co3O4:N (N= Mn, La, Sn and Zn) thin films compared to those of undopedCo3O4 one.

II.2. Film thickness

The thickness (t_h) of N-doped Co_3O_4 thin films as a function of the PWN(N= Mn, La, Sn and Zn) was calculated from UV-visible data using the following equation [22-23].

$$t_h = \frac{\lambda_1 \lambda_2}{2n(\lambda_1 - \lambda_2)} \qquad (1)$$

Where, n is the refractive index at two adjacent maxima or minima at wavelengths λ_1 and λ_2 . The variation of thickness shown in Figure.1. It is clear that thickness is not a function of the proportion of dopant with N (N= Mn, La, Sn and Zn). This can be explained that doping has no effect on the thickening of the thin films; this is due to the low percent of dopant N (WPN).

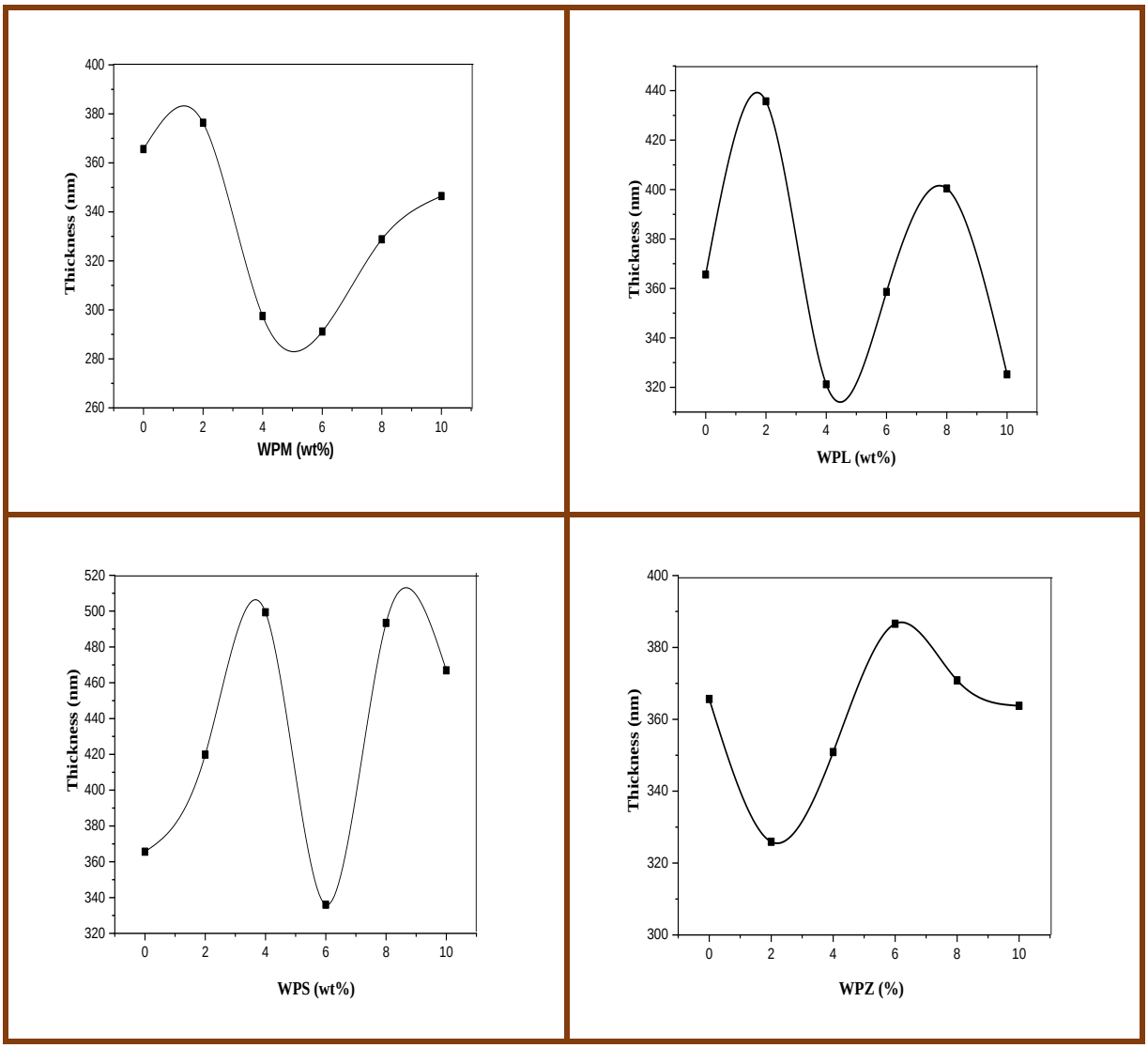

Figure 2. Variation of theCo_3O_4 thin films thickness as a function of the WPN(N= Mn, La, Sn and Zn).

II.3. Band gap energy (E_{gop}) and Urbach energy(Eu)

The absorption edges correspond to the electronic excitation of the valence band at the conduction band. The direct band gap value is determined by the valence level related to the strong O^{2-} ($2p^6$) properties, and the conduction level at which the main contribution is given by the Co^{2+}($3d^7$) orbital's. The direct band gap value is determined by the valence level related to the strong O properties, and the conduction level at which the main contribution is given by the Co orbitals. The presence of Co^{3+}($3d^6$) in Co_3O_4 gives rise to a sub-band located within the energy gap. So, that coincide with E_{gop1}(is corresponds to the onset of O^{2-}(2p) to the Co^{3+}(t2g)) excitation as highlighted in the enlarged $(\alpha h\nu)^2$ versus $(h\nu)$ plots in the figure 3and E_{gop2}(is corresponds to the onset of O^{2-}(2p) to the Co^{2+}(t2g)), which determines the valence to conduction band excitation. The optical band gap E_{gop1} and E_{gop2} values for all samples are summarized in Tables.1 with the WPN (N=M,L,S and Z).

Co_3O_4 is known to possess strong photo absorption in the visible region, which is easily evidenced by its dark black color. To calculate the energy gap E_{gop}associated with the incident photon energy $(h\nu)$and the absorption coefficient (α), we use the classical equation [24-25].

$$(\alpha h\upsilon)^2 = A\left(h\upsilon - E_{gop}\right)$$

Two linear regions appear indicating the existence of two different band gap values, which may be ascribed to the spin-orbit fragmenting of the valence band. The extrapolation of two straight lines to $(\alpha h\upsilon)^2 = 0\ (eV)^2$ give values of the direct band gaps of N-doped Co_3O_4(N=Mn, La, Sn and Zn)thin films (see tables.1, 2, 3 and 4).It is found of E_{gop1} values of the energy band gap for Mn doping varies between 1.42±0,07 and 1.46±0.07 eV while E_{gop2} values, which are obtained from the extrapolation of the first linear region, found to be varying between 1.873±0.10 and 2.11±0,11eV (see figure.3). Increased film thickness could explain the increase in the optical band gap E_{gop2} and vice versa [26]. For La doping, it is found of E_{gop1} values varies between 1.45 and 1.48 eV while E_{gop2} values found to be varying between 2.02 and 2.06 eV, the enhancement trend in the optical band gap may be explained by the effect of introduction of La doping which cause a distortion of network within Co_3O_4 matrix and forming an impurity energy levels (acceptor level) within the band gap [8,27].For Sn doping, it is found of E_{gop1} values varies between 1.46 and 1.47 eV while E_{gop2} values are found to be varying between 2.02 and 2.065eV.And for Zn doping, it is found of E_{gop1} values

varies between 1.39 and 1.48 eV while E_{gop2} values are found to be varied between 1.73 and 2.16 eV.

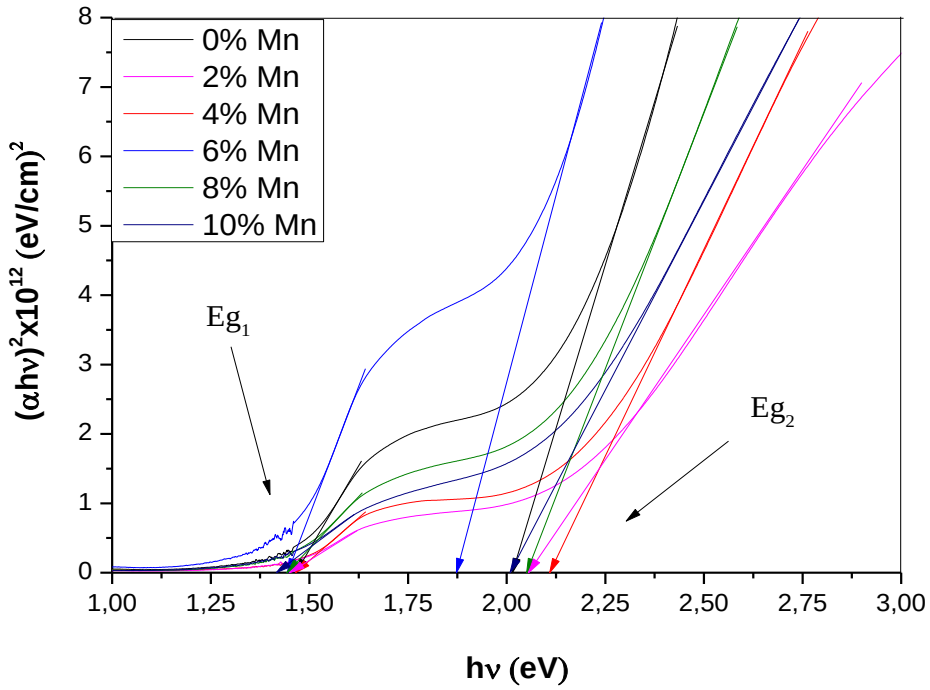

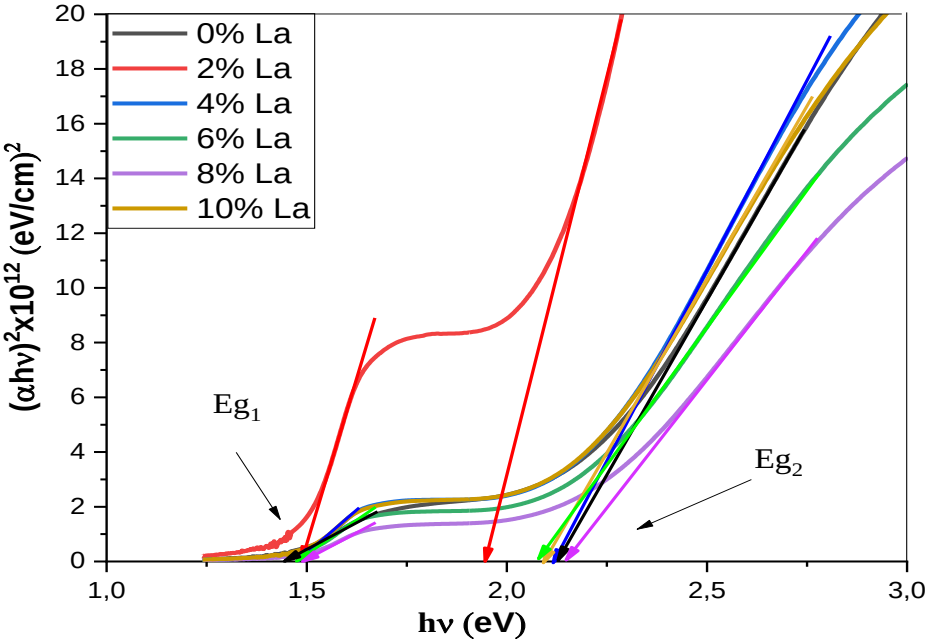

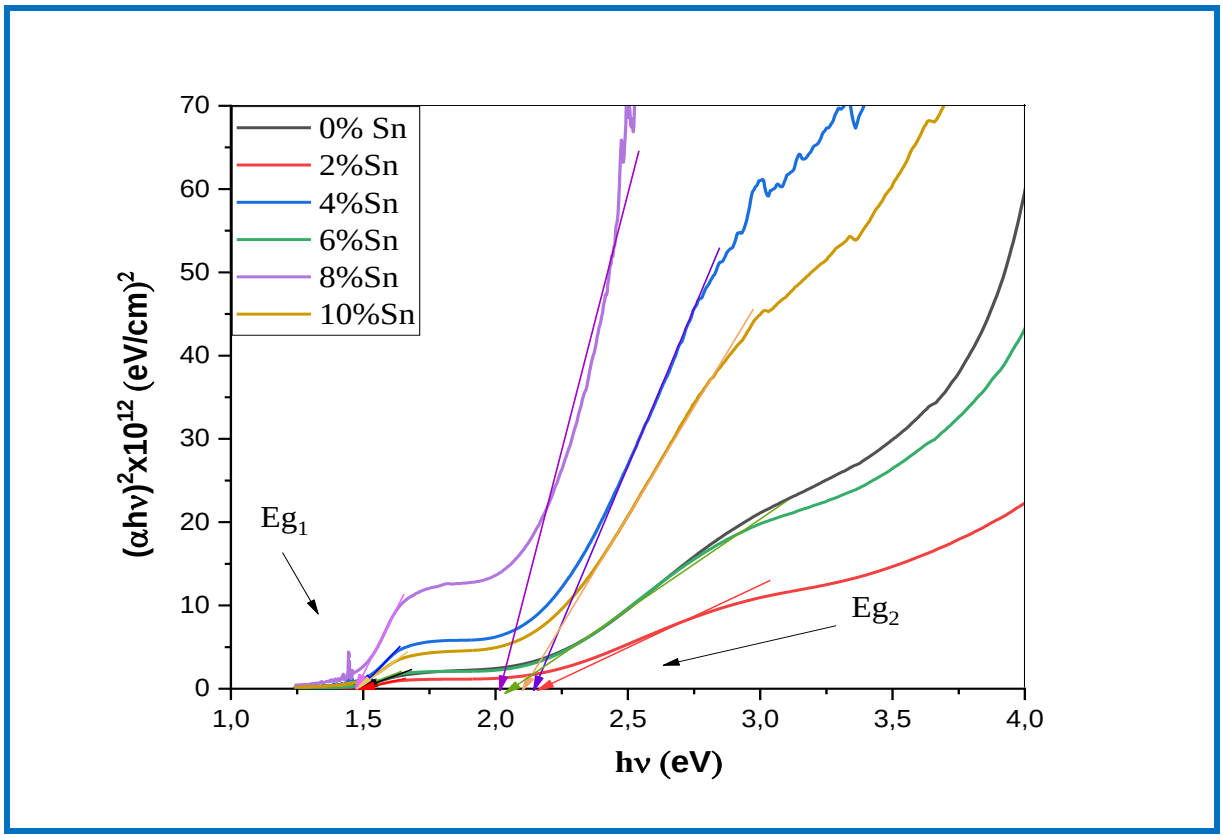

Figure 3. Plots of $(\alpha h\upsilon)^2$ against $h\upsilon$of pneumatic spray method (CVD) made Co_3O_4:N (N= Mn, La, Sn and Zn) thin films compared to those of undoped Co_3O_4 one.

The presence of Co^{3+} ions in Co_3O_4 thin films is attributed to an intermediate band located inside the energy gap. The band gaps E_{gop1} are generally associated with a charge transfer Co^{3+} d (t2g) →Co^{2+} d (t2) while the band gaps E_{gop2} are associated with O^{2-} (2p6) → Co^{2+}(3d7) and O2– (2p6) → Co^{3+} (3d6) charge transfer [8]. The transition band between the Co^{3+}- Co^{2+} ions indicating the charge transfer in the films is localized because of many vacancies and acts as an acceptor band.

Co^{3+} substituted by $Mn^{2+\ or3+}$, La^{3+}, $Sn^{2+or\ 4+}$ and Zn^{2+} leads to the formation of impurity energy levels created between CB band and VB band. This increases the amount of Co^{3+}vacancy. The observed marginal difference or the decrease in the E_{gop2} values is also due to the presence of a high amount of acceptor states (cation vacancies) near the top edge of the range, which belong to Co^{3+}or Co^{2+}(3dt2g). This can occur as a result of overlapping upper-edge states and donor-edge states upon doping, resulting in a narrowing of the range of E_{gop2}[28,29]. Of the band gap energy increased; This can be explained by the increase in Urbach energies (see figure 4), that is, as the Urbach energy increases, the random energy increases, and thus the absence of crystal structural organization.

The refractive index is related to optical band gap (E_{gop2}) of a semiconductor by the following relationship [23,30]:

$$n = 4{,}084 - 0{,}68\ E_{gop2}$$

The observed marginal difference or shift in the E_{gop2} values is further due to the formation of impurity energy levels or localized energy states that are created between the conduction domain and the straightness band upon doping observed from EDS [28,29].

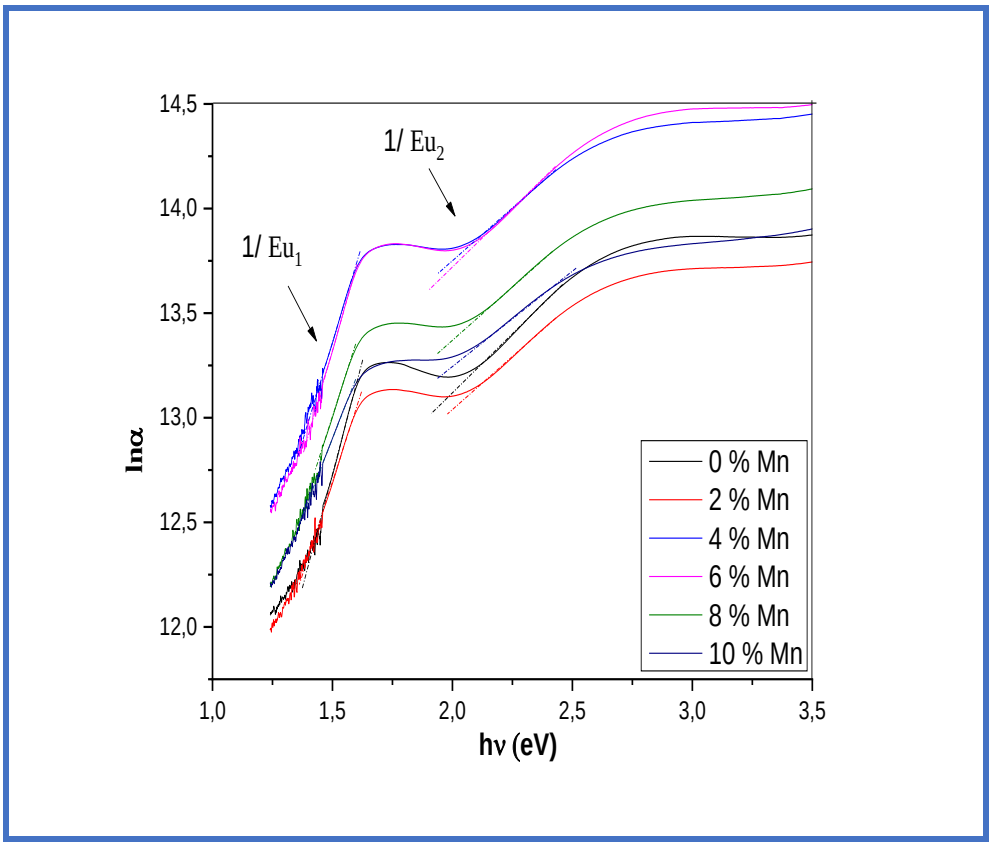
1/ Eu2
1/ Eu1
0 % Mn
2 % Mn
4 % Mn
6 % Mn
8 % Mn
10 % Mn
lnα
hν (eV)

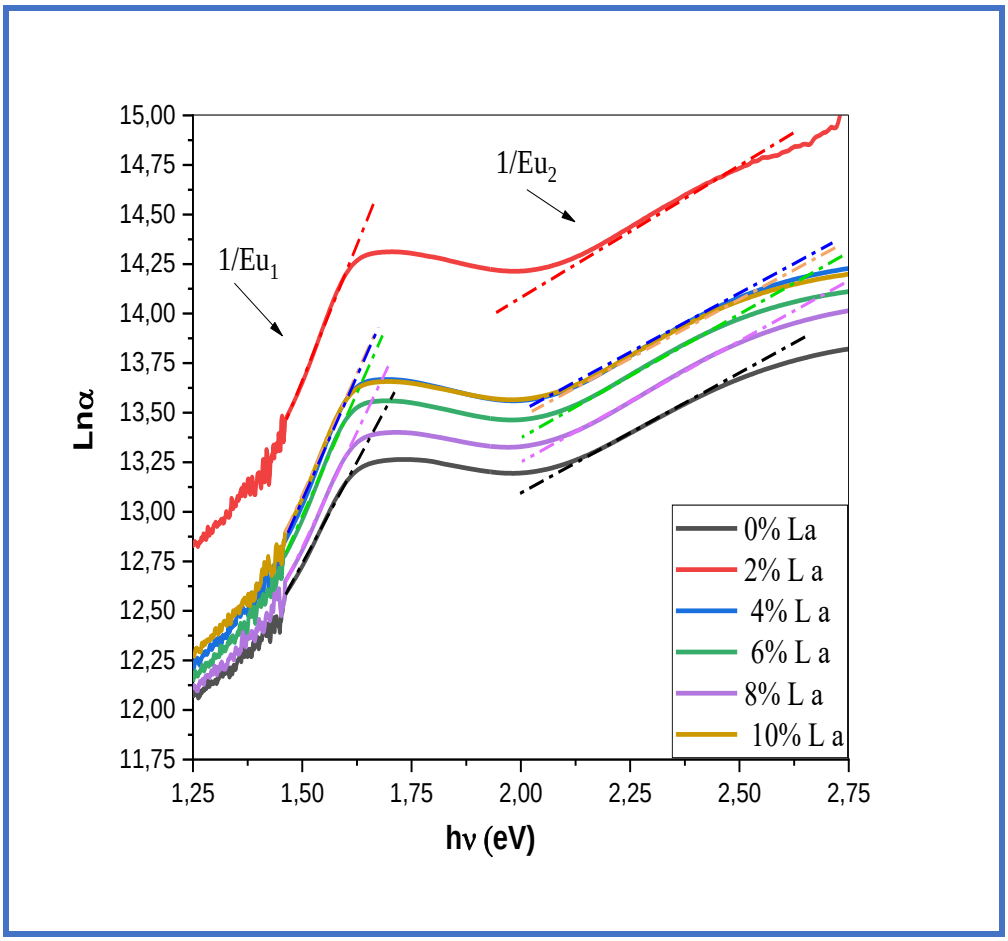
1/Eu2
1/Eu1
0% La
2% L a
4% L a
6% L a
8% L a
10% L a
Lnα
hν (eV)

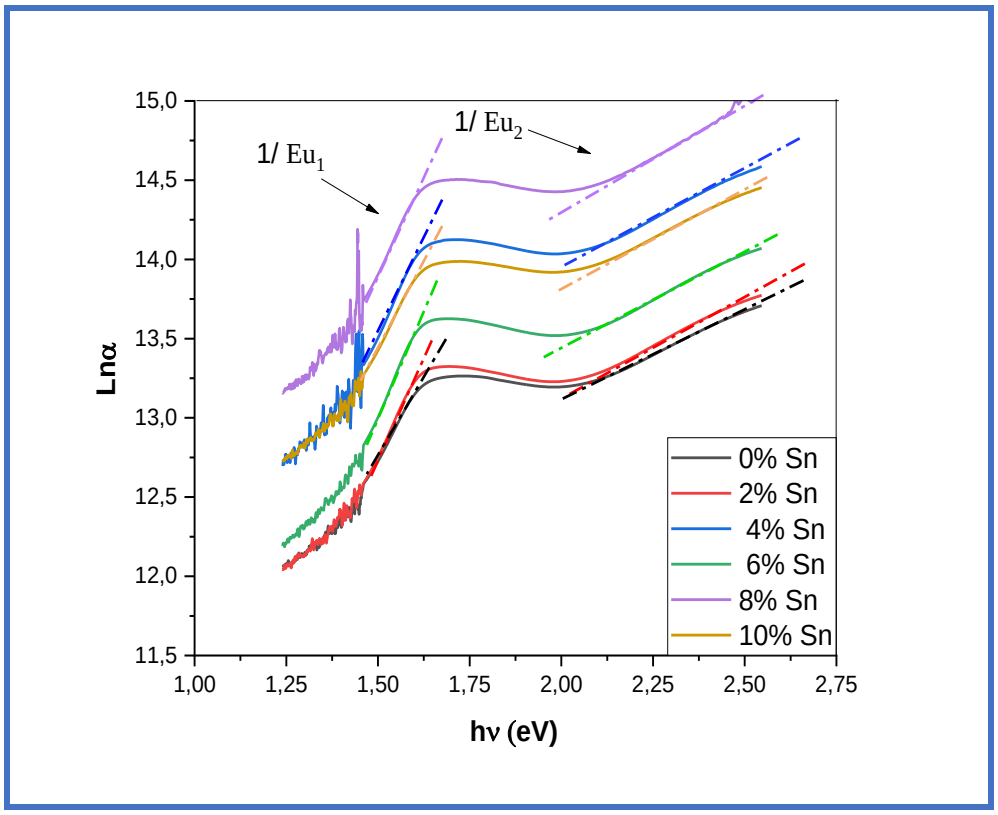

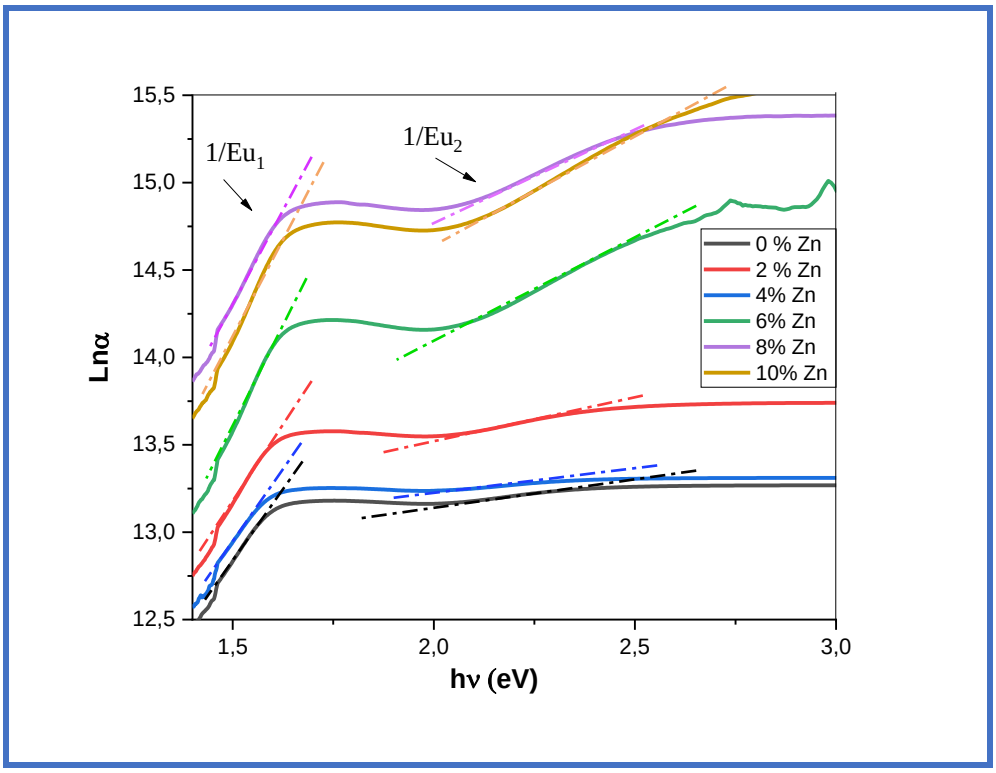

Figure.4. Plots of ($h\upsilon$) against $ln\ \alpha$ of the Co_3O_4: N thin films with different WPN (N= Mn, La, Sn and Zn).

Table.1. Optical and electrical parameters values of the deposited N-doped Co_3O_4 thin films(N= Mn, La, Sn and Zn).

		Band gap energy (eV)		Urbach energy Eu (eV)				
	WPN (wt%)	E_{gop1}	E_{gop2}	Eu_1	Eu_2	**Thickness t_h(nm)**	**Refractive index *n***	**Electrical conductivity σ $(\Omega.cm)^{-1}$**
WPM (wt%)	0	1.47	2,016	0,24	0,894	365,64	2,71	1,623
	2	1.45	2,056	0,28	0,993	376,38	2,68	2,074
	4	1.47	2,11	0,23	0,995	297,47	2,64	2,633
	6	1,44	1,873	0,25	0,917	291,14	2,81	15,536
	8	1,43	2,051	0,28	1,0	328,81	2,69	0,992
	10	1,42	2,01	0,34	1,12	346,45	2,72	0,631
WPL (wt%)	2	1.48	2,059	0,18	0,894	321,22	2,68	1,252
	4	1.48	2,074	0,19	0,804	435,71	2,67	2,578
	6	1,45	2,072	0,19	0,785	358,61	2,68	4,112
	8	1,46	2,118	0,22	0,846	425,26	2,64	3,425
	10	1,46	2,075	0,19	0,860	400,85	2,67	22,858
WPS (wt%)	2	1.46	2,065	0,22	0,832	419,81	2,68	9,778
	4	1.47	2,062	0,21	0,829	499,32	2,68	9,863
	6	1,46	2,065	0,19	0,823	336,01	2,68	10,237
	8	1,47	2,031	0,22	0,794	493,38	2,70	16,875
	10	1,46	2,045	0,24	0,856	466,93	2,69	10,001
WPZ (wt%)	2	1.47	2,097	0,29	2,372	325,92	2,66	15,708
	4	1.39	1,730	0,31	0,534	350,87	2,91	17,481
	6	1,48	2,100	0,20	0,870	386,58	2,66	24,266
	8	1,47	2,000	0,22	0,971	370,83	2,72	22,333
	10	1,49	2,016	0,21	0,817	363,75	2,71	21,236

III. Electrical properties

For measuring the sheet resistance (R_{sheet}) by the four-point probe technique, the current (I=0.01 μA) is applied between the outer two wires and the value of potential difference (V) is read across the two internal probes. Thus, the sheet resistance is calculated from the following relation:

$$R_{sheet} = \frac{\pi}{In2} * \frac{V}{I}$$

The conductivity (σ) values of films are calculated from the following formula:

$$\sigma = 1/(R_{sheet} * t_h)$$

Where t_h: is thickness of thin films.

The values of electrical conductivity (σ) of N-doped Co_3O_4thin films are listed in Table 1. The variation of conductivity (σ) of thin films as a function of the WPN is illustrated in figure 5.

The conductivity (σ) is found to increase with 6wt% of Mn reaching a value of 15,536. then, it starts to decrease with further increase of Mn content reaching a value of 0,631 for 10 wt% of Mn (WPM).

The conductivity (σ) is found to increase slightly with 6 wt% of La reaching a value of 4,112. Then, it starts to increase significantly with further increase of La content reaching a value of 22,858 for 10 wt% of La (WPL).

The conductivity (σ) is found to increase significantly with 8 wt% of Sn reaching a value of 16,875. Then, it starts to decrease with further increase of Sn content reaching a value of 10,001 for 10 wt% of Sn (WPS).

Finally, the conductivity (σ) is found to increase significantly with 6 wt% of Zn reaching a value of 24,266. Then, it starts to decrease slightly with further increase of Zn content reaching a value of 21,236 for 10 wt% of Zn (WPZ).

This increase in conductivity is mainly explained by an increase in the carrier concentration (holes) of the valence band due to electronic shifts in the conduction band and holes resulting from the non-stoichiometry of the oxygen network in the p-Co3O4 grain [30]. On the other hand, the reduction of the size of the grains and increasing of doping gives rise to the

appearance of the separate energy levels. These levels manifest in the gap as electronic defects, which probably work like donors inducing the increase in conductivity.

At a high value of doping, the decreases electrical conductivity (σ) can be explained as follows; the increase in the resistance is attributed to the reduced crystallization of thin films, resulting in a decrease in the electron scattering centers due to the increase of the WPM [31].

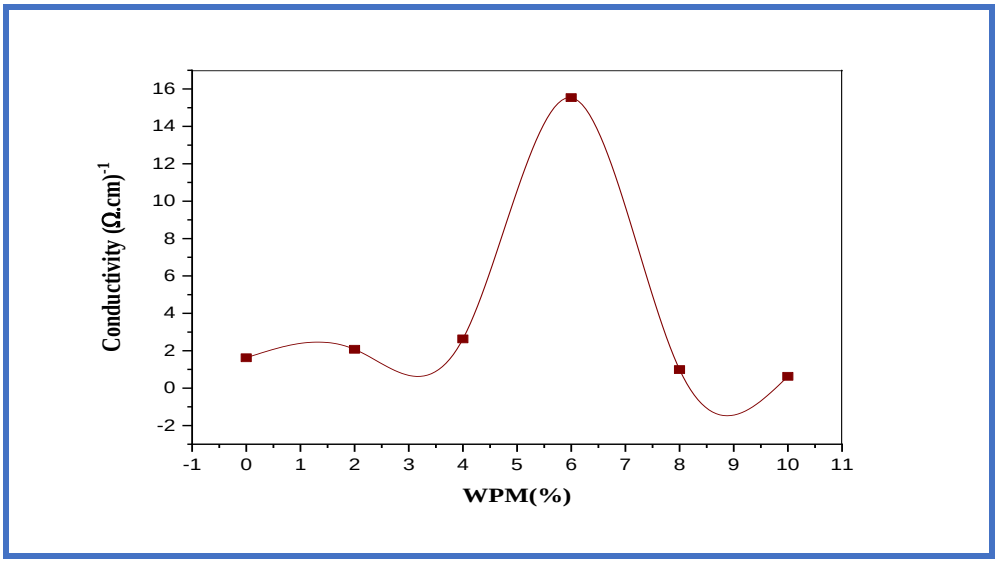

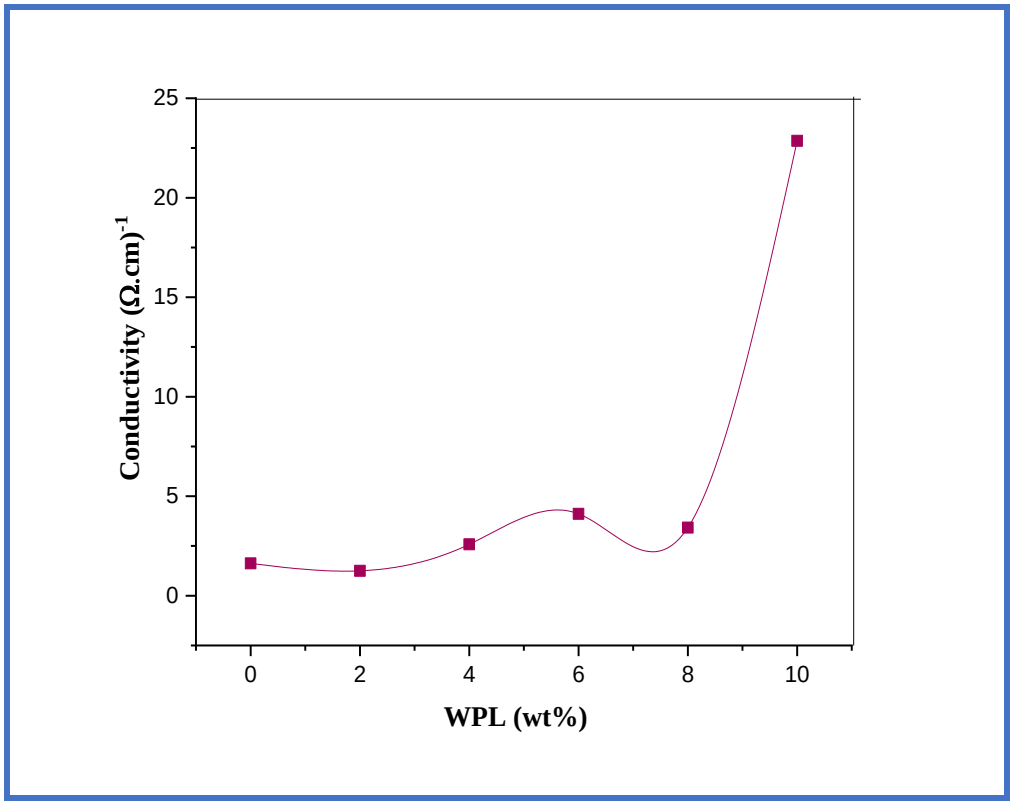

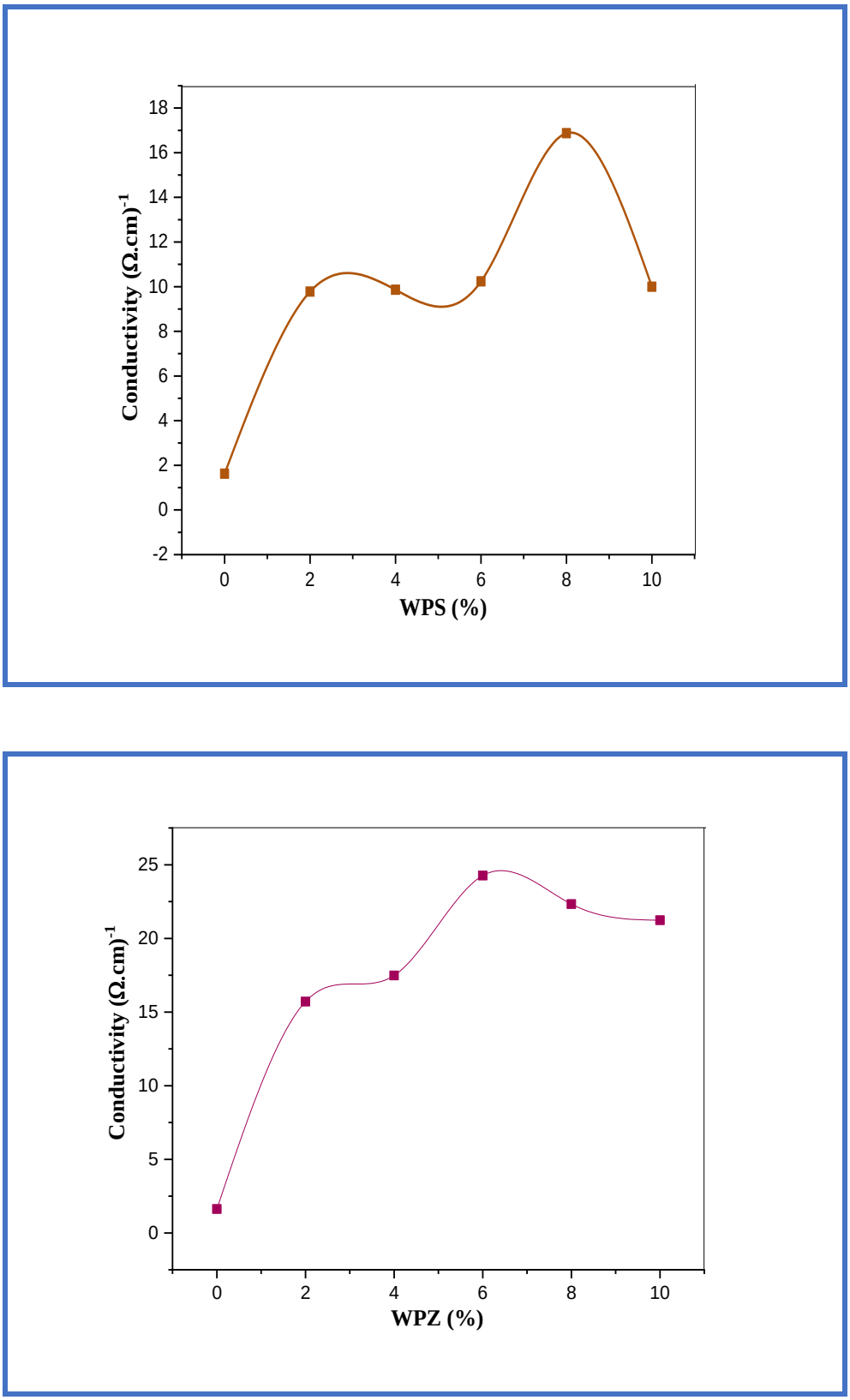

Figure.5 Electrical conductivity of the Co_3O_4:N thin films as a function of the WPN(N= Mn, La, Sn and Zn).

IV. Conclusion

This chapter focuses on the effect of manganese, lanthanum, tin and zinc doping on the optical and electric properties of chemically deposited Co_3O_4 thin films. It is found that all the films exhibit a low optical transmittance in the transparency region with two direct band gap around E_{gop1}= 1,4 eV and E_{gop2}= 2,0 eV. Moreover, cover method is employed in order to estimate the film thickness and some optical constants. Electrical study show that the maximum of conductivity is obtained for 6 wt% of Mn, 10 wt% of La, 8wt% of Sn and 6wt% of Zn by values 15,536; 22,858; 16,875 and 24,266 $(\Omega.cm)^{-1}$ respectively.

References

[1] Nabila Kouidri,Saâd Rahmane,Abdelkrim Allag, Substrate temperature-dependent properties of sprayed cobalt oxide thin films, Journal of Materials Science: Materials in Electronics 30 (2019) 1153–1160.

[2] Nabila Kouidri. Contribution à l'étude de couches minces d'oxydes transparents conducteurs à base de zinc et cobalt par spray pneumatique, Doctorat thesis, University Mohamed Khider of Biskra, 2019.

[3] Z. Bencharef, A. Chala, R. Messemeche, Y. Benkhetta, The physical properties of spinel cupic Co_3O_4 thin films prepared by a PSM, Main Group Chemistry 21(2022) 329-340.

[4] C. Ravi Dhas, R. Venkatesh, R. Sivakumar, A. Moses Ezhil Raj, C. Sanjeeviraja. Effect of solution molarity on optical dispersion energy parameters and electrochromic performance of Co_3O_4 films. Journal of Optical Materials 72 (2017) 717-729.

[5] AbdelhakLakehal, BedhiafBenrabah, AmarBouaza, CherifaDalache, BenhebalHadj. Tuning of the physical properties by various transition metal doping in Co_3O_4: TM (TM = Ni, Mn, Cu) thin films: A comparative study. Chinese Journal of Physics. 56 (2018) 1845-1852.

[6] C. Ravi Dhas, R. Venkatesh, R. Sivakumar, T. Dhandayuthapani, B. Subramanian, C. Sanjeeviraja, A. Moses Ezhil Raj. Electrochromic performance of chromium-doped Co_3O_4 nanocrystalline thin films prepared by nebulizer spray technique. Journal of Alloys and Compounds 784 (2019) 49-59

[7] MohdShkir, Z.R. Khan, Aslam Khan, Kamlesh V. Chandekar, M.A. Sayed, S. AlFaify. A comprehensive study on structure, opto-nonlinear and photoluminescence properties of Co_3O_4 nanostructured thin films: An effect of Gd doping concentrations. Journal of Ceramics International (2022).

[8] Mohd. Shkir, Aslam Khan, Mohd Imran, M. Ajmal Khan, Rayees Ahmad Zargarf, ThamraaAlshahrani g, K. Deva Arun Kumar, P. Mohanraji, Kamlesh V. Chandekarj, S. AlFaify. Spray pyrolysis developed Nd doped Co_3O_4 nanostructured thin films and their structural, and opto-nonlinear properties for optoelectronics applications. Optics and Laser Technology 150 (2022) 107959.

[9] S. Fareed, R. Medwal, J.V. Vas, I.A. Khan, R.S. Rawat, M.A. Rafiq, Tailoring oxygen sensing characteristics of Co3O4 nanostructures through Gd doping, Ceramics International. 46 (7) (2020) 9498–9506.

[10] L. Xu, G. Zheng, J. Miao, F. Xian, Dependence of structural and optical properties of sol–gel derived ZnO thin films on sol concentration. Appl. Surf. Sci. **258**, 7760 (2012).

[11] N.Lehraki, M.S.Aida, S.Abed, N. Attaf, A. Attaf, M. Poulain,ZnO thin films deposition by spray pyrolysis: Influence of precursor solution properties, Current Applied Physics 12 (2012) 1283-1287.

[12] L. Abdelhak, B. Amar, B. Bedhiaf, D. Cherifa, B. Hadj, Characterization of Mn-Doped Co 3 O 4 Thin Films Prepared by Sol Gel-Based Dip-Coating Process, High.Temp. Mater. Process. 38(2019)237–247.

[13] W. Zhang, P. Anguita, D. Javier, C. Descorme, J.L. Valverde, A. Giroir-fendler, Comparison of different metal doping effects on Co_3O_4 catalysts for the totaloxidation of toluene and propane, Catalyst (2020) 1–14.

[14] C. Zhang, J. Wei, L. Chen, S. Tang, M. Deng, Y. Du, All-solid-state asymmetric supercapacitors based on Fe-doped mesoporous Co_3O_4 and three-dimensionalreduced graphene oxide electrodes with high energy and power densities,Nanoscale 9 (2017) 15423–15433.

[15] N. Zhang, Q. Qin, X. Ma, J. Zhou, L. Sun, C. Chen, S. Wen, Y. Chen, S. Ruan, One-step synthesis and gas sensing properties of hierarchical Fe doped Co3O4 nanos-tructures, J. Alloy. Compd. 723 (2017) 779–786.

[16] J.W. Kim, S.J. Lee, P. Biswas, T. Il Lee, J.M. Myoung, Solution-processed n-ZnOnanorod/p- Co_3O_4 nanoplate heterojunction light-emitting diode, Appl. Surf. Sci. 406 (2017) 192–198.

[17] C. Dalache, H. Benhebal, B. Benrabah, A. Ammari, A. Kharroubi, A. Lakhal,Cadmium-doped Co3O4 thin films: synthesis and characterization, Surf. Rev.Lett. 26 (2019) 1–9.

[18] G.F. Zhang, P. Qin, J.M. Song, Facile fabrication of Al2O3-doped Co_3O_4/graphene nanocomposites for high performance asymmetric supercapacitors, Appl. Surf. Sci. 493 (2019) 55–62.

[19] Mohamed Shaban, Adel M.El Sayed, Influence of the spin deposition parameters and La/Sn double doping on the structural, optical, and photoelectrocatalytic properties of $CoCo_2O_4$photoelectrodes, Solar Energy Materials and Solar Cells, 217(2020) 110705.

[20] OzkanBayram, Erdalİgman, HarunGuney, OnderSimsek, The role of cobalt doping on the optical and structural properties of Mn_3O_4 nanostructured thin films obtained by SILAR technique, Superlattices and Microstructures, 128(2019) 212-220.

[21] Jingwei Huang, TingtingLiu ,Rongfang Wang , Mingyi Zhang, Lei Wang , Houde She , Qizhao Wang, Facile loading of cobalt oxide on bismuth vanadate: Proved construction of p-n junction for efficient photoelectrochemical water oxidation, Journal of Colloid and Interface Science 570(2020) 89-98.

[22] J. A. K. Tareen. A. Malecki, J. P. Doumerc, J. C. Launay, P. Dordor, M. Pouchard, P. Hagenmuller, Growth and electrical properties of pure and Ni-doped Co_3O_4 single crystalsMaterials research bulletin. Materials Research Bulletin 19 (1984) 989-997.

[23] R.C. Ambare, S.R. Bharadwaj, B.J. Lokhande,Electrochemical characterization of Mn: Co_3O_4 thin films prepared by spray pyrolysis via aqueous route, Current Applied Physics, 14(2014) 1582-1590.

[24] J. Tauc., R. Grigorovici., and A. Vancu, "Optical properties and electronic structure of amorphous germanium", Physica Status Solidi (B), 15(2), (1966) 627- 637.

[25] J.H. Richter, Electronics Properties of Metal Oxide Films Studied by Core Level Spectroscopy, Digital Comprehensive Summaries of Uppsala Faculty of Science and Technology, 228 (1969).

[26] Y. Benkhetta, A. Attaf, H. Saidi, A. Bouhdjar, H. Bendjedidi, I.B. Kherkhachi, M. Nouadji, N. Lehraki, Influence of the solution flow rate on the properties of zinc oxide (ZnO) nano-crystalline films synthesized by ultrasonic spray process, Optik 127 (2016) 3005–3008

[27] A. Lakehal, B. Bedhiaf, A. Bouaza, B. Hadj, A. Ammari, C. Dalache, Structural, optical and electrical properties of Ni-doped Co3O4 prepared via Sol-Gel technique, Mater. Res. 21 (3) (2018).

[28] R.Perekrestov, A.Spesyvyi, J.Maixner, K.Mašek, O.Leiko, I.Khalakhan, J.Maňák, P.Kšírová, Z.Hubička, M.Čada, The comparative study of electrical, optical and catalytic properties of Co_3O_4 thin nanocrystalline films prepared by reactive high-power impulse and radio frequency magnetron sputtering, Thin Solid Films, 686 (2019) 137427.

[29] R. Venkatesha , C. Ravi Dhasa, R. Sivakumarb , T. Dhandayuthapanib , B. Subramanianc, C. Sanjeevirajad , A. Moses EzhilRaje, Tailoring the physical properties

and electrochromic performance of nebulizer spray coated Co3O4 films through copper doping ,Solid State Ionics. 334 (2019) 5-13.

[30] N.M. Ravindra, Energy gap-refractive index relation—some observations , Infrared physics,21 (1981)283-285.

[31] A. Bouhdjer, A. Attaf, H. Saidi, Y. Benkhetta, M.S. Aida, I. Bouhaf, A. Rhil, Influence of annealing temperature on In2O3 properties grown by an ultrasonic spray CVD process, Optik 127 (2016) 6329–6333.

General conclusion and future work

1. General conclusion

In this thesis, cobalt oxide thin films have been successfully deposited using a homemade pneumatic spray method (PSM) by varying doping weight percentages (0, 2,4,6,8 and 10 wt %) on glass substrate at temperature 400°C. So, two main objectives will be pursued in this investigation: study of the effect of manganese, lanthanum, tin and zinc doping concentration on the physical properties. The present study shows that the variation of doping concentration induces pronounced physical modifications in the Co3O4 thin films. The X-ray diffraction patterns reveals that the crystalline quality of pristine and N-doped cobalt oxide (Co_3O_4) thin films self-cubic spinel structure is oriented along to (111) plane. The crystal size (D) and lattice strain (ε) are calculated based on X-ray diffraction and Williamson-Hall relationship. Thus, batter crystalline quality is obtained for doping weight percent Mn (2 wt%), La (8wt%), Sn (2wt%) and Zn (10 wt%).

The morphology of pristine and N-doped Co_3O_4 (N= Mn, La, Sn and Zn) thin films are shown in SEM top view images are almost homogeneous and well covered without any pinholes and cracks. However, the SEM top view observations show no modification at the surface morphology of the produced thin films after doping. According to AFM micrographs with three dimensional (3D), the straight acicular nanorods (SANRs) are shown. However, 3D images show that the films are rough surface. Furthermore, the transmittance is decreased in both visible and infrared regions after Mn, Sn, La and Zn doping and is increases only when doped with Mn for 2 wt% in visible region and for 2, 8 and 10 wt% in infrared region. The thickness is estimated using Swanepoel method. To conclude thickness is not a function of the proportion of dopant with N (N= Mn, La, Sn and Zn).

The optical studies showed two direct band gaps E_{gop1} and E_{gop2} which are varied between 1,42to 1,49 eV and from 1,730 to 2,118 eV respectively. With doping, the optical bandgap, Egop2 narrows to 1,873 eV, 2,059 eV, 2,031 eV and to 1,730 eV at 6 wt% of manganese, 2 wt% of lanthanum, 8 wt% of tin and 4 wt% of zinc respectively. The electrical conductivity increasing with of doping so that it reaches 15,536$(\Omega.cm)^{-1}$ of Manganese doping (in 6 wt% of Mn), 22,858 $(\Omega.cm)^{-1}$ of lanthanum doping (in 10 wt% of La), 16,875 $(\Omega.cm)^{-1}$ of tin doping (in 8 wt% of Sn) and 24,266$(\Omega.cm)^{-1}$ of zinc doping (in 6 wt% of Zn).

Finally, the optimization of doping concentration may be useful guidelines to the synthesis of some optoelectronic devices based on the Co_3O_4 thin films.

2. Future work

As suggestions for further work, there are several areas of research involving Co_3O_4 thin films that will appear to be promising. Indeed, other dopants will be imagined in addition to the introduction of different percentages in to have further improvement in the physical properties. Thus, we can test our findings for the selection of ratios for Co-doping.

Moreover, practical applications of N-doped Co_3O_4 (N= Mn, La, Sn and Zn) thin films can be pursued under sunlight, for example photocatalysis, self-cleaning and water splitting for H_2 production.

ANNEXES

Name and formula

Reference code:	00-042-1467
Compound name:	Cobalt Oxide
PDF index name:	Cobalt Oxide
Empirical formula:	Co_3O_4
Chemical formula:	Co_3O_4

Crystallographic parameters

Crystal system:	Cubic
Space group:	Fd-3m
Space group number:	227
a (Å):	8,0837
b (Å):	8,0837
c (Å):	8,0837
Alpha (°):	90,0000
Beta (°):	90,0000
Gamma (°):	90,0000
Calculated density (g/cm^3):	6,05
Volume of cell (10^6 pm^3):	528,24
Z:	8,00
RIR:	3,10

Subfiles and quality

Subfiles:	Alloy, metal or intermetalic Common Phase Corrosion Inorganic
Quality:	Star (S)

Comments

Color:	Black
Creation Date:	01/01/1970
Modification Date:	01/01/1970
Color:	Black
Sample Source or Locality:	Sample obtained from Fischer Scientific. Average relative standard deviation in intensity of the ten strongest reflections for three specimen mounts=4.0%. Validated by calculated pattern
Additional Patterns:	To replace 00-009-0418.

References

Primary reference: Martin, K., McCarthy, G., North Dakota State University, Fargo, North Dakota, USA., *ICDD Grant-in-Aid*, (1990)

Peak list

No.	h	k	l	d [A]	2Theta[deg]	I [%]
1	1	1	1	4,66700	19,001	19,0
2	2	2	0	2,85800	31,272	34,0
3	3	1	1	2,43700	36,853	100,0
4	2	2	2	2,33400	38,542	9,0
5	4	0	0	2,02100	44,810	19,0
6	4	2	2	1,65010	55,656	8,0
7	5	1	1	1,55570	59,359	29,0
8	4	4	0	1,42900	65,238	34,0
9	5	3	1	1,36640	68,630	2,0
10	6	2	0	1,27820	74,119	2,0
11	5	3	3	1,23280	77,341	7,0
12	6	2	2	1,21870	78,406	4,0
13	4	4	4	1,16680	82,627	2,0
14	7	1	1	1,13200	85,762	1,0
15	6	4	2	1,08020	90,977	3,0
16	7	3	1	1,05240	94,100	9,0
17	8	0	0	1,01050	99,334	3,0
18	6	6	0	0,95270	107,908	2,0
19	7	5	1	0,93340	111,230	6,0
20	6	6	2	0,92730	112,340	2,0
21	8	4	0	0,90380	116,923	2,0

Stick Pattern

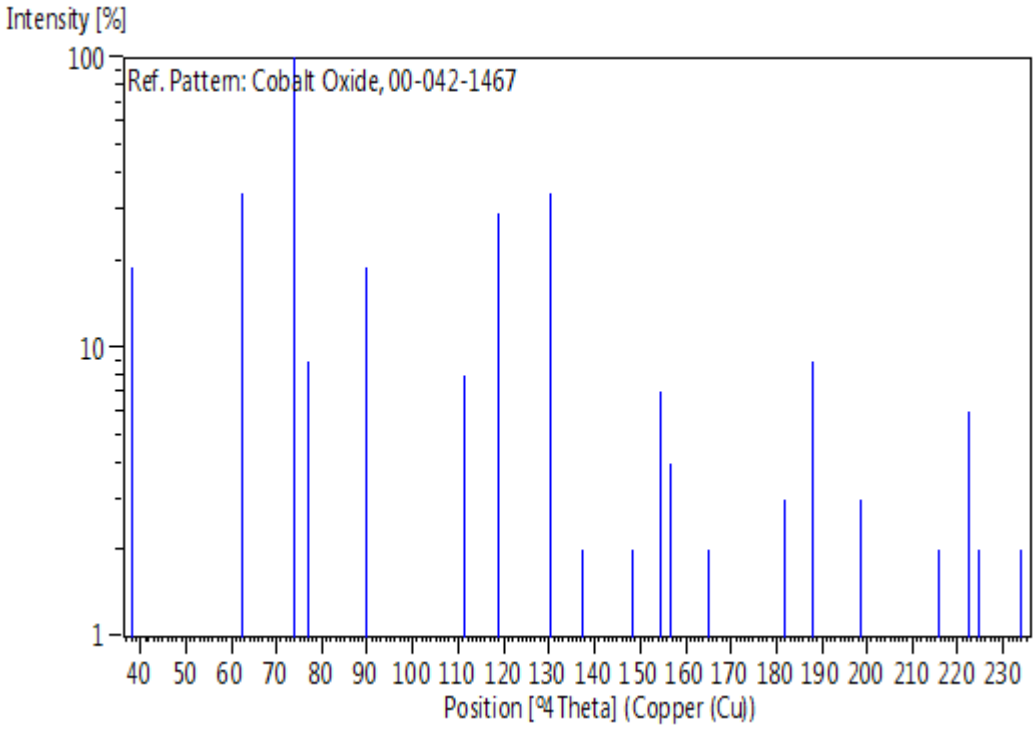

Main Group Chemistry 21 (2022) 329–340
DOI 10.3233/MGC-210090
IOS Press

The physical properties of spinel cubic Co_3O_4 thin films prepared by a PSM

Z. Bencharef[a,b,*], A. Chala[a,b], R. Messemeche[a,b] and Y. Benkhetta[a,b]
[a]*Department of Material Sciences, Faculty of Science, University of Biskra, Biskra, Algeria*
[b]*Physic Laboratory of Thin Films and Applications (LPCMA), University of Biskra, Biskra, Algeria*

Abstract. Undoped and Mn-doped Co_3O_4 films were deposited on heated glasses substrates ($T_S = 400°C$) using a homemade pneumatic spray method (PSM). The solution concentration and deposition time are 0.1 M and 4 min respectively. The effect of manganese doping concentration on structural, optical and electrical properties of cobalt oxide were investigated. The elaborated films were characterized by X-ray diffraction, UV-Vis spectroscopy, atomic force microscopy (AFM) the three-dimensional (3D), energy dispersive spectroscopy (EDS), and four points probe measurements. The XRD study showed that all films were polycrystalline consisting with spinel cubic phase orientated along to (111) plane. The lattice strain and crystallite size were estimated by Williamson-Hall method. The morphology of Mn-doped Co_3O_4 thin films shows a homogeneous surface with straight acicular nanorods (SANRs). EDS analysis showed the presence of peaks associated with Co, O and Mn elements which confirm the composition of the thin films. The optical band gaps varies from 1.42 ± 0.07 to 1.47 ± 0.07 eV of E_{gop1} and E_{gop2} varies from 1.87 ± 0.10 to 2.11 ± 0.11 eV. In addition, the electrical measurement show a maximum electrical conductivity ($\sigma = 15.54 \pm 0.78$ $(\Omega.cm)^{-1}$) at 6% wt of Mn.

Keywords: Mn-Co_3O_4 thin films, Manganese doping, pneumatic spray method (PSM), weight percentages of Manganese (WPM), spinel cubic structure (SCS), X-ray diffraction (XRD)

1. Introduction

Absorbent conducting oxide (ACO) materials such as Fe_2O_3, Cu_2O, NiO and Co_3O_4 have attracted a lot of research. The development of ACO are importance to their interesting optoelectronic, chemical optical and physical properties [1]. Among the ACO is cobalt oxide, which is one of the most remarkable material in experimental examination of scientific and technological importance [1]. Cobalt oxide has a three phases different crystalline are: Co_2O_3 (cubic structure), CoO (cubic structure) and Co_3O_4 (cubic spinel structure of the type AB_2O_4; where Co^{3+} ions occupy the octahedral sites and Co^{2+} occupy the tetrahedral sites) is high stability compared to other phases [2]. It has a high optical absorbance in the spectral range of UV-Vis and electrical conduction.

Co_3O_4 thin films suitable for many applications such as catalyst for gaz sensors [3] and catalysers[4, 5], super-capacitors [6], solar selective absorber due to the p-type semiconducting [7], energy storage [8], photocatalytic[9], etc. Co_3O_4 can be produsd by several techniques such as magnetron sputtering (MST), pulsed laser deposition (PLD), chemical vapor deposition (CVD), sol-gel process (SGP), reactive evaporation (RE), electrochemical deposition (ECD) and 400 °C molecular beam epitaxy (MBE). Previous studies indicate that doping of the transition metal elements (Fe, Mn, Cu, Cr, Ni) in

*Corresponding author: Z. Bencharef, University of Biskra, Biskra, Algeria. E-mail: zahia.bencharef@univ-biskra.dz.

ISSN 1024-1221/$35.00

Co_3O_4 can enhance electrocatalytic activity [10–14]. A. Lakehal et al. reported the optical absorption studies have shown they pure Co_3O_4 and Mn doped Co_3O_4 (9wt%) prepared by ultrasonic bath exhibits multiple band gap energies ($Eg_1 = 1.33$ eV and $Eg_2 = 1.87$ eV) for 45 min [7]. R. Venkatesha et al. have prepared Cu-doped Co_3O_4 films by nebulized spray pyrolysis method by varying the Cu dopant concentration, found band gap energie $Eg_2 = 1.72$ eV of 6% Cu [15].

In this work, undoped and Mn-doped Co_3O_4 films are deposited using a homemade pneumatic spray method (PSM). The used technique has many advantages, such as it can produce homogeneous thin films with very regular crystallites sizes [16, 17]. It facilitates the control of the solution concentration, the control of temperature stabilization for glass substrates, the control of time for spraying, large-area spraying, and control of composition. In addition, the morphology of films can be controlled; therefore, it is one of the most important methods for the preparation of Co_3O_4 thin films. The effect of manganese doping on Co_3O_4 thin films crystallinity, transmittance, bandgap energy, and electrical conductivity of Co_3O_4 was investigated.

2. Experimental procedure

Mn-doped Co_3O_4 films thin films prepared using a simple homemade PSM on highly cleaning glass substrates. Cobalt chloride dehydrate ($CoCl_2.6H_2O$) with 0,1 M and manganese (II) chloride tetrahydrate ($MnCl_2.4H_2O$) were used as chemicals sources in the solvent which contained equal volumes of distilled water (H_2O) with a volume of 50 ml too and two drops of chloride acid (HCl) also used as a stabilizer for the all samples in this work. Then use manganese doping with different PWM (Mn/Co = 0; 2; 4; 6; 8 and 10 weight %).The produced mixture was stirred for 1 h at temperature between 50 °C –60°C to yield a transparency and homogenous solutions. The glass substrates were cleaned using acetone and methanol solutions for 15 min respectively and rinsed by distilled water. The normalized distance of 20 cm between the spray nozzle (0,5 mm) and the substrates was maintained. The solution quantity of 50 ml was fixed during the preparation of thin films. The spray rate of 3 (ml/min) was maintained by using filtered compressed air (1bar) as a gas carrier. The deposition time was fixed to 4 min at 400 °C as substrate temperature for each film. The structural and crystalline properties of Mn-doped Co_3O_4 films were analyzed by X-Ray diffraction (Rigaku-Type MiniFlex600) with Cu K_α radiation ($\lambda = 0{,}1541874$ nm) in the scanning range of (2θ) was between 10° and 80°.

The optical transmission of thin films was obtained at room temperature in the range of 300 –1000 nm by using a JASCO V-770 spectrophotometer. The morphological properties were studied using (KLA-Tencor Stylus P7) atomic force microscopy (AFM) with three-dimensional (3D). EDS, associated with SEM (TESCAN-VEGA3 scanning electron microscope) was used to determine the films chemical composition. As for electrical conductivity of thin films was measured by four probe points.

3. Results and discussions

3.1. Thin films thickness

The thickness (t_h) of Mn-doped Co_3O_4 thin films as a function of the PWM was calculated from UV-visible data using the following equation [18, 19].

$$t_h = \frac{\lambda_1 \lambda_2}{2n\,(\lambda_1 - \lambda_2)} \tag{1}$$

Where, n is the refractive index at two adjacent maxima or minima at wavelengths λ_1 and λ_2. The variation of thickness shown in Fig. 1. It is clear that thickness is not a function of the proportion of

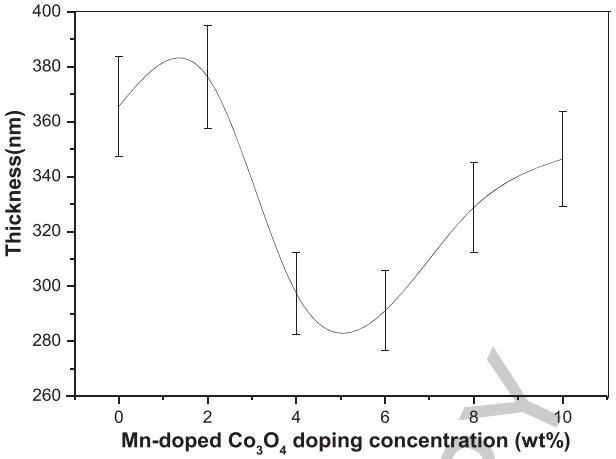

Fig. 1. VariationCo_3O_4 thin films thickness as a function of the WPM.

manganese (WPM). This can be explained that manganese doping has no effect on the thickening of the thin films; this is due to the low percent of manganese (WPM).

3.2. Structural properties of Mn-doped Co_3O_4 thin films

The XRD spectra of thin films of undoped and Mn-doped Co_3O_4 deposited at temperature of 400 ° C and 0.1 M as a solution concentration are shown in Fig. 2. It can be noted that all thin layers exhibit several diffraction peaks around 2 θ = 19.01 °; 31.196 °; 36.834 °; 38. 482 ° and 59.393 ° which correspond respectively to the planes (111), (220), (311), (222) and (511). These peak reflections indicate the phase of Co_3O_4 according to (JCPDS 42-1467) [19]. The peaks position (θ values) were used to determine the d-spacing according to Bragg's Iaw; $\lambda = 2d*\sin\theta$. The lattice parameter (a) of Co_3O_4 thin films as cubic system is determined from $a = d_{hkl} \times \sqrt{h^2 + k^2 + l^2}$, where (hkl) are the Miller indices the diffraction peaks. The value of a was determined for each film considering the three main peaks (111), (311) and (222) can be noted in Table 1.

Mn-doped Co_3O_4 thin films are oriented preferentially along to the plane (111) in substrate temperature 400°C, Manickam et al. [20], Manogowri et al. [21], Louardi et al. [22], and Kouidri et al. [23] have obtained the same result for the Co_3O_4 thin films prepared by spray method. This direction has no diffraction relation with another oxide (CoO or Co_2O_3), this indicates that the thin films of Co_3O_4: Mn are more stable [24], and have minimum energy of the growth. The disappearance of the plane (220) and the decrease in the intensity of the plane (311) in the sample of 8% Mn may be due to the removal of crystal orientations with a preference for growth in the direction of the lowest energy, which is the plane (111).

This due to the increase of stress caused by the rise of Mn doping rate. However, good crystallization was obtained in the low doping. This is attributed to the increase in nucleation sites [25, 26].

The crystallite size (D) and lattice strain (ε), was analyzed using the williamson-hall method [26], being based on the following equation:

$$\frac{\beta * cos\theta}{\lambda} = \frac{0,9}{D} + \frac{4\varepsilon * sin\theta}{\lambda} \tag{2}$$

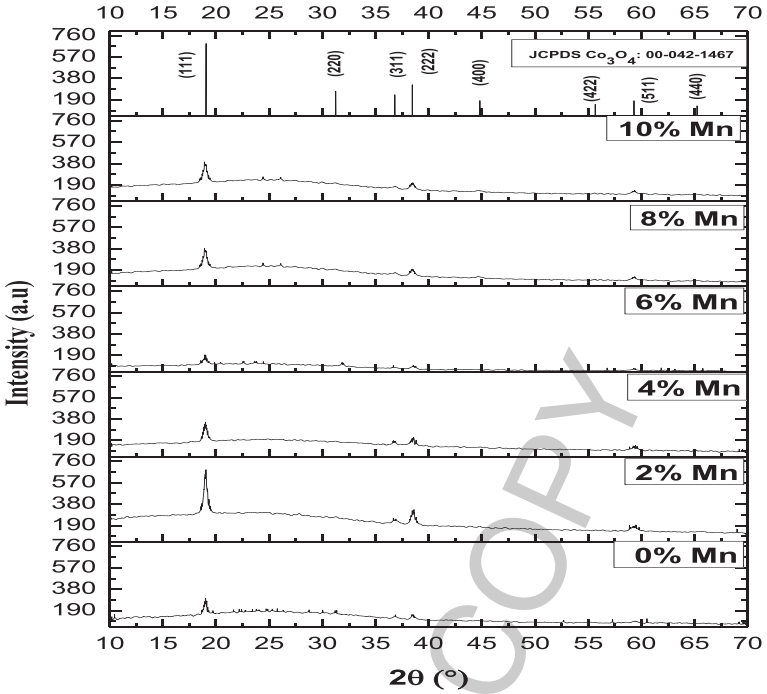

Fig. 2. DRX patterns of Co_3O_4: Mn thin films deposited by different PWM.

Table 1
Structural parameters of Co_3O_4:Mn thin films

Mn-doped	θ (deg)			d_{hkl} (nm)			a (nm)		
Co_3O_4 (wt%)	(111)	(311)	(222)	(111)	(311)	(222)	(111)	(311)	(222)
0	9.51	18.41	19.25	0.46	0.24	0.234	0.80855	0.8093	0.8097
2	9.512	18.42	19.26	0.46	0.24	0.234	0.80816	0.8091	0.8093
4	9.501	18.38	19.24	0.47	0.24	0.234	0.808963	0.8109	0.8102
6	9.49	18.35	19.27	0.46	0.24	0.235	0.8099	0.8119	0.8089
8	9.492	18.38	19.27	0.46	0.24	0.236	0.8096	0.8106	0.8090
10	9.492	18.39	19.22	0.46	0.24	0.237	0.8096	0.8101	0.8109

Where β: measured full width at half maximum (in radians), θ: Bragg angle (in degree), and λ: wavelength of X-rays.

Using the Williamson-Hall plot of Mn-doped Co_3O_4, the lattice strain and crystallite sizes were calculated respectively from the slope of the linear fit and y-intercept in Fig. 3. This analysis was applied to (111), (311), (222), and (511) corresponding peaks of the Co_3O_4:Mn thin films.

Table 2 shows the results obtained of W-H analysis for the cubic spinel phase. As can be seen, increasing the WPM(for$\leqslant$ 4% Mn) is accompanied with the crystallite sizes and lattice strain decrease (see Fig. 4). This results demonstrate that the substitution of Mn atom in cubic spinal lattice develops a lattice distortion and an intrinsic stress leading to the growth of smaller grains (up to 4 wt% Mn WPM) [27], a smiling correlation between the compressive strain and crystallite size has been reported by Mahdjoub et all in their study of ZnMgO thin films [7]. After this value, the crystallite sizes and lattice strain increased, and that is called coalescence step [28, 29].

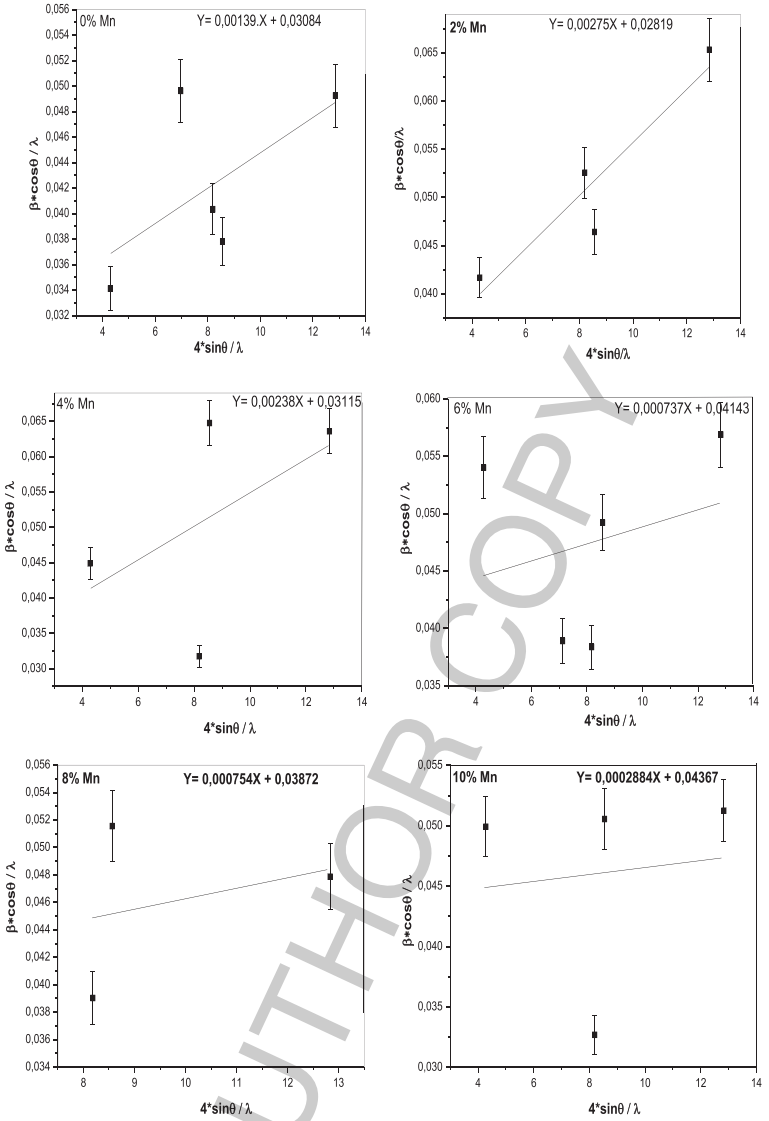

Fig. 3. Williamson-Hall plots of Mn-doped Co_3O_4 for cubic spinel structure.

3.3. Surface morphology of Mn-doped Co_3O_4 thin films

The morphological arrangement of the Mn-doped Co_3O_4 thin films deposited at 400°C with different weight percentage of manganese (WPM) was analyzed using atomic force microscopy(AFM) with three dimensional (3D)and is presented in Fig. 6. From AFM micrographs it is shown that the straight acicular nanorods (SANRs) is consistent with the results reported elsewhere [30], whereas, thin films of lower WPM, it shows fewer the SANR compared to the films witha higher WPM. A quantitative analysis of surface roughness upon small-scale image using the roughness function of the weigth percentage of Mn led to Rms values nm of 217 and 566 nm for lower WPM and higher WPM, respectively. The evolution of film surface as a function of the WPM as a function of the deposition rate can be explained as follows; at low percentage rat, this means that a few amounts of the Mn-doped Co_3O_4 have been deposited; therefore, fewer SANRs appear, so the surface is less rough. Increasing the WPM leads to an increase in the number of SANRs, and thus increased roughness.

Table 2
Williamson-Hall XRD analysis of Mn-doped Co_3O_4 for cubic spinel structure

(hkl)		%0	%2	%4	%6	%8	%10
111	4 sin θ/λ	4,284334	4,286396	4,282140	4,277017	4,278158	4,278534
	β cos θ/λ	0,0341223	0,041662	0,044905	0,054003	0,046282	0,049922
220	4 sin θ/λ	6,975272	–	–	7,122787	–	–
	β cos θ/λ	0,0496311	–	–	0,038893	–	–
311	4 sin θ/λ	8,195901	8,197707	8,180243	8,1564149	8,183030	8,188084
	β cos θ/λ	0,04034	0,05256	0,031759	0,049207	0,039036	0,032692
222	4 sin θ/λ	8,555871	8,560096	8,551267	8,5641499	8,562878	8,543538
	β cos θ/λ	0,0378099	0,045747	0,056475	0,049207	0,051553	0,050556
511	4 sin θ/λ	12,851565	12,83506	12,841683	12,827709	12,834534	12,834636
	β cos θ/λ	0,0492499	0,065345	0,063590	0,0568862	0,047879	0,0512542
Crystallite size D (nm)		32,42	35,47	32,10	24,13	25,82	22, 90
Lattice strain ε (x 10^{-3})		1,39	2,75	2,38	0,737	0,754	0,288

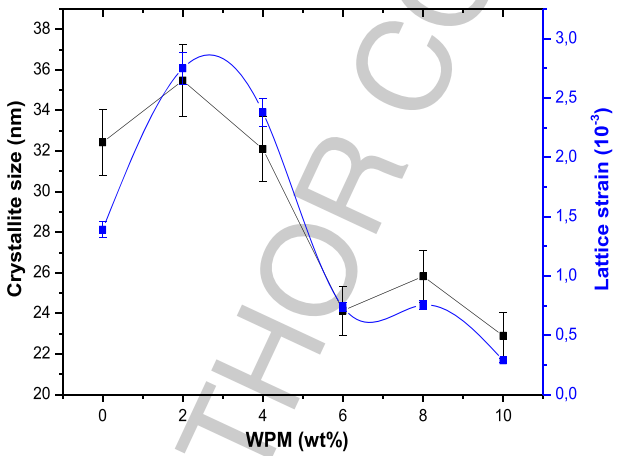

Fig. 4. Lattice strain and crystallite size of Mn-doped Co_3O_4 from Williamson-Hall plots.

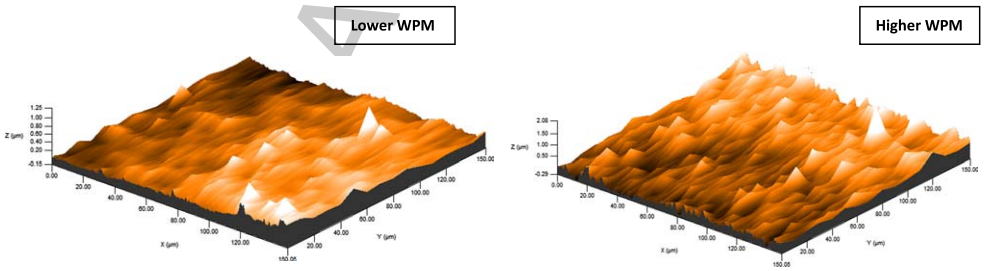

Fig. 5. 3DAFM images of Co_3O_4: Mn thin films with different WPM.

The chemical composition of elements present in the Mn-doped Co_3O_4 thin films was determined using EDS spectra with the scanning electron microscopy(SEM). Figure 6 shows the atomic percentages of elements present in the Mn-doped Co_3O_4. The oxygen and manganese density increases, but the cobalt density decreases in thin films. From the EDS spectra, from percentages for chemical com-

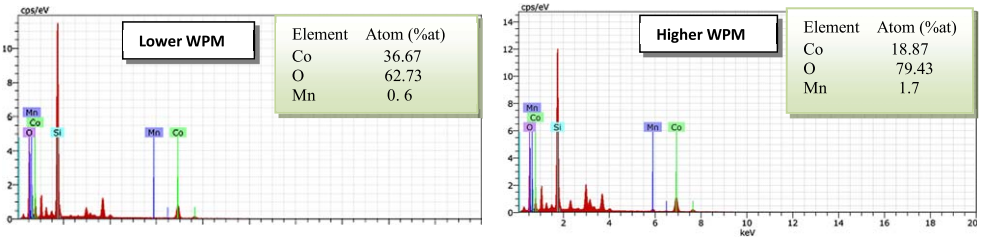

Fig. 6. EDS spectra of Mn-doped Co_3O_4 thin films with different WPM.

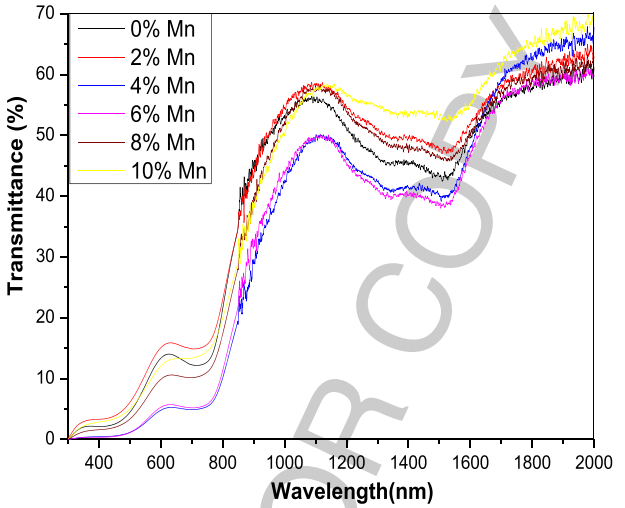

Fig. 7. Transmittance spectra of Co_3O_4: Mn thin films with different WPM.

positions of the films obtained near to the stoichiometric in nature. Such surface morphology may offer expanded surface area, beneficial for gas sensing [15] and electrochromic applications [31].

3.4. Optical properties

Figure 7 shows the optical transmittance spectra of Mn-doped Co_3O_4 thin films deposited on glasses substrates at 400°C under a function of WPM. It can be seen, the Mn-doped Co_3O_4 thin films have exhibit a similar optical behavior over the wavelength of 300–2000 nm, but there is noticeable high transmittance of 16% for 6 WPM in the range visible (UV-Vis). The optical transmittance of the thin films deposited at low WPM values with a spinel phase was 5% because this thin films of spinel phase have low crystalline size ($D = 24$, 39 nm) which increasing light scattering. This leads to minimum transmittance in the films. These films are allowed to be use in solar cells and the PN junction [32–34].

The absorption edges correspond to the electronic excitation of the valence band at the conduction band. The direct band gap value is determined by the valence level related to the strong O^{2-} ($2p^6$) properties, and the conduction level at which the main contribution is given by the $Co^{2+}(3d^7)$ orbital's. The direct band gap value is determined by the valence level related to the strong Op properties, and the conduction level at which the main contribution is given by the Co orbitals. The presence of $Co^{3+}(3d^6)$ in Co_3O_4 gives rise to a sub-band located within the energy gap. So, that coincide with E_{gop1}(is corresponds to the onset of $O^{2-}(2p)$ to the $Co^{3+}(t2g)$) excitation as highlighted in the enlarged $(\alpha h\nu)^2$ versus $(h\nu)$ plots in the Fig. 8 and E_{gop2}(is corresponds to the onset of $O^{2-}(2p)$ to the

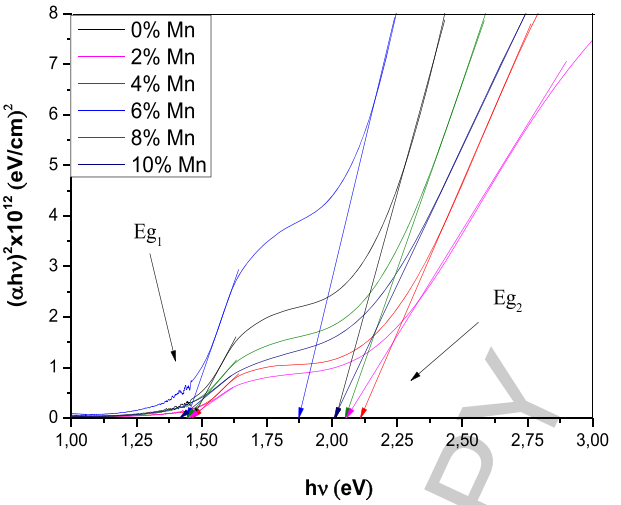

Fig. 8. Plots of $(\alpha h\upsilon)^2$ against $h\upsilon$ of Co_3O_4: Mn thin films with different WPM.

Table 3
Optical and electrical parameters values of the deposited Mn-doped Co_3O_4 thin films

WPM (wt%)	Band gap energy (eV)		Urbach energy Eu (eV)		Thickness t_h(nm)	Refractive index n	Electrical conductivity σ $(\Omega.cm)^{-1}$
	E_{gop1}	E_{gop2}	Eu_1	Eu_2			
0	$1.47 \pm 0,07$	$2,016 \pm 0,10$	$0,24 \pm 0,0117$	$0,894 \pm 0,05$	$365,64 \pm 18,30$	2,71	$1,623 \pm 0,10$
2	$1.45 \pm 0,07$	$2,056 \pm 0,10$	$0,28 \pm 0,0137$	$0,993 \pm 0,05$	$376,38 \pm 18,82$	2,68	$2,074 \pm 0,104$
4	$1.47 \pm 0,07$	$2,11 \pm 0,11$	$0,23 \pm 0,014$	$0,995 \pm 0,05$	$297,47 \pm 14,87$	2,64	$2,633 \pm 0,132$
6	$1,44 \pm 0,07$	$1,873 \pm 0,1$	$0,25 \pm 0,011$	$0,917 \pm 0,05$	$291,14 \pm 14,56$	2,81	$15,536 \pm 0,78$
8	$1,43 \pm 0,08$	$2,051 \pm 0,10$	$0,28 \pm 0,014$	$1 \pm 0,05$	$328,81 \pm 16,44$	2,69	$0,992 \pm 0,05$
10	$1,42 \pm 0,07$	$2,01 \pm 0,10$	$0,34 \pm 0,020$	$1,12 \pm 0,06$	$346,45 \pm 17,32$	2,72	$0,631 \pm 0,032$

Co^{2+}(t2g)), which determines the valence to conduction band excitation. The optical band gap E_{gop1} and E_{gop2} values for all samples are summarized in Table 3 with the WPM.

Co_3O_4 is known to possess strong photo absorption in the visible region, which is easily evidenced by its dark black color. To calculate the energy gap E_{gop} associated with the incident photon energy $(h\upsilon)$ and the absorption coefficient(α), we use the classical equation [24].

$$(\alpha h\upsilon)^2 = A\left(h\upsilon - E_{gop}\right) \tag{3}$$

Where A is the proportionality constant and E_{gop} is the band gap. Two linear regions appear indicating the existence of two different band gap values, which may be ascribed to the spin-orbit fragmenting of the valence band. The extrapolation of two straight lines to $(\alpha h\upsilon)^2 = 0\,(eV)^2$ give values of the direct band gaps of Mn-doped Co_3O_4 thin films (see Table 3). It is found of E_{gop1} values of the energy band gap varies between $1.42 \pm 0,07$ and 1.46 ± 0.07 eV while E_{gop2} values, which are obtained from the extrapolation of the first linear region, found to be varying between 1.873 ± 0.10 and $2.11 \pm 0,11$eV (see Fig. 8). Increased film thickness could explain the increase in the optical band gap E_{gop2} and vice versa [35]. The marginal variation or shift observed in E_{gop2} values might be due to formation of impurity energy levels or localized energy states created between conduction band and valance band upon Mn doping. Co^{+3} substituted by Mn^{+3} leads to the formation of impurity energy levels created

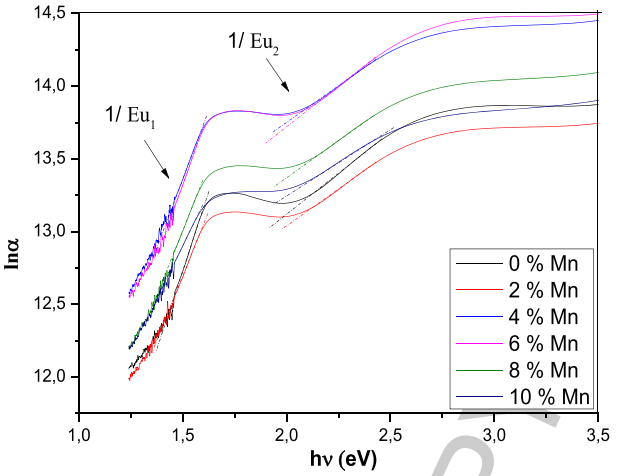

Fig. 9. Plots of $(h\upsilon)$ against $ln\alpha$ of Co_3O_4: Mn thin films with different WPM

between CB band and VB band. This increase the amount of Co^{+3} vacancy. The observed marginal difference or decrease in the E_{gop2} values is also due to the presence of a high amount of acceptor states (cation vacancies) near the top edge of the range, which belong to Co^{3+} or Co^{2+}(3dt2g). This can occur as a result of overlapping upper-edge states and donor-edge states upon doping of manganese observed from EDS, resulting in a narrowing of the range of E_{gop2} [3, 15]. After 6 wt% of Mn, the band gap energy increased; This can be explained by the increase in Urbach energies (see Fig. 9), that is, as the Urbach energy increases, the random energy increases, and thus the absence of crystal structural organization. The refractive index is related to optical band gap (E_{gop2}) of a semiconductor by the following relationship [19, 36]:

$$n = 4,084 - 0,68E_{gop2} \tag{4}$$

The observed marginal difference or shift in the E_{gop2} values is further due to the formation of impurity energy levels or localized energy states created between the conduction domain and the straightness band upon doping of manganese observed from EDS [3, 15].

3.5. *Electrical properties*

For measuring the sheet resistance (R_{sheet}) by the four-point probe technique, the current ($I = 0.01\mu A$) is applied between the outer two wires and the value of potential difference (V) is read across the two internal probes. Thus, the sheet resistance is calculated from the following relation:

$$R_{sheet} = \frac{\pi}{In2} * \frac{V}{I} \tag{5}$$

The conductivity (σ) values of films are calculated from the following formula:

$$\sigma = 1/(R_{sheet} * t_h) \tag{6}$$

Where t_h: is thickness of thin films.

The values of electrical conductivity (σ) of Mn-doped Co_3O_4 thin films are listed in Table 2. The variation of conductivity (σ) of thin films as a function of the WPMis illustrated in Figure 10. It can

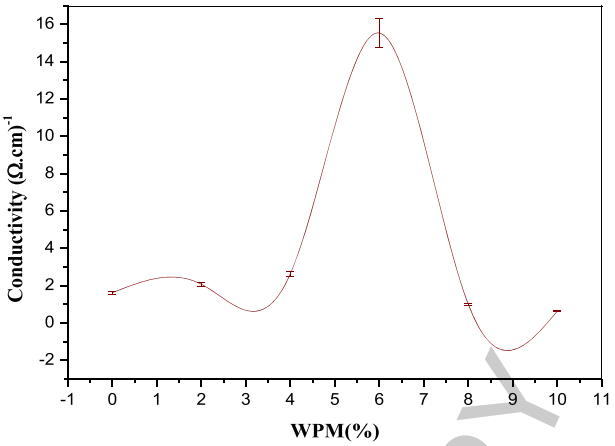

Fig. 10. Electrical conductivity of Mn-doped Co_3O_4 thin films as a function of the WPM.

be observed that the conductivity (σ) increases with the increase of the WPM upto 6% Mn. After this value, the conductivity decreases. This increase is mainly due to an increase in the carrier concentration (holes) of the valence band due to electronic shifts in the conduction band and holes resulting from the non-stoichiometry of the oxygen network in the p-Co_3O_4 grain [37]. On the other hand, the reduction of the size of the grains and increasing of manganese gives rise to the appearance of the separate energy levels.

These levels manifest in the gap as electronic defects, which probably work like donors inducing the increase in conductivity. After the value of 6% Mn, the electrical conductivity (σ) decreases can be explained as follows; the increase in resistance is attributed to the reduced crystallization of thin films, resulting in a decrease in the electron scattering centers due to the increase of the WPM [38].

4. Conclusion

Undoped and Mn-doped Co_3O_4 thin films were deposited using a homemade pneumatic spray method (PSM) by varying manganese doping weight percentages (0, 2,4,6,8 and 10 wt %) on glass substrate at temperature 400°C. The X-ray diffraction patterns revealed that the crystalline quality of pristine and Mn-doped cobalt oxide (Co_3O_4) thin films self cubic spinel structure oriented along to (111) plane. The crystal size (D) and lattice strain (ε) were calculated based on X-ray diffraction and Williamson-Hall relationship. The morphology of pristine and Mn-doped Co3O4 thin films is almost homogeneous and with the forms straight acicular nanorods (SANRs).The optical studies showed tow direct band gaps E_{gop1} and E_{gop2} varied between $1{,}416 \pm 0{,}0708$ to $1{,}466 \pm 0{,}0733$ eV and from $1{,}873 \pm 0{,}0936$ to $2{,}11 \pm 0{,}1055$ eV respectively. The electrical conductivity increased get to $15, 536 \pm 0, 7768\ (\Omega.\text{cm})^{-1}$ with increasing percentages weight of Manganese doping (in 6 wt% of Mn) determined from four point probe technique. Co^{+3} substituted by Mn^{+3} leads to an increase in the amount of oxygen vacancy. The latter engenders the increase of electrical conductivity at 6% wt% of Mn.

It can be concluded, Manganese doping has a significant impact on the structural, morphological, optical, and electrical properties of Co_3O_4 thin films. Through the obtained results, it can be said that the pneumatic spray method (PSM) is important in obtaining homogeneous films with good structural, optical, and electrical properties. It can also be said that the Mn-doped cobalt oxide thin films prepared by the pneumatic spraying method (PSM) are applicable in photovoltaics, photocatalysis, and gas sensing applications.

References

[1] A. Louardi, A. El Bachiri, L. Soussi, H. Erguig, B. Elidrissi, M. Khaidar and M. Monkade,Optical Properties of Mg Cobalt Oxide (Mg $_x$ Co_{3-x} O_4) Thin Films, *Materials Focus* **7** (2018), 459–463.

[2] F. Alema, A. Osinsky, P. Mukhopadhyay and Winston V. Schoenfeld, Epitaxial growth of Co_3O_4 thin films using $Co(dpm)_3$ by MOCVD, *Journal of Crystal Growth* **525** (2019), 125207.

[3] R. Perekrestov, A. Spesyvyi, J. Maixner, K. Mašek, O. Leiko, I. Khalakhan, J. Maňák, P. Kšírová, Z. Hubička and M. Čada, The comparative study of electrical, optical and catalytic properties of Co_3O_4 thin nanocrystalline films prepared by reactive high-power impulse and radio frequency magnetron sputtering, *Thin Solid Films* **686** (2019), 137427.

[4] O. Kilo, J. Jabbour, R. Habchi, N. Abboud, M. Brouche, A. Khoury and D. Zaouk, Electrospray deposition and characterization of cobalt oxide thin films, *Materials Science in Semiconductor Processing* **24** (2014), 57–61.

[5] P. Shia, R. Sua, S. Zhua, M. Zhua, D. Li and S. Xu, Supported cobalt oxide on graphene oxide: Highly efficient catalysts for the removal of Orange II from water, *Journal of Hazardous Materials* **229–230** (2012), 331–339.

[6] [6]S.G. Kandalkar, J.L. Gunjakar and C.D. Lokhande, Preparation of cobalt oxide thin films and its use in supercapacitor application, *Applied Surface Science* **254** (2008), 5540–5544.

[7] A. Lakehal, B. Benrabah, A. Bouaza, C. Dalache and B. Hadj, Tuning of the physical properties by various transition metal doping in Co_3O_4: TM (TM = Ni, Mn, Cu) thin films: A comparative study, *Chinese Journal of Physics* **56** (2018), 1845–1852.

[8] L. Yao, Y. Xi and G. Xi, Y. Recycling and synthesis of LiNi 1/3 Co 1/3 Mn 1/3 O 2 from waste lithium ion batteries using d, l-malic acid. Feng, *J Alloys Compd* **680** (2016), 73–79.

[9] A.B. Vennela, D. Mangalaraj, N. Muthukumarasamy, S. Agilan and K.V. Hemalatha, Structural and Optical Properties of Co3O4 Nanoparticles Prepared by Sol-gel Technique for Photocatalytic Application, *International Journal of Electrochemical Science* **14** (2019), 3535–3552.

[10] A.I. Nguyen, D.L. Suess, L.E. Darago, P.H. Oyala, D.S. Levine, M.S. Ziegler, R.D. Britt and T.D. Tilley, Manganese-Cobalt Oxido Cubanes Relevant to Manganese-Doped Water Oxidation Catalysts, *Journal of the American Chemical Society* **139** (2017), 5579–5587.

[11] S. Liu, K. Hui and K. Hui, ACS Appl. Vertically stacked bilayer CuCo 2 O 4/MnCo 2 O 4 heterostructures on functionalized graphite paper for high-performance electrochemical capacitors, *Journal of Materials Interfaces* **8** (2016), 3258–3267.

[12] X. Zou, J. Su, R. Silva, A. Goswami, B.R. Sathe and T. Asefa, Efficient oxygen evolution reaction catalyzed by low-density Ni-doped Co3O4 nanomaterials derived from metal-embedded graphitic C3N4, *Chem Commun* **49** (2013), 7522–7524.

[13] T. Baidya, T. Murayama, P. Bera, O.V. Safonova, P. Steiger, N.K. Katiyar, K. Biswas and M. Haruta, Low-Temperature CO Oxidation over Combustion Made Fe- and Cr-Doped Co_3O_4 Catalysts: Role of Dopant's Nature toward Achieving Superior Catalytic Activity and Stability, *Journal of Physical Chemistry* **121** (2017), 15256–15265.

[14] T. Grewe, X. Deng and H. Tüysüz, Influence of Fe Doping on Structure and Water Oxidation Activity of Nanocast Co3O4, *Chemistry of Materials* **26** (2014), 3162–3168.

[15] R. Venkatesha, C. Ravi Dhasa, R. Sivakumarb, T. Dhandayuthapanib, B. Subramanianc, C. Sanjeevirajad and A. Moses Ezhil Raje, Tailoring the physical properties and electrochromic performance of nebulizer spray coated Co3O4 films through copper doping, *Solid State Ionics* **334** (2019) 5–13.

[16] W. Daranfed, N. Guermat and K. Mirouh, Experimental Study of Precursor Concentration the Co3O4 Thin Films Used as Solar Absorbers, *Annales de Chimie - Science des Matériaux* **44** (2020), 121–126.

[17] S. Salman Chiad, H. Ali Noor, O. Mazin Abdulmunem and N. Fadhil Habubi, Optical and Structural properties of Ni-doped Co3O4Nanostructure Thin films Via CSPM, *Journal of Physics: Conference Series* **1362** (2019), 012115.

[18] J.A.K. Tareen, A. Malecki, J.P. Doumerc, J.C. Launay, P. Dordor, M. Pouchard and P. Hagenmuller, Growth and electrical properties of pure and Ni-doped Co_3O_4 single crystalsMaterials research bulletin, *Materials Research Bulletin* **19** (1984), 989–997.

[19] R.C. Ambare, S.R. Bharadwaj and B.J. Lokhande, Electrochemical characterization of Mn: Co_3O_4 thin films prepared by spray pyrolysis via aqueous route, *Current Applied Physics* **14** (2014), 1582–1590.

[20] M. Manickam, V. Ponnuswamy, C. Sankar, R. Mariappan and R. Suresh, Influence of Substrate Temperature on the Properties of Cobalt Oxide Thin Films Prepared by Nebulizer Spray Pyrolysis (NSP) Technique, *Silicon* **8** (2016), 351–360.

[21] R. Manogowri, R. Mary Mathelane, S. Valanarasu, I. Kulandaisamy, A. Benazir Fathima and A. Kathalingam, Effect of annealing temperature on the structural, morphological, optical and electrical properties of Co_3O_4 thin film by nebulizer spray pyrolysis technique, *Journal of Materials Science: Materials in Electronics* **27** (2016), 3860–3866.

[22] A. Louardi, A. Rmili, F. Ouachtari, A. Bouaoud, B. Elidrissi and H. Erguig, Characterization of cobalt oxide thin films prepared by a facile spray pyrolysis technique using perfume atomizer, *Journal of Alloys and Compounds* **509** (2011), 9183–9189.
[23] N. Kouidri, S. Rahmane and A. Allag, Substrate temperature-dependent properties of sprayed cobalt oxide thin films, *Journal of Materials Science: Materials in Electronics* **30** (2019), 1153–1160.
[24] J.H. Richter, Electronics Properties of Metal Oxide Films Studied by Core Level Spectroscopy, *Digital Comprehensive Summaries of Uppsala Faculty of Science and Technology* 228 (1969).
[25] A. Bouhdjer, A. Attaf, H. Saidi, H. Bendjedidi, Y. Benkhetta and I. Bouhaf, Correlation between the structural, morphological, optical, and electrical properties of In2O3 thin films obtained by an ultrasonic spray CVD process, *J Semiconduct* **36** (2015), 082002-1
[26] R. Messemeche, H. Saidi, A. Attaf,Y. Benkhetta, S. Chala, R. Azizi, R. Nouadji, Elaboration and characterization of nano-crystalline layers of transparent titanium dioxide (Anatase-TiO_2) deposited by a sol-gel (spin coating) process, *Surfaces and Interfaces* **19** (2020), 100482.
[27] R. Venkatesh, C. RaviDhas, R. Sivakumar, T. Dhandayuthapani, P. Sudhagar, C. Sanjeeviraja and A. Moses EzhilRaj, Analysis of optical dispersion parameters and electrochromic properties of manganese-doped Co_3O_4 dendrite structured thin films, *Journal of Physics and Chemistry of Solids* **122** (2018), 118–129.
[28] J. Yan, G. Wu, W. Dai, N. Guan and L. Li, Synthetic Design of Gold Nanoparticles on Anatase TiO2 001 for Enhanced Visible Light Harvesting ACS Sustainable Chem, *Eng* **2** (1940), (2014).
[29] D. Georgescu, L. Baia, O. Ersen, M. Baia and S. Simon, Experimental assessment of the phonon confinement in TiO2 anatase nanocrystallites by Raman spectroscopy, *J Raman Spectrosc* **43**(7) (2012), 876–883.
[30] O. Herzallah, H.B. Temam, A. Ababsa and A. Gana, Electrodeposited Ni-Co Films from Electrolytes with Different Co Contents, *Defect and Diffusion Forum* **406** (2021), 219–228.
[31] C. RaviDhas, R. Venkatesh, R. Sivakumar, A. Moses EzhilRaj and C. Sanjeeviraja, Effect of solution molarity on optical dispersion energy parameters and electrochromic performance of Co_3O_4 films, *Optical Materials* **72** (2017), 717–729.
[32] M. Shaban and A.M. El Sayed, Influence of the spin deposition parameters and La/Sn double doping on the structural, optical, and photoelectrocatalytic properties of $CoCo_2O_4$ photoelectrodes, *Solar Energy Materials and Solar Cells* **217** (2020), 110705.
[33] O. Bayram, E. İgman, H. Guney and O. Simsek, The role of cobalt doping on the optical and structural properties of Mn_3O_4 nanostructured thin films obtained by SILAR technique, *Superlattices and Microstructures* **128** (2019), 212–220.
[34] J. Huang, T. Liu, R. Wang, M. Zhang, L. Wang, H. She and Q. Wang, Facile loading of cobalt oxide on bismuth vanadate: Proved construction of p-n junction for efficient photoelectrochemical water oxidation, *Journal of Colloid and Interface Science* **570** (2020), 89–98.
[35] Y. Benkhetta, A. Attaf, H. Saidi, A. Bouhdjar, H. Bendjedidi, I.B. Kherkhachi, M. Nouadji and N. Lehraki, Influence of the solution flow rate on the properties of zinc oxide (ZnO) nano-crystalline films synthesized by ultrasonic spray process, *Optik* **127** (2016), 3005–3008.
[36] N.M. Ravindra, Energy gap-refractive index relation—some observations, *Infrared Physics* **21** (1981), 283–285.
[37] S. Rahmane and N. Kouidri, effect Of Cobalt Chloride Concentration On Structural, Optical And Electrical Properties Of Co3o4 Thin Films Deposited By Pneumatic Spray, *Journal of New Technology and Materials* **10**(01) (2020), 56–62.
[38] A. Bouhdjer, A. Attaf, H. Saidi, Y. Benkhetta, M.S. Aida, I. Bouhaf and A. Rhil, Influence of annealing temperature on In2O3 properties grown by an ultrasonic spray CVD process, *Optik* **127** (2016), 6329–6333.

Abstract

Study of the effect of dopant on oxide thin films for optoelectronic applications.

In this work, we chose to deposit dopant cobalt oxide with manganese, lanthanum, tin and zinc by spray pneumatic method. The Co3O4:N (N= Mn, La, Sn and Zn) thin films were deposited on heated glasses substrates (T_S = 400°C) using a homemade pneumatic spray method (PSM). The solution concentration and deposition time are 0.1 M and 4min respectively. The effect of N doping concentration on structural, optical and electrical properties of cobalt oxide were investigated. The elaborated films were characterized by X-ray diffraction, UV-Vis spectroscopy, atomic force microscopy (AFM) the three-dimensional (3D), energy dispersive spectroscopy (EDS), and four points probe measurements. The XRD study showed that all films were polycrystalline consisting with spinel cubic phase orientated along to (111) plane. The lattice strain and crystallite size were estimated by Williamson-Hall method. The morphology of N-doped Co_3O_4 thin films shows a homogeneous surface with straight acicular nanorods (SANRs). EDS analysis showed the presence of peaks associated with Co, O and N elements which confirm the composition of the thin films. The optical band gaps vary from 1,42 to 1,49 eV of E_{gop1} and E_{gop2} varies from 1,730 to 2,118 eV. In addition, the electrical measurement shows a maximum electrical conductivity (σ_M = 15,536 $(\Omega.cm)^{-1}$) at 6% wt of Mn, (σ_L = 22,858 $(\Omega.cm)^{-1}$) at 10 wt% of La, (σ_S = 16,875 $(\Omega.cm)^{-1}$) at 8% wt of Sn and (σ_Z = 24,266 $(\Omega.cm)^{-1}$) at 6% wt of Zn.

Keywords: N-doped Co_3O_4 thin films, pneumatic spray method (PSM), weight percentages of N (WPN), spinel cubic structure (SCS), X-ray diffraction (XRD).

الملخص

دراسة تأثير التطعيم على شرائح الأكسيد الرقيقة للتطبيقات الكهروضوئية

في هذا العمل، اخترنا في دراستنا أكسيد الكوبالت المطعم بالمنغنيز، اللانثانيوم, القصدير والزنك. تم ترسيب الشرائح الرقيقة Co_3O_4: N حيث على مساند زجاجية ساخنة (T_S = 400°C) باستخدام طريقة رش هوائي محلي الصنع (PSM) . تركيز المحلول ووقت الترسيب 0.1 مول/ل و4 دقائق على التوالي. تم دراسة تأثير تركيز التطعيم على الخواص التركيبية والبصرية والكهربائية لأكسيد الكوبالت. تميزت الشرائح بانحراف الأشعة السينية، والتحليل الطيفي للأشعة المرئية وفوق البنفسجية، والفحص المجهري للقوة الذرية (AFM)ثلاثي الأبعاد (3D)، والتحليل الطيفي المشتت للطاقة (EDS) ، وقياسات مسبار بأربع نقاط. أظهرت دراسة XRD أن جميع الأفلام كانت متعددة البلورات وتتكون من طور مكعب من الإسبينيل موجه على طول مستوى (111). تم تقدير إجهاد الشبكة وحجم البلورات بواسطة طريقة Williamson-Hall. يُظهر الشكل المورفولوجي للشرائح الرقيقة Co_3O_4: N سطحًا متجانسًا مع العصي النانوية المستقيمة (SANRs).أظهر تحليل EDS وجود قمم مرتبطة بعناصر Co و O و N التي تؤكد تكوين الأغشية الرقيقة. تختلف فجوات النطاق الممنوع من 1.42 إلى 1.49 eV من E_{gop1} و E_{gop2} من 1.730 إلى 2.118 eV. بالإضافة إلى ذلك، يُظهر القياس الكهربائي الموصلية الكهربائية القصوى ($\sigma_M = 15{,}536\ (\Omega.\mathrm{cm})^{-1}$)عند 6٪ بالوزن من Mn ،

($\sigma_L = 22{,}858\ (\Omega.\mathrm{cm})^{-1}$) عند 10٪ بالوزن من La, ($\sigma_S = 16{,}875\ (\Omega.\mathrm{cm})^{-1}$) عند 8٪ بالوزن منSn و ($\sigma_Z = 24{,}266\ (\Omega.\mathrm{cm})^{-1}$) عند 6٪ بالوزن من الزنك.

كلمات المفتاحية:

الشرائح الرقيقة Co_3O_4 المطعمة ب N ، طريقة الرش بالهواء المضغوط (PSM) ، النسب المئوية للوزن من N (WPN)، هيكل مكعب الإسبينيل (SCS)، انعكاس الأشعة السينية (XRD) .

Résumé

Etude de l'effet du dopant sur les couches minces d'oxyde pour applications optoélectroniques.

Dans ce travail, nous avons choisi de déposer de l'oxyde de cobalt dopé avec du manganèse, du lanthane, de l'étain et du zinc par pulvérisation pneumatique. Les couches minces de Co_3O_4:N (N=Mn, La, Sn et Zn) ont été déposées sur des substrats de verre chauffés (TS = 400°C) en utilisant une méthode de pulvérisation pneumatique (PSM) artisanale. La concentration de la solution et le temps de dépôt sont respectivement de 0,1 M et 4 min. L'effet de la concentration de dopage N sur les propriétés structurelles, optiques et électriques de l'oxyde de cobalt a été étudié. Les films élaborés ont été caractérisés par diffraction des rayons X, spectroscopie UV-Vis, microscopie à force atomique (AFM) tridimensionnelle (3D), spectroscopie à dispersion d'énergie (EDS) et mesures par sonde à quatre points. L'étude XRD a montré que tous les films étaient polycristallins constitués d'une phase cubique spinelle orientée le long du plan (111). La déformation du réseau et la taille des cristallites ont été estimées par la méthode de Williamson-Hall. La morphologie des couches minces de Co_3O_4 dopé N montre une surface homogène avec des nanobâtonnets aciculaires droits (SANR). L'analyse EDS a montré la présence de pics associés aux éléments Co, O et N qui confirment la composition des couches minces. Les bandes interdites optiques varient de 1,42 à 1,49 eV d'Egop1 et Egop2 varie de 1,730 à 2,118 eV. De plus, la mesure électrique montre une conductivité électrique maximale (σ_M = 15 536 $(\Omega.cm)^{-1}$) à 6 % en poids de Mn, (σ_L = 22 858 $(\Omega.cm)^{-1}$) à 10 % en poids de La, (σ_S = 16 875 $(\Omega.cm)^{-1}$) à 8 % en poids de Sn et (σ_Z = 24 266 $(\Omega.cm)^{-1}$) à 6 % en poids de Zn.

Mots clés : couches minces de Co_3O_4 dopé N, méthode de spray pneumatique (PSM), pourcentages massiques de N (WPN), structure cubique spinelle (SCS), diffraction des rayons X (XRD).